USING NMR CHEMICAL SHIFT PERTURBATIONS TO MAP INTERACTIONS BETWEEN ACYL-ACYL CARRIER PROTEINS AND ACYL HOMOSERINE LACTONE SYNTHASES

by

Madison N. Rizzo

A thesis

submitted in partial fulfillment

of the requirements for the degree of

Master of Science in Chemistry

Boise State University

May 2023

BOISE STATE UNIVERSITY GRADUATE COLLEGE

DEFENSE COMMITTEE AND FINAL READING APPROVALS

of the thesis submitted by

Madison N. Rizzo

Thesis Title: Using NMR Chemical Shift Perturbations to Map Interactions Between Acyl-Acyl Carrier Proteins and Acyl Homoserine Lactone Synthases

Date of Final Oral Examination: 28 November 2022

The following individuals read and discussed the thesis submitted by student Madison Nicole Rizzo, and they evaluated the student's presentation and response to questions during the final oral examination. They found that the student passed the final oral examination.

Lisa R. Warner, Ph.D.	Chair, Supervisory Committee
Rajesh Nagarajan, Ph.D.	Member, Supervisory Committee
Don L. Warner, Ph.D.	Member, Supervisory Committee

The final reading approval of the thesis was granted by Lisa R. Warner, Ph.D., Chair of the Supervisory Committee. The thesis was approved by the Graduate College.

DEDICATION

I would like to dedicate this thesis to my friends, family and mentors who have supported me in this journey. From getting accepted into the Air Force's Advanced Academic Degree program to reviewing drafts, I could not have done this without your support and commitment. Thank you from the bottom of my heart.

"Last but not least, I want to thank me. I want to thank me for believing in me, I want to thank me for doing all this hard work. I wanna thank me for having no days off. I wanna thank me for never quitting. I wanna thank me for always being a giver and trying to give more than I receive. I wanna thank me for trying to do more right than wrong. I wanna thank me for being me at all times." – Snoop Dogg

ACKNOWLEDGMENTS

I would like to thank Drs. Lisa Warner, Rajesh Nagarajan, and Don Warner for participating in my thesis committee. I would also like to thank Dr. Eric Baggs, Ms. Amanda Spencer, Ms. Yvette Russell, Ms. Stacey “Ace” Pedraza, and Ms. Jayden Brandt for their hard work and dedication to this project. Without these people, this research would not be possible. Thank you to the United States Air Force and the Air Force Institute of Technology for sending me to get my advanced academic degree at Boise State University. Finally, I would like to thank the Department of Chemistry and Biochemistry for their academic and administrative support. The work presented here was funded in part by the NSF (CHE 190531). The Boise State University NMR facility instrumentation was funded through an NSF CRIF-MU/RUI (Grant Number 0639251) as well as funding from the State of Idaho and Departmental funding.

ABSTRACT

A pandemic of antibiotic resistance is underway and affecting multiple industries, including veterinary, agricultural, and healthcare. High bacterial population density is a major form of defense for bacterial cells against drugs, contributes to antibiotic resistance, and is one of the requirements for the formation of biofilms. Quorum sensing is a form of cell-to-cell communication that both gram-negative and gram-positive bacteria use to account for density behavior. When the population density of bacteria reaches a certain level (a "quorum"), there is an observed coordinated shift in gene expression that leads to optimized growth or virulence. Acyl carrier proteins (ACP) and the enzyme acyl-homoserine lactones synthase (AHLS), which are the building blocks for the formation of quorum sensing molecules, and acyl-homoserine lactone (AHL) molecules signal the regulation of some of these expressed genes. AHLs are chemical autoinducers used in quorum sensing. This project contributes to an effort to map interactions between ACP1 and RhlI from *Pseudomonas aeruginosa*, using nuclear magnetic resonance (NMR) spectroscopy to better predict drug target sites to inhibit the production of AHL molecules. Here, I present the chemical shift backbone assignments for ACP1 and the optimized expression and purification of ACP1 and RhlI.

TABLE OF CONTENTS

LIST OF TABLES

LIST OF FIGURES

LIST OF ABBREVIATIONS

ACP	acyl carrier protein
AcpH	acyl carrier protein phosphodiesterase
AHL	acyl homoserine lactone
AHLS	acyl homoserine lactone synthase
B-PER	bacterial protein extraction reagent
CoA	coenzyme A
DNA	deoxyribonucleic acid
DTT	dithiothreitol
D_2O	deuterated water
EDTA	ethylenediaminetetraacetic acid
FAB	fatty acid biosynthesis
FPLC	fast protein liquid chromatography
GMQE	global model quality estimation
GST	glutathione S-transferase
His_6MBP	hexahistidine-tagged maltose-binding protein
HRV-3C	human rhinovirus 3-chymotrypsin
IPTG	Isopropyl ß-D-1-thiogalactopyranoside
LB	luria-Bertani
MWCO	molecular weight cut-off
NMR	nuclear magnetic resonance

OD_{600}	optical density at 600nm
PDB	protein data bank
SAM	S-adenosyl-L-methionine
SDS PAGE	dodecyl sulfate–polyacrylamide gel electrophoresis
SEC	size exclusion chromatography
Sfp	surfactin phosphopantetheinyl transferase
TCEP	tris-2-carboxyethyl phosphine
TSP	trimethylsilyl propanoic acid
UHPLC	ultra high-performance liquid chromatography
UV	ultraviolet

CHAPTER ONE : INTRODUCTION

Quorum Sensing

Quorum sensing is a form of cell-to-cell communication used to control population density in Gram-negative and Gram-positive bacteria [1]. Bacteria use quorum sensing to increase their population to form plaques or biofilms as a mechanism for antibiotic resistance [2]. These biofilms and plaque form when biofilm-producing bacteria are in an aqueous environment and adhere to solid surfaces to produce a network of extracellular polymeric substances. These substances include biomolecules such as proteins, polysaccharides, lipids, and deoxyribonucleic acid (DNA) to form a protective barrier around the bacteria [2].

Gram-negative bacteria utilize the regulatory protein LuxI for quorum sensing. LuxI is an enzyme responsible for the biosynthesis of autoinducing molecules or acyl-homoserine lactone (AHL) molecules. The autoinducer concentration increases with increasing cell-population density and signal further growth (Figure 1.1).

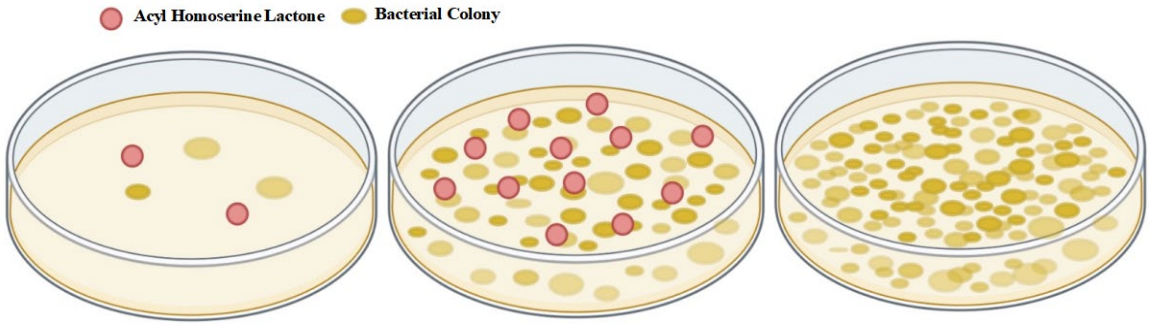

Figure 1.1 Quorum Sensing and Biofilm Formation.
Visual representation of increased AHL molecules correlating to increased cell density to form a biofilm [created with BioRender.com].

The human pathogen *P. aeruginosa*, has two LuxI homologues: LasI and RhlI. Both LasI and RhlI are autoinducer synthases that catalyze the formation of the AHL autoinducers N-(3-oxododecanoyl)-homoserine lactone and N-butyryl-homoserine lactone [3].

Acyl Carrier Proteins are an essential component of quorum sensing

ACPs are a product of fatty acid biosynthesis (FAB), with a wide range of functions, and are found in all living things. Universally, ACPs consist of four alpha-helices connected by three loops, and acyl chain carrying Serine (37Ser; ACP1) located near the N-terminal region of helix II [4]. When a phosphopantetheine linker is covalently attached to the Serine in helix II, it is referred to as holo-ACP; when an acyl group is loaded onto the phosphopantetheine linker, it is referred to as acyl-ACP (Figure 1.2).

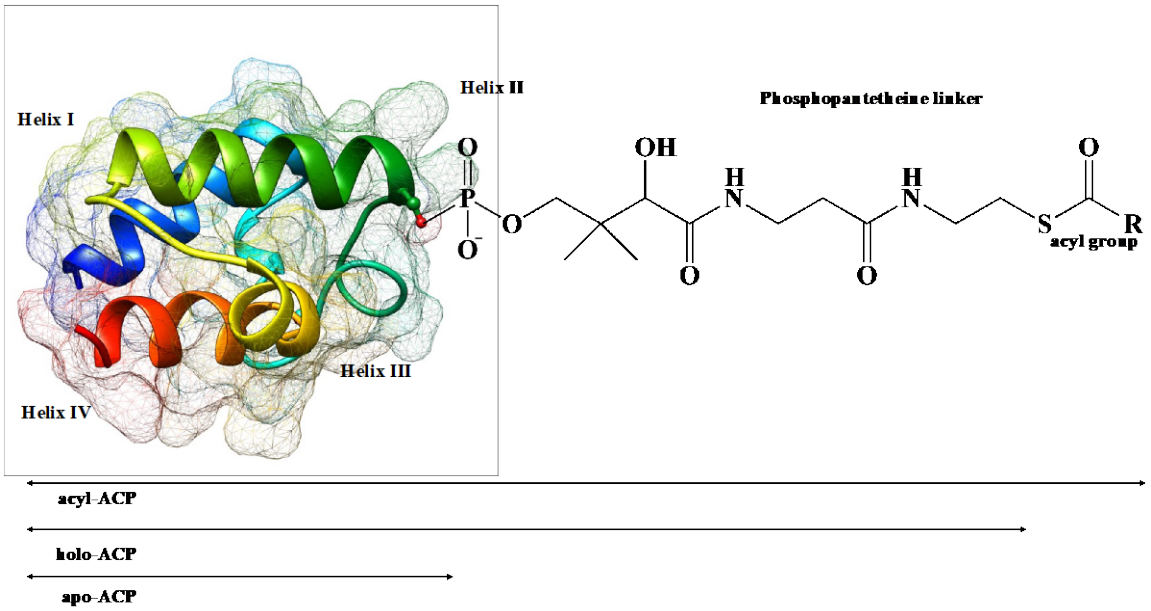

Figure 1.2 Visual of apo-, holo- and acyl-ACP.
ACP1 has four helices, and without a phosphopantetheine linker, the domain is known as apo-ACP. Holo-ACP are the four helices with the addition of a phosphopantetheine linker, and acyl-ACP is the grouping of the four helices, phosphopantetheine linker, and an acyl group [5, 6, 7, 8].

Bacteria use a diversity of chemical languages for communication

A variety of combinations of ACPs and acyl groups can result in the synthesis of different autoinducing molecules or acyl homoserine lactones (AHL). Different AHLs communicate different needs or states both inter- and intraspecies. AHLs are produced based on combinations of acyl chain length, the particular ACP, and acyl homoserine lactone synthases (AHLSs) (Figure 1.3) [9]. Similar reactions between acyl-ACP and AHLS occur in different strains of bacteria, with different acyl groups. The difference in acyl group requires alternate AHLS enzymes and produce a variety of different acyl-homoserine lactone molecules. Having a variety of AHL molecules allows bacteria to communicate inter- and intraspecies. The focus of this research is to map the structure of ACP for *P. aeruginosa* (ACP1) in apo- form and with acyl cargo loaded (C4I-ACP1) to

better understand the synthesis of AHL molecules and ultimately the inhibition of these signals.

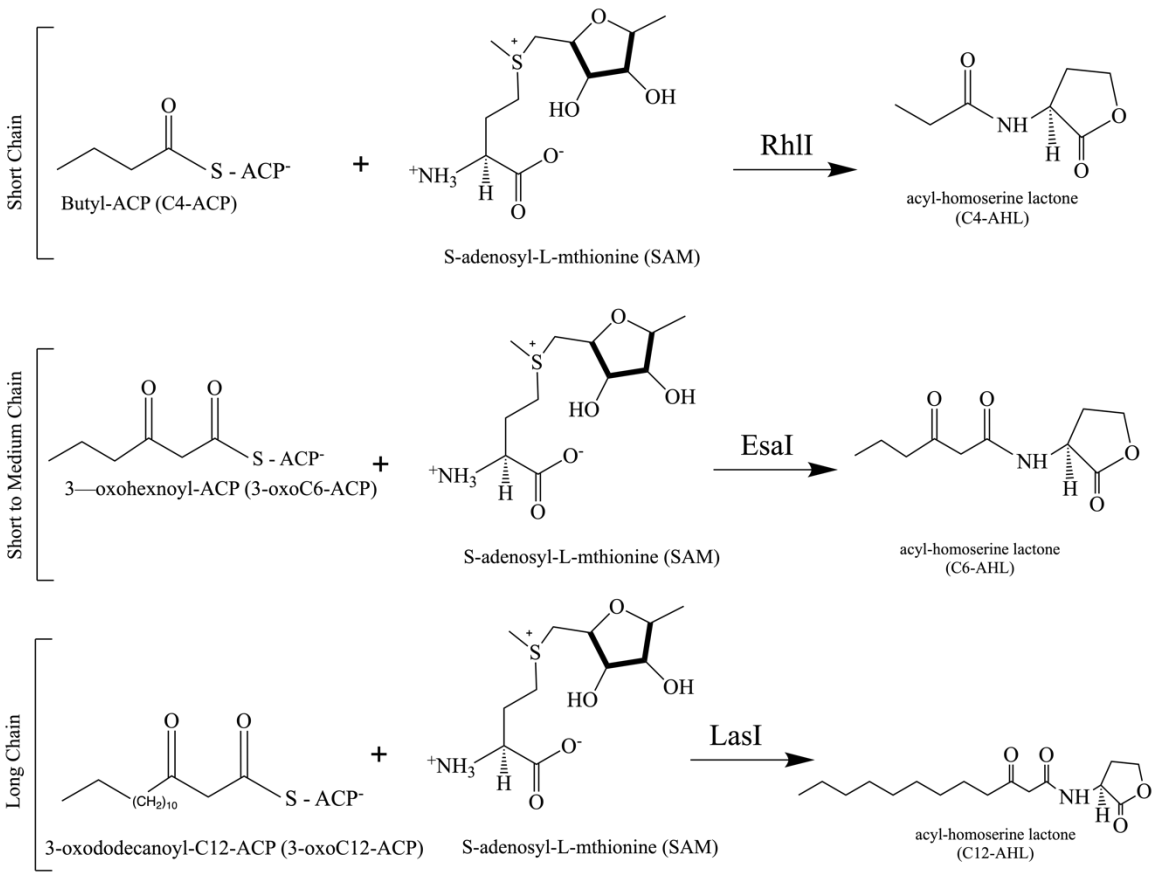

Figure 1.3 Production of different autoinducing AHL molecules from cognate enzyme/substrate pairs.

Production of different AHL molecules with different acyl groups lengths and corresponding native AHLS enzymes [8].

AHL Synthases are the enzymes that create quorum sensing chemicals

Acyl bonded ACP (Acyl-ACP) are a product of the fatty acid biosynthesis. S-adenosyl-L-methionine (SAM) molecules are general purpose bio-building blocks found in living organisms. SAM is commonly known for as a substrate involved in methyl group transfers and for its role in cysteine biosynthesis. In quorum sensing in *Pseudomonas arugenosa*, the AHLS enzyme RhlI reacts with SAM and acyl-ACP1, undergoing lactonization and creating a lactone ring. The nitrogen group on the lactone

ring acylates the acyl group on the acyl-ACP1, to form the end product of holo-ACP, 5'-methyl-thioadenosine (MTA) after lactonization, and the AHL molecule used for quorum sensing [10]. Figure 1.4 is a representation of this mechanism with an inactive butyl (C4I) acyl group attached to ACP to form the C4-AHL molecule. An inactive acyl group is cargo loaded onto ACP for Nuclear Magnetic resonance (NMR) spectroscopy so that the protein and enzyme will bind, but a reaction does not occur. The interface data from NMR could be uses as a potential drug target to disrupt formation of the AHL autoinducer. Because ACPs have so many pivotal roles in living things, it is important to define only the interactions between the acyl-ACPs and their enzymes for bacterial growth and communication.

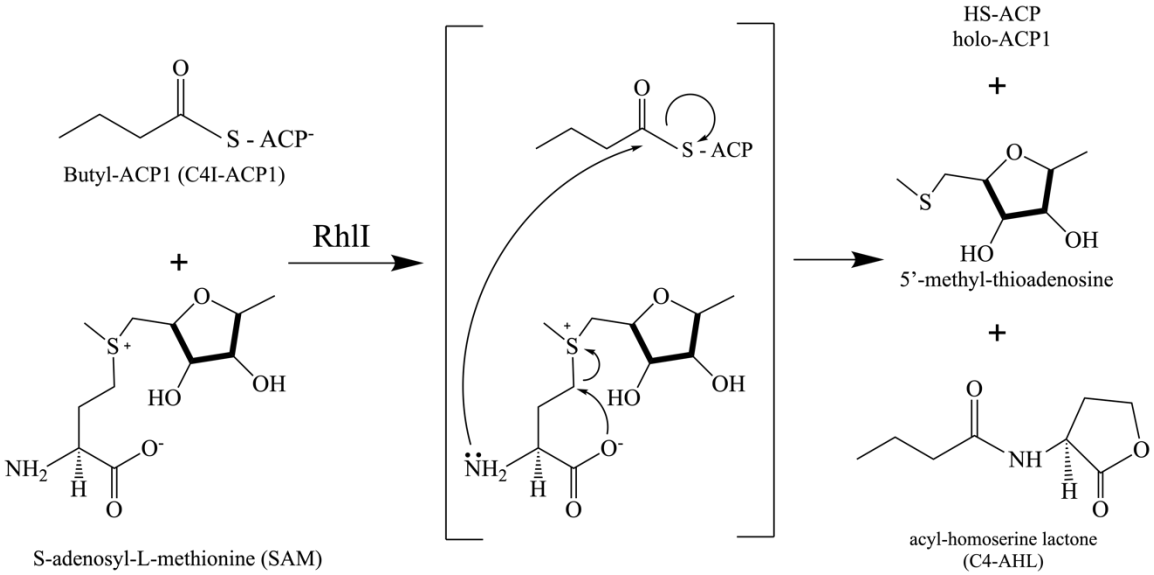

Figure 1.4 Mechanism for C4-AHL production.
S-adenosyl-L-methionine (SAM) undergoes lactonization creating the lactone ring for the AHL. The C4I-ACP1 is acylated and the acyl group is attached to the lactone ring by RhlI to form the acyl-homoserine lactone molecule [8, 10].

NMR In Determination of Protein-Protein Interfaces

NMR is an important tool to understand protein-protein interfaces. The amide backbone of the protein is a sensitive probe of structural changes in proteins. NMR spectroscopy measures the chemical shift of nuclei with the quantum mechanical property of spin (or gyromagnetic ratio; γ) by exciting the spins with radio frequency waves (ω). Briefly, a sample is placed inside of a magnet, where it is subjected to a static magnetic field (B_0 in Figure 1.5). An NMR sample has millions of molecules in it, so for simplicity, we refer to the NMR observed signal as resulting from the bulk magnetization vector. In the ground state in the magnet, the NMR active nuclei (or spins) align with the Z-axis. When perturbed from the Z-axis, the spins will precess in the X-Y plane. This principle of nuclear spin is also known as Lamar's Frequency (Equation 1.1). Over time, this precession of nuclei will relax back to the ground state, or aligned with the Z-axis.

$$\textbf{Equation 1.1} \quad \boldsymbol{\omega = \gamma \beta_0}$$
$$\boldsymbol{\omega} = \textbf{frequency} \quad \boldsymbol{\gamma} = \textbf{gyromagnetic ratio} \quad \boldsymbol{\beta_0} = \textbf{magnetic field}$$

The nuclear presession frequency (ω) is then measured by detecting the precession of the nuclei in the x-y plane. To get a typical 1D NMR spectrum (frequency vs. intensity), the resonance in the time domain is then transformed using the Fourier transformation equation (Equation 1.2, Figure 1.6) to the frequency domain and then normalized to the static magnetic field by dividing by the resonance frequency to yield the chemical shift in parts per million (ppm).

$$\textbf{Equation 1.2} \quad \boldsymbol{F(\omega) = \alpha \int_{-\infty}^{\infty} f(t) e^{-i2\pi\omega t} dt}$$
$$\boldsymbol{\omega} = \textbf{frequency} \quad \boldsymbol{\alpha} = \textbf{signal} \quad \boldsymbol{t} = \textbf{time}$$

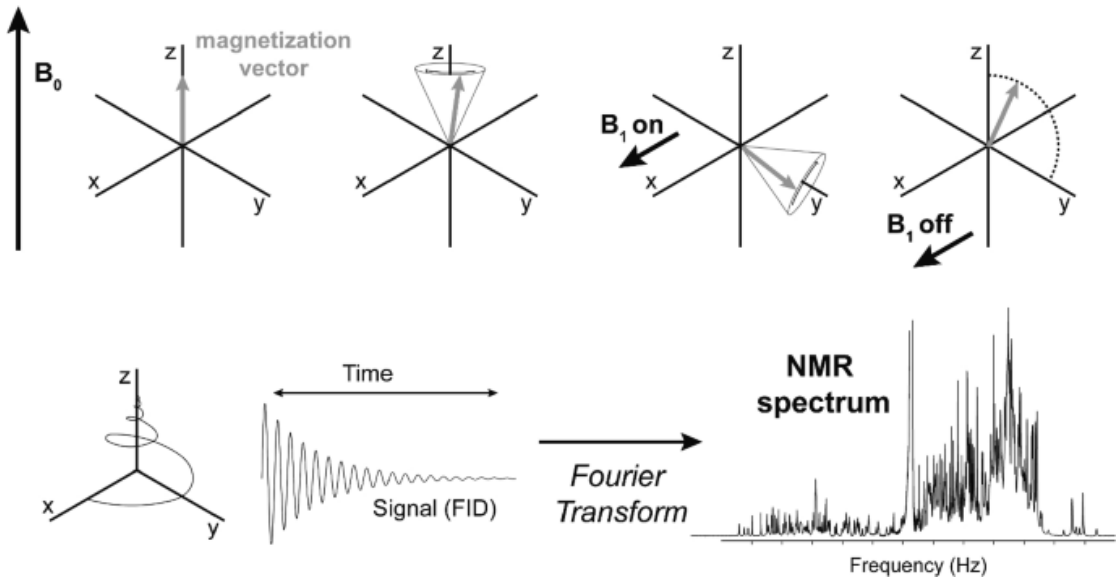

Figure 1.5 Theory of NMR spectroscopy for magnetization vector and Fourier transform.

Bulk magnetization vectors and nuclear presession frequency in the time domain transformed using the Fourier transformation [11].

A combination of ^{1}H, ^{13}C, and ^{15}N 1D spectra are then plotted in the X, Y, and Z planes to get a 2D and 3D NMR spectra.

Using NMR spectroscopy, structural changes in proteins can be monitored through changes in chemical shift perturbations in response to changes in the experimental conditions. The chemical shifts of the backbone amide ^{1}H and ^{15}N are sensitive to changes in the electromagnetic environment around the nuclei (Figure1.5 (a) & (b)) [11]. The chemical shift perturbation can be seen visually with NMR spectra by comparing overlapped spectra with assigned protein backbone peaks and identifying peak changes. An example of this can be seen in Figure 1.6, where the dashed rectangle represents the area of a peak shift (peak 4), in the proton and nitrogen planes. Overlapping peaks indicate little to no change in structure (peaks 1-3). For this information to be used for structural conformation, the peaks from the 2D NMR spectra

must be assigned using 3D NMR data Figure 1.6 (c). Spectra in a 3D plane is then used to identify amide backbones of a protein structure Figure 1.6 (a).

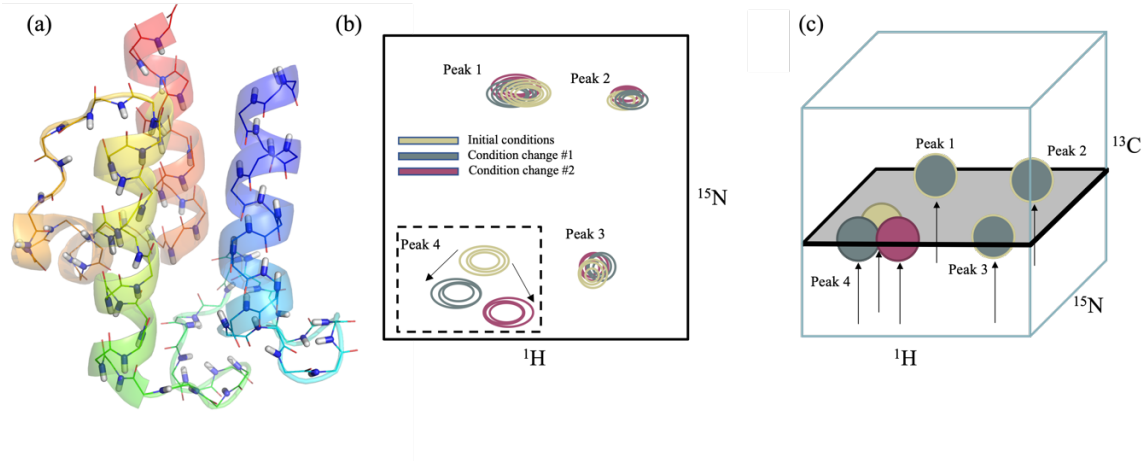

Figure 1.6 Protein NMR: 2D and 3D NMR spectra examples. Chemical shift perturbations can be used to determine conformational changes using **(a)** ribbon diagram of ACP1 with the amide atoms of the backbone shown in stick representation **(b)** 2D NMR spectrum and **(c)** 3D NMR. A visual shift can be seen in the hypothetical 2D spectra for peak 4 [12, 13].

An example of chemical shift perturbations being used for protein structure is from the Sztain et al. study, where they used chemical shifts to indicate structural changes of acyl-ACPp. ACPp is an ACP found in *E. coli* that also contains a phosphopantetheine linker. Stzain identified residues with chemical shift perturbations correlating to acyl groups with increasing carbon chain lengths. The study demonstrates how ACPp uses patterned structural changes to communicate with partner enzymes and allosteric regulation of chain flipping [14]. This study mirrors the identification of chemical shift perturbations for ACP1 and the protein-enzyme interactions in quorum sensing.

Chemical shift perturbation experiments are planned to study the ACP1-RhlI axis, however, first, the chemical shifts of the backbone amide ^{1}H, and ^{15}N shifts must be assigned to the atoms in the ACP1 protein. A combination of 1D, 2D, and 3D ^{1}H, ^{13}C,

and ^{15}N spectra are typically collected to assign the backbone of a protein smaller than 20 kDa (Table 1.1). For proteins larger than 20 kDa, side chain deuteration is often required and the backbone assignment spectra are different [12, 15].

Table 1.1 Collected NMR spectra names and provided information.
Spectra collected for protein backbone assignments and the information provided from each spectra [12].*'Root' resonances: Identification peaks for residues

Spectra Name	Information provided
^{15}N-HSQC	Backbone H-N resonances that will be used as 'root' resonances or the identification peaks for individual residues
CBCAcoNH	Backbone Cβ and Cα resonances of the *i*-1 residue and H-N resonances of the *i* residue
HNCACB	Backbone Cβ and Cα resonances and H-N resonances of the *i* and *i*-1 residues
HNCO	Backbone C=O resonance of the *i*-1 residue and H-N resonances of the *i* residue

The ^{1}H, ^{15}N-HSQC spectrum is collected by exciting the ^{1}H protons and transferring the magnetization from ^{1}H to the covalently attached ^{15}N nuclei via J-coupling. The ^{15}N chemical shift is evolved on the ^{15}N and transferred back to the ^{1}H for detection. The HNCACB experiment starts with magnetization on the ^{1}H nucleus, which is then transferred to ^{15}NH via 1H-15N coupling, then on to the $^{13}C\beta$ and $^{13}C\alpha$, where the chemical shift is evolved. From here it is transferred first to ^{15}NH with chemical shift evolution and then to ^{1}HN for detection. The J-coupling between the ^{15}N and $^{13}C\alpha$ on *i* and *i*-1 residues is similar and therefore magnetization is transferred to ^{15}N on the *i*

residue from both ^{13}Cα's on the *i* and *i*-1 residues [12]. Because of this transfer, each NH group has two Cα and Cβ peaks visible, for the *i* and *i*-1 peaks. To identify which peaks are the *i*-1 peaks, the CBCAcoNH spectrum is used. This spectrum transfers magnetization from ^{1}H to the ^{13}Cβ on the *i*-1 residue, and then to ^{13}Cα like the HNCACB. However, it is then transferred to the ^{13}CO, then to ^{15}NH and then to ^{1}HN on the *i* residue for detection. This shows only the *i*-1 peaks, which overlap with the HNCACB's *i*-1 peaks and distinguishing between the *i* and *i*-1 peaks. Because protein backbones assemble in the *i* and *i*-1 format, the protein can be reconstructed in a 3D space. The HNCO spectrum can be used to identify the structure of the protein correlating the amide ^{1}H and ^{15}N shifts of the *i* residue with the ^{13}C shift of *i*-1 residue [12, 16] (Figure 1.7).

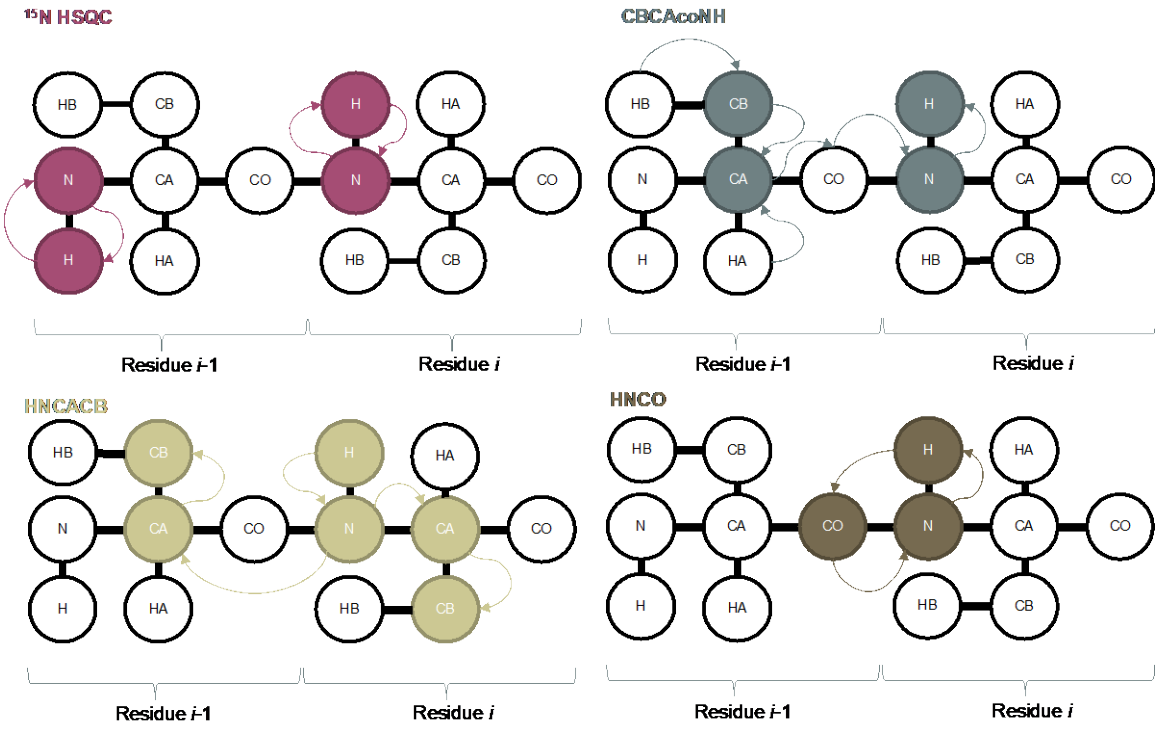

Figure 1.7 Visualization of NMR spin systems.
Protein backbone assignment requires each NMR spectra to connect the *i*-1 and *i* residue as formatted. ^{15}N HSQC, CBCAcoNH, HNCACB, and HNCO spectra were collected to identify chemical shift perturbations [12, 13, 17].

Thesis Goal

(**AIM 1**) Backbone NMR assignments of apo-ACP1 and C4I-ACP1

Approach Aim 1: Use NMR chemical shift perturbations to understand the structural changes of apo-ACP1 and ACP1 when native (C4I) cargo is loaded.

(**AIM 2**) Optimization of protein expression and purification of proteins required for ACP conversion and cargo loading.

Approach Aim 2: Identify optimal conditions for protein expression and purification required for ACP conversion and cargo loading

Ultimately, the results from this research will be used to map the interaction of C4I-ACP1 and the AHLS enzyme, RhlI, from *P. aeruginosa* (ACP1). By understanding the selective interaction that maintains fidelity in the synthesis of the quorum molecule, AHL, inhibitors can be designed to target the ACP-AHLS interface to decrease bacteria population growth and reduce antibiotic resistance as a whole Figure 1.8).

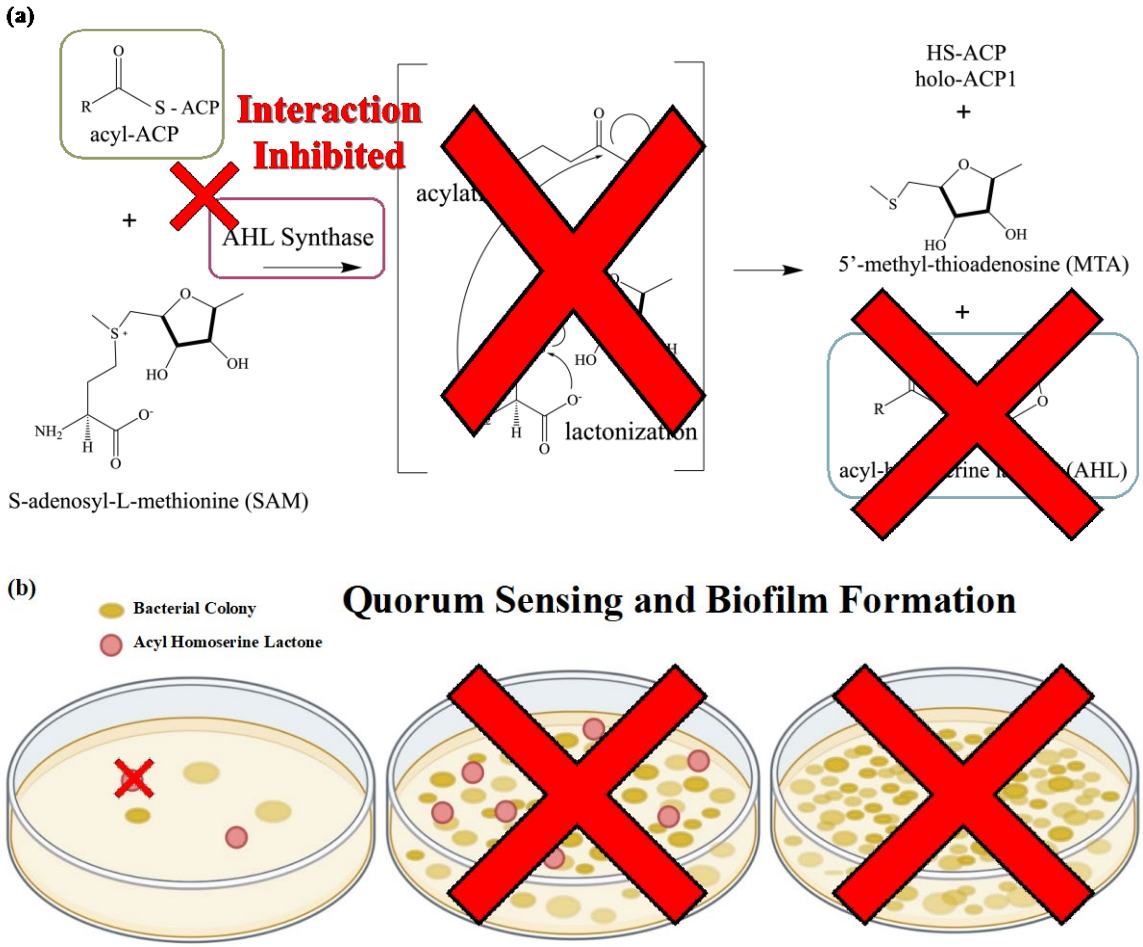

Figure 1.8 Visualization of thesis goal.
The overarching goal of this thesis is to define the interaction between acyl-ACP and AHLS so that the specific interaction can be **(a)** inhibited, therefore inhibit the AHL molecule from being produced, and ultimately **(b)** stopping the formation of biofilms and antibiotic resistance for increasing [8]. [created with BioRender.com].

CHAPTER TWO: APO-ACP1 PROTEIN BACKBONE ASSIGNMENTS

Introduction

Protein backbone assignments for protein can be identified using NMR spectra. Apo-ACP1 was expressed with isotopic enrichment with ^{13}C, ^{15}N, purified, and confirmed that it was the apo form of the protein prior to ^{13}C, ^{15}N backbone chemical shift assignments. This chapter discusses the production of ^{13}C, ^{15}N ACP1, the conversion to apo-ACP1, and the NMR data collection and analysis for apo-ACP1.

Materials and Methods

Expression and Purification of ^{13}C, ^{15}N ACP1

Expression and purification of isotope enriched proteins for NMR studies in an *Escherichia coli* platform requires growth of the bacteria and expression in a defined medium. M9 medium is a salt based medium derived from the laboratory manual provided by Miller [18]. The medium is used to isotopically enrich atoms in proteins such as ^{2}H, ^{13}C, and ^{15}N by preparing the medium with isotopes as the sole source. In this study, enriched medium uses ^{13}C-glucose and/or ^{15}N-ammonium chloride as a sole source of carbon and nitrogen to isotopically enrich the ACP1 proteins. Isotopic enrichment is necessary for NMR studies because the nuclear spins of ^{12}C and ^{14}N are not as magnetically active, and signals are not strong enough for the NMR instrument [15].

E. coli BL21 (DE3) cells were transformed with pD441-NH plasmid encoding the ACP1 protein from *P. aeruginosa* with a His_6 tag. The transformed cells were plated on Luria-Bertani (LB)-agar with 1mM kanamycin for selection. Several colonies were used

to inoculate 5 mL of LB supplemented with 1mM kanamycin and grown overnight at 37 °C, shaking at 250 rpm. Cells were separated from the LB by centrifugation for 5 mins at 4,000×g and used to inoculate isotopically enriched ^{13}C, ^{15}N M9 minimal media broth (2.0 g/L ^{13}C-glucose, 0.5 g/L ^{15}N-ammonium chloride, 0.5 g/L ^{13}C, ^{15}N-isogro, 1 mM magnesium sulfate, 0.3 mM calcium chloride, 1 mM biotin, 1 mM thiamin, 10 mL 100×trace element, 100 mL 10×M9 salt, 1 mM kanamycin). The 1 L culture was grown at 37 °C shaking at 250 rpm until reaching an optical density at 600nm (OD_{600}) = 0.6-0.8. A pre-induced sample with the same OD_{600} was collected for SDS-PAGE analysis. The remaining culture was induced with 1 mM isopropyl ß-D-1-thiogalactopyranoside (IPTG) and incubated overnight (~16 hrs) at 37 °C, 250 rpm. A 1 mL induced sample was collected for SDS-PAGE analysis. The remaining induced cells were harvested by centrifugation, and frozen for at least 30 min prior to lysing. The harvested pellets were lysed using the bacterial protein extraction reagent (B-PER) complete, 1 mM lysozyme, 1 mM DNase and ½ tablet Pierce™ protease inhibitor. The lysed cells were clarified by centrifugation and filtered with a 0.45 μm polyethersulfone syringe filter prior to application on the immobilized nickel affinity column (HisTrap™ HP 1 mL column) using an ÄKTA Start instrument (Cytiva) and imidazole. The HisTrap™ HP was washed with 10 column volumes (CV) of I20 buffer (20 mM imidazole, 20 mM Tris HCl, 200 mM NaCl, 10% glycerol, pH 7.9), loaded with the clarified lysate, and eluted with 10 CV of I200 buffer (200 mM imidazole, 20 mM Tris HCl, 200 mM NaCl, 10% glycerol, pH 7.9). Fractions containing purified protein were identified using 16% Tris-Tricine polyacrylamide gel electrophoresis (PAGE) and peak identification from the chromatogram, pooled, concentrated using a 3,000 molecular weight cut-off (MWCO) centrifugal concentrator

(Sartorius), and exchanged into a Tris protein storage buffer (50 mM Tris-Cl pH 7.5, 150 mM NaCl, 0.1 mM tris(2-carboxyethyl)phosphine (TCEP) and 0.1 mM ethylenediaminetetraacetic acid (EDTA)). Concentrated samples were further purified using size exclusion chromatography (SEC) on a HiLoad™ Superdex™ 75 pg (Cytiva) (Figure 2.1). Fractions containing purified protein were again identified using 16% Tris-Tricine-PAGE, pooled, and concentrated using a 3,000 MWCO centrifugal concentrator (Sartorius). Aliquots were stored in a 4°C before enzymatic conversion to apo-ACP1.

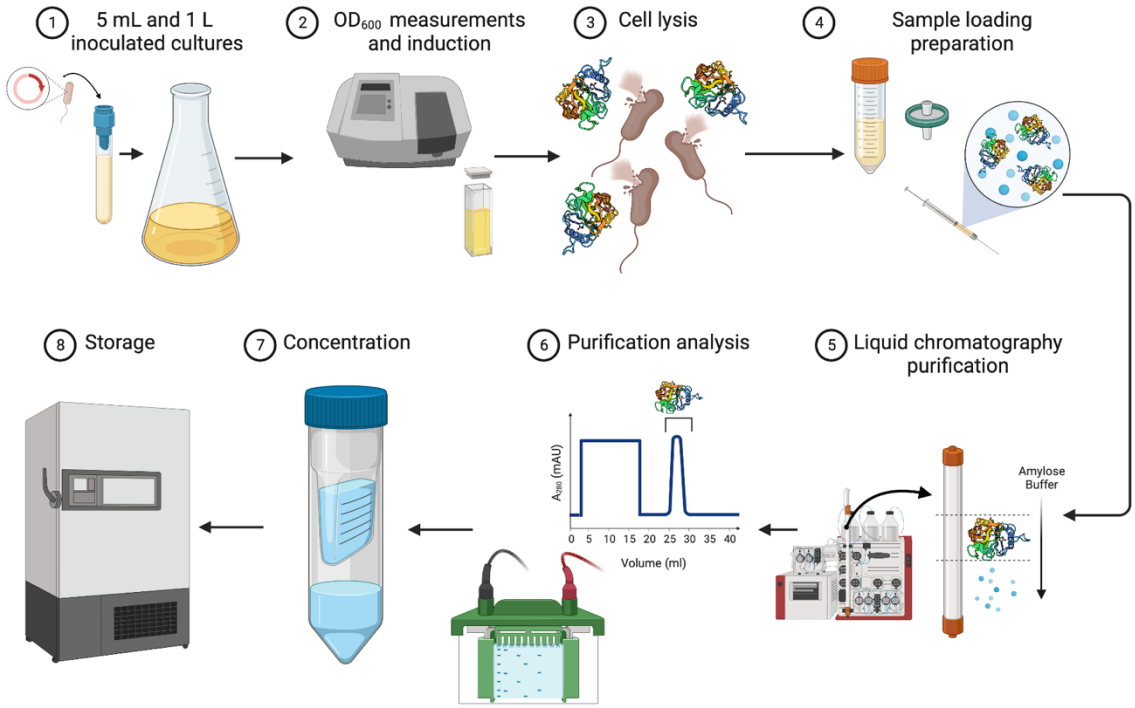

Figure 2.1 Protein expression and purification for labeled ACP1.
1) Plasmid encoding ACP1 was transformed, inoculated into LB culture and transferred to ^{13}C, ^{15}N isotopically enriched M9 minimal media until 2) the culture reached an OD_{600} between 0.6-0.8 and was induced. 3) Cells are then lysed and 4) clarified prior to 5) affinity chromatography purification. 6) Protein is then analyzed before 7) being further purified using size exclusion chromatography (SEC) and 8) NMR data collection. [Adapted from "Protein Overexpression and Purification from Bacteria", by BioRender.com (2020). Retrieved from https://app.biorender.com/biorender-templates].

Holo- and Apo-ACP Conversion and Purification of apo-ACP1

Expression of ACPs in *E. coli* produces a mixture of apo-ACP and holo-ACP naturally. Purified ACP samples were converted to apo-ACP using the enzyme acyl carrier protein phosphodiesterase (AcpH). First, the ratio of apo:holo was determined using ultra high-performance liquid chromatography (UHPLC) prior to incubation with AcpH. A 50 µL sample of the ACP1 was filtered using costar 0.22 µm centrifuge tubes and centrifuged for 1 min at 5,000×g. The collected flowthrough was then diluted with 70 µL Nanopure water (120 µL total). The diluted sample was then injected in a HyprSil gold 2.1/100 mm, 1.9 µm particle size column, washing with an increasing gradient of acetonitrile from 25% to 75%. The UV spectrum was observed at 220 nm, 280 nm, and 340 nm. The area under the 220 UV peaks was then used to calculate the percentage of holo- and apo-ACP. The remaining holo- and apo-ACP mixture was converted to apo-ACP using the AcpH enzyme in a reaction buffer consisting of 1M NaCl, 150 mM $MgCl_2$, 10 mM $MnCl_2$, 500 mM Tris at pH 8. AcpH was then added to the reaction mixture (3.2 µM final) and incubated at 37 °C overnight. The final apo-ACP1 solution was purified again with SEC on a HiLoad™ Superdex™ 75 pg (Cytiva) in ACP NMR buffer (40 mM PO_4 and 1 mM EDTA at pH 6.5) on an ÄKTA Pure fast protein liquid chromatography (FPLC) instrument. The reaction product was checked again using the area under the 220 nm UV chromatography from the UHPLC (50 µL of the reaction sample is filtered using costar 0.22 µm centrifugal filters. The collected flowthrough was then diluted with 70 µL nanopure MilliQ water; 120 µL total). The mixture should be at least 90% apo-ACP and 10% holo-ACP before data collection or cargo loading. Once confirmed, the appropriate fractionated samples from the SEC purification were pooled

based on the UV peaks from chromatogram and 16% Tris-Tricine PAGE. The pooled fractions are then concentrated using 6 mL sartorius Vivapin centrifuge tubes with a membrane containing a 3,000 MWCO. The samples are centrifuged at 4,000×g until concentration is at least 300 µL and 300 µM. The concentration for all samples were calculated with a Thermo Scientific NanoDrop One, using the protein analysis A280 program. Apo-ACP1 construct with a His_6 tag had an extinction coefficient of 1.49 Ɛ/1000 and molecular weight of 10.03 kDa [5]. Concentrated samples were either prepared for NMR or used for cargo loading.

NMR Methodology

The ^{13}C, ^{15}N apo-ACP1 protein was analyzed using NMR. The final apo-ACP1 NMR sample was 0.94 mM. 1.25 mM deuterated dithiothreitol (d-DTT) in deuterated water (D_2O), 25 µM TSP in D_2O, and 0.1× Halt protease inhibitor cocktail were added to the sample, which was then placed in a 5 mm Shigemi NMR tube.

NMR data was obtained on a Bruker AVANCE III 600 MHz spectrometer equipped with a cryogenically cooled TCI cryoprobe. 1D ^{1}H, 2D ^{1}H, ^{15}N HSQC, and 3D HNCO, HNCA, HNCACB, and HNcoCACB NMR spectra were collected, processed with NMRPipe and analyzed with the CCPN Analysis 2.0 on NMRBox [19, 20, 21]. For reproducibility, the parameters for each of the spectra are included below in APPENDIX B: NMR Parameters.

Results and Discussion

Expression and purification of ^{13}C, ^{15}N ACP1 results

^{13}C, ^{15}N ACP1 was produced with a concentration of 67 µM prior to enzymatic conversation. Expression and purification used isotopically enriched ^{13}C**,** ^{15}N M9

minimal media for bacterial growth and expression for the carbon and nitrogen atoms to have a nuclear spin visible by the NMR instrument. Nickel affinity chromatography was used because of the His_6 tag attached to the ATUM pD441-NH plasmid encoding the ACP1 protein from *P. aeruginosa*. The chromatogram of from the affinity chromatography (Figure 2.2 (a)) shows the loading of clarified sample at the 20 mL mark, after equilibration. The large block like peak of sample loading comes from protein saturation, where the UV detector cannot differentiate proteins, and are in the flowthrough fraction of the gel image. These proteins are not the protein of interest and do not bind to the column. The next peak at 64 mL suggests ACP1 eluted off of the column in fraction 3, and is confirmed in 16% Tris Tricine PAGE (Figure 2.2 (b)). The molecular weight of ACP1 is ~10 kDa, and the strongest band at fraction 3 corresponds to the chromatogram and the size of ACP1. The flow through and wash wells show some purification did occur, and product was not lost in the loading and wash steps of the liquid chromatography. However, based on the impurities still seen in the fractions, a second round of purification with SEC was necessary for the most potent fractions, fractions 3-4. The ladder used for ACP1 was a low range PAGE ruler because of the small size of ACP1. The pre-induced and induced samples were used to as a control, displaying the expression of protein pre- and post-induction with IPTG.

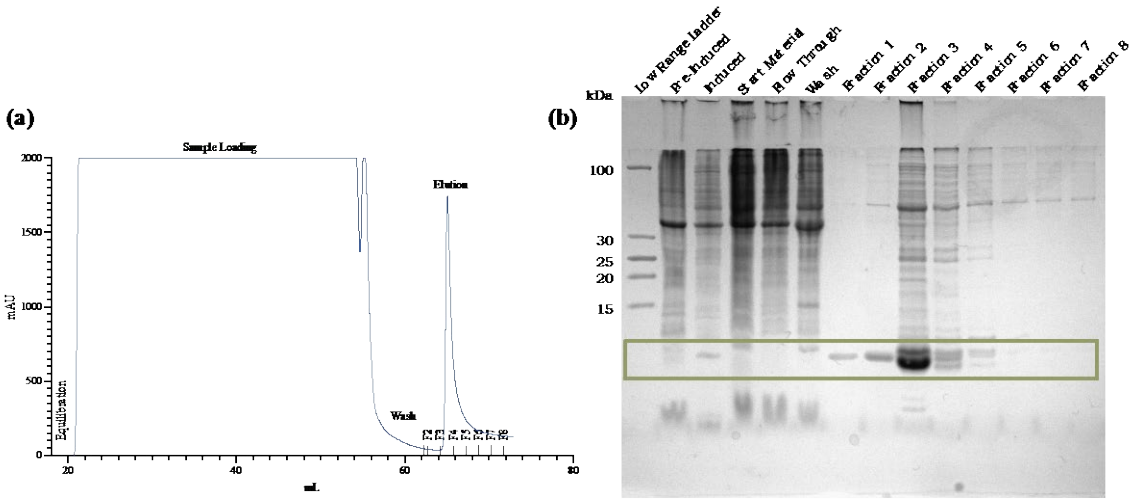

Figure 2.2 ^{13}C, ^{15}N ACP1 affinity chromatography purification.
An example ÄKTA Start Nickel Column (HisTrap™) Chromatography **(a)** chromatogram and corresponding **(b)** 16% Tris Tricine Gel for ^{13}C, ^{15}N ACP1. ACP1 is ~10 kDa and can be found mostly in fractions 3 and 4 from the chromograph and gel image.

SEC was used to purify ^{13}C, ^{15}N ACP1 from impurities and showed potential dimerization. The SEC chromatogram (Figure 2.3 (a)) was collected with two UV measurements, 280 nm (blue) and 220 nm (red). Even though most proteins are seen in 280 nm range, ACP1 has better peak definition at 220 nm because it has fewer aromatic groups, with only one tyrosine (80Tyr) and no tryptophan and phenylalanine residues in its sequence [22].

The first and largest peak are larger impurities which corresponds to fraction A8 in the 16% Tris Tricine PAGE (Figure 2.3 (b)). The last, peak near 120 mL is known as the void, and is the imidazole buffer molecules eluting from the column.

ACP1 was observed in multiple fractions between B4-C6, within two dominate peaks with fractions B6-C6. SEC elutes larger molecules first because smaller molecules are retained longer in the small crevasses and pores on the resin beads of the column. The presence of ACP1 in multiple peaks suggests intermolecular dimers, which could be

formed by disulfide bridges from the sulfur atoms between cystine (21Cys) residues, or between the exposed sulfur of the holo-ACP1 phosphopantetheine linker [23].

The 16% Tris Tricine PAGE in Figure 2.3 (b) confirms the protein presence in fractions B4-C6 with strong bands near ~10 kDa. Though there were still some impurities in the protein, the protein was clean enough to be treated with AcpH for apo-ACP1 conversion. Dimerization bands are not seen in the gel because the gel sample buffer contains the reducing agent 2-Mercaptoethanol (BME). Fractions B4-C6 were collected and converted to apo-ACP1 (Figure 2.9) prior to SEC (Figure 2.10) and NMR data collection.

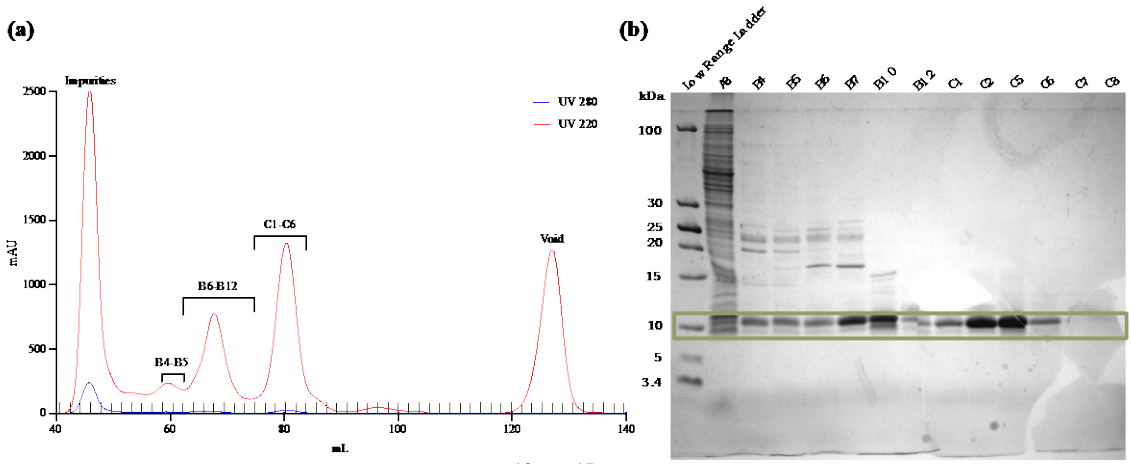

Figure 2.3 SEC ^{13}C, ^{15}N ACP1 purification.
ÄKTA Pure 25 SEC with UV detection at 280 nm (blue) and 220 nm (red) show isolated ^{13}C, ^{15}N ACP1 in holo- and apo- form. In the (a) SEC chromatogram and (b) 16% Tris-Tricine PAGE, ACP can be in wells B4-C6 in a 96-well block.

ACP1 chromograms show possible dimerization

ACP1 has the ability to dimerize because of the sulfur atoms, from either the cystine (21Cys) residues or the phosphopantetheine linker which can form disulfide bonds [23]. Possible dimerization peaks were first noticed in 220 nm chromatograms from SEC with multiple peaks with ^{13}C, ^{15}N ACP1 (Figure 2.4 (a)). The chromatogram

shows the protein eluting at 64 mL and 76 mL. The peaks were pooled as peak 1 (B6-B12) and peak 2 (C1-C6) for experimentation with BME. BME is a reducing agent for disulfide bonds, and disrupts the ACP1 dimerization [24]. 16% Tris Tricine PAGE (Figure 2.4 (b)), shows with a low range PAGE ruler to see the small size differences in ACP1. The first sample well is a sample from peak 1 without BME (-BME), and the second well is the same sample with BME (+ BME). Wells 3 and 4 are the same with samples from peak 2. The 16% Tris Tricine PAGE indicates that the peak 1 contains mostly dimers, with a weak band at ~10 kDa for ACP1 alone and stronger band appearing at ~20 kDa (double ACP1). This is confirmed with a strong, singular band at ~10 kDa with the addition of BME. Peak 2 is assumed to be a monomer because the strongest bands appear at the ~10 kDa mark with and without BME. A faint band does appear at ~20 kDa -BME Peak 2, but this could be from peak overlap in the B11 fraction from the 96-well block. The elution of the peaks also correlated to SEC, where the larger dimer peak elutes before the smaller monomer peak.

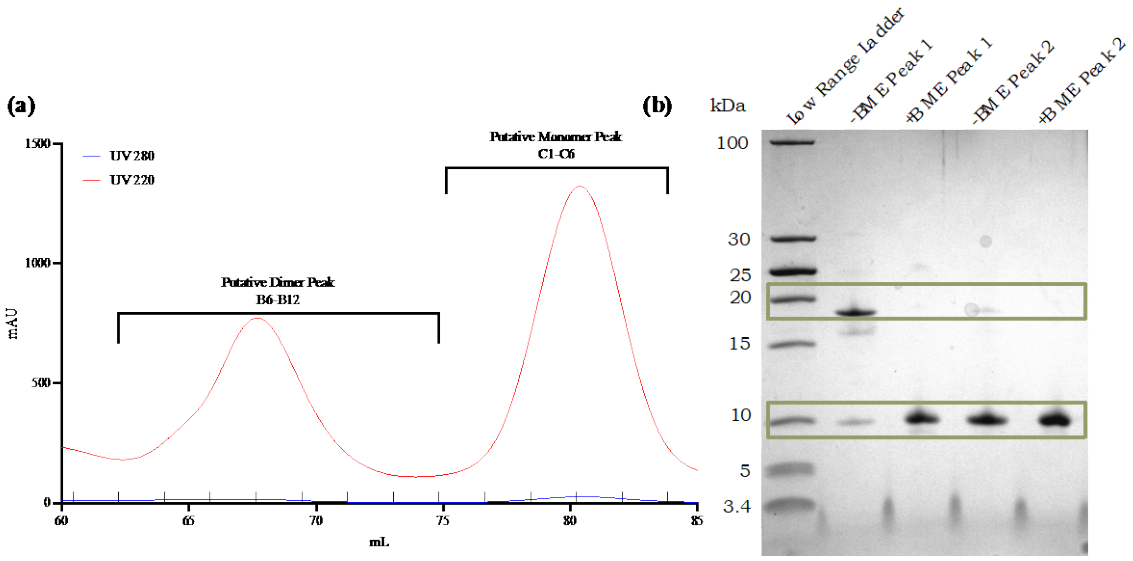

Figure 2.4 Dimerization and Disulfide Reduction of ACP1 of SEC peaks. ÄKTA Pure 25 SEC **(a)** chromatogram with UV detection at 280 nm (blue) and 220 nm (red) show isolated ACP1 with peak multiplicity. **(b)** 16% Tris-Tricine PAGE of peaks 1 and 2 from the SEC chromatogram with and without the reducing agent BME.

Additional experiments were conducted on the ACP1 using the UHPLC and DTT. DTT is a reducing agent known to reduce dimers into monomers [25]. Unlabeled ACP1 was injected in a HyprSil gold 2.1/100 mm, 1.9 µm particle size column, washing with an increasing gradient of acetonitrile from 25% to 75%. The UV spectrum was observed at 220 nm, 280 nm, and 340 nm. The resulting chromatograms (220 nm) for untreated (without DTT) ACP1 (black) and DTT treated ACP1 (blue) are seen in Figure 2.5. The untreated ACP1 chromatogram shows two peaks, or a monomer and a dimer peak, while the DTT treated ACP1 chromatogram shows only one peak, a reduced monomer peak.

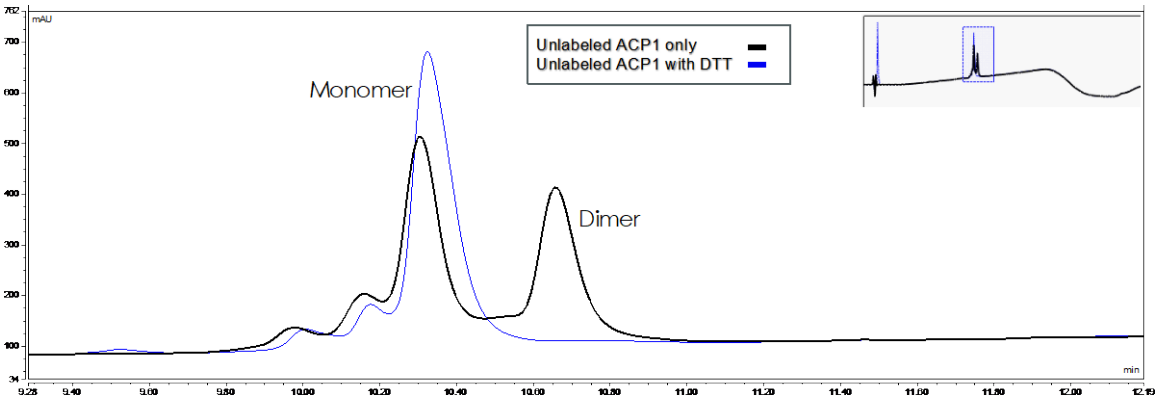

Figure 2.5 Dimerization of UHPLC chromatogram peaks.
Chromatograms for untreated ACP1 UHPLC chromatogram (black) compared to DTT treated ACP1 UHPLC chromatogram (blue) measured at 220 nm.

Possible locations in the ACP1 sequence where dimerization can occur

The two possible locations (21Cys and the phosphopantetheine linker) for dimer formation required additional experimentation to confirm the form of the ACP1 (Figure 2.6).

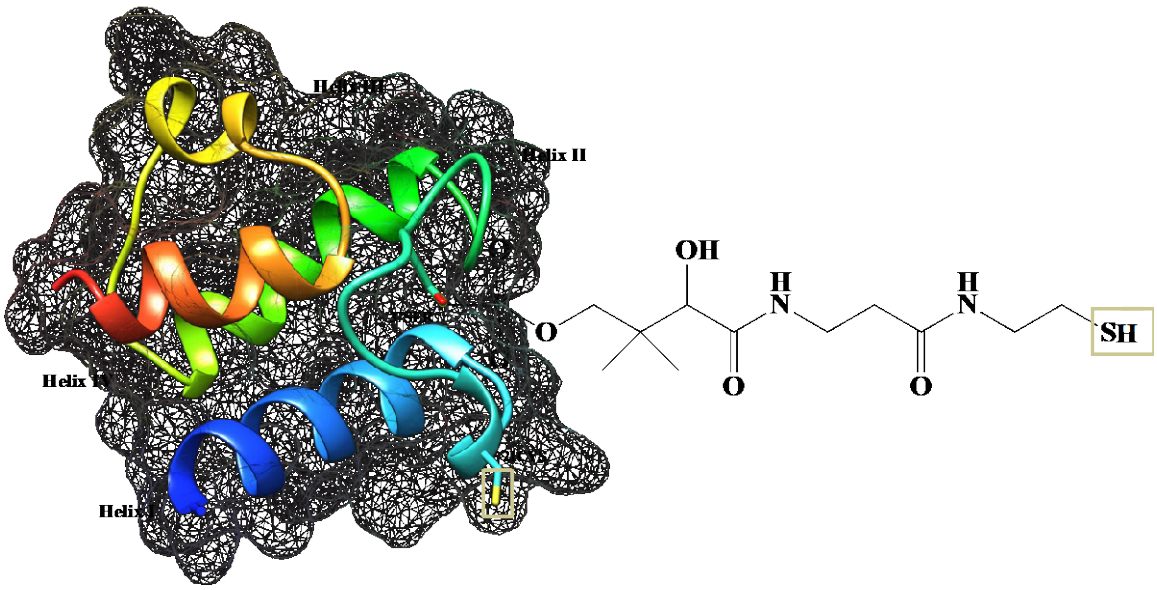

Figure 2.6 Possible dimerization locations on APC1.
The disulfide bridge formed in dimers could occur at 21Cys or at the sulfur atom on the phosphopantetheine linker at 37Ser (yellow boxes) on ACP1.

If ACP1 is in apo- form, then a disulfide bond could not form on the phosphopantetheine linker because apo-ACP1 does not have this linker. To confirm the final form of ACP1, the enzymes AcpH and Sfp were used for conversion.

AcpH is the enzyme used to convert holo-ACP to apo-ACP by removing the phosphopantetheine for the protein. *Bacillus subtilis* produces an enzyme called Sfp, which is used for cargo loading acyl groups onto apo-ACP [8]. Sfp can also be used in the conversion for apo-ACP to holo-ACP, catalyzing the transfer of the phosphopantetheine linker [26]. Form conformation studies used the Sfp reaction to convert apo-ACP1 into holo-ACP1 and the reserve reaction to convert holo-ACP1 to apo-ACP1 using the enzyme AcpH (Figure 2.7).

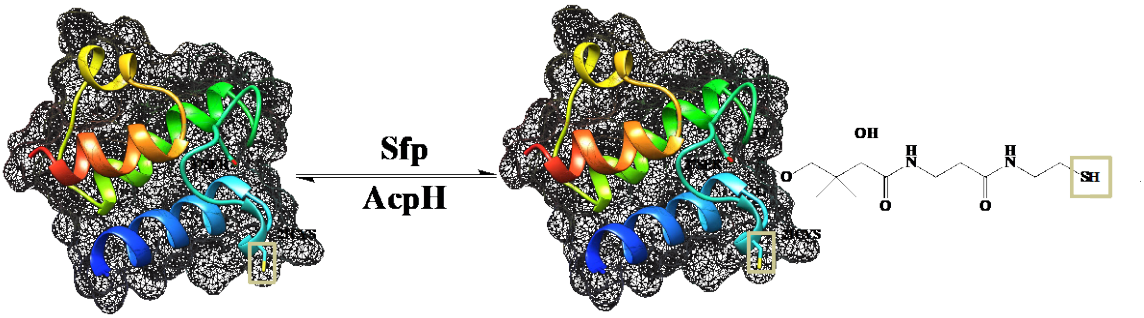

Figure 2.7 Holo- and apo- conversion of ACP1 with AcpH and Sfp.
The addition of the phosphopantetheine linker to apo-ACP1 to make holo-ACP1 and the reverse reaction with AcpH and the removal of the phosphopantetheine linker.

A UHPLC chromatogram shows a peak appears around the 10 min 10 sec mark for untreated (no Sfp) holo-/apo-ACP1(blue) and shifts to 9 min 20 sec mark for holo-ACP1 (black) (Figure 2.8). Sfp (maroon) and CoA (pink) only chromatograms are used as a baseline control to show peaks are not enzymes. These results are as expected with apo-ACP1 being less polar than holo-ACP1.

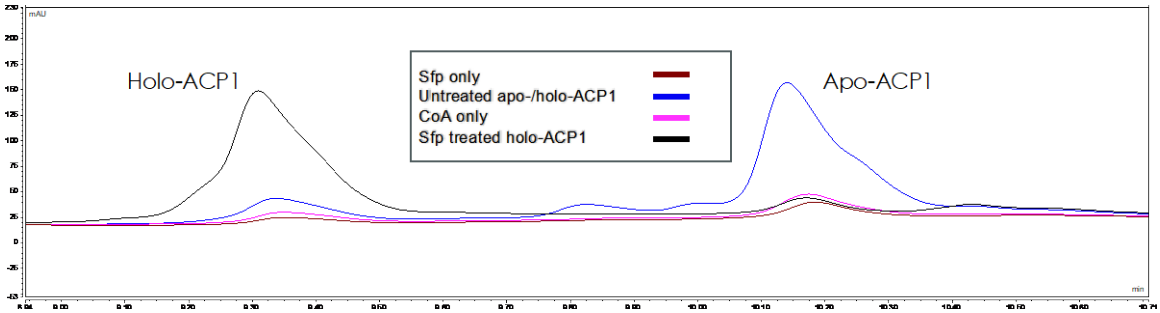

Figure 2.8 UHPLC control of holo-/apo-ACP1 conversion to holo-ACP1 chromatographs.
An untreated holo-/apo-ACP1 (without Sfp) UHPLC chromatogram (blue) compared to Sfp treated holo-ACP1 UHPLC chromatogram (black). Sfp (maroon) and CoA (pink) only chromatograms are used as a baseline control for peaks.

Holo- and Apo-ACP1 conversion and purification of ACP1

Results for the ^{13}C, ^{15}N ACP1 reaction with AcpH contained unstable baselines, and the described methodology to calculate the area under the curve could not be completed for apo:holo ratios. Only the tops of the chromatogram peaks were identifiable, and the instability affected the area under the peaks. The mixture of holo-/apo-ACP1 was still treated with AcpH and purified (Figure 2.9) prior to UHPLC data collection. Because the tops of the peaks were still identifiable, the results show a retention time shift from 9 min and 35 sec to 10 mins. This shift was expected because a reverse phase column with non-polar resin was used for UHPLC. Even though apo-ACP1 is smaller in size, it is also less polar than holo-ACP1, and has a stronger attraction to the non-polar resin and eluting later from the column [27]. With the conversion results, it can be concluded that the dimerization of ACP1 is at least occurring on the 21Cys sulfur atom because ACP1 is in apo- form, and does not have a phosphopantetheine linker. While dimerization could still be occurring on the sulfur atom of the phosphopantetheine linker if the protein in holo- form, dimerization is still occurring on the 21Cys residue. To prevent dimerization, APC1 should include a reducing agent for analysis.

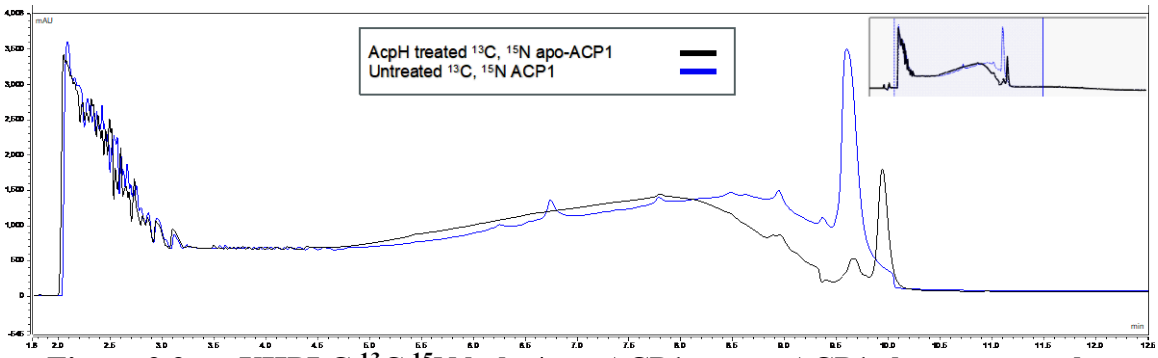

Figure 2.9 UHPLC $^{13}C,^{15}N$ holo-/apo-ACP1 to apo-ACP1 chromatographs. Untreated $^{13}C,^{15}N$ holo-/apo-ACP1 UHPLC chromatogram (blue) compared to a AcpH treated $^{13}C,^{15}N$ apo-ACP1 UHPLC chromatogram (black). Peak retention appears at the 9 mins 45 secs for $^{13}C,^{15}N$ holo-/apo-ACP1 and the 10 mins for $^{13}C,^{15}N$ apo-ACP1, indicating a completed conversion to apo-ACP1.

The purified ^{13}C, ^{15}N apo-ACP1 for SEC can be seen in the chromatogram (Figure 2.10 (a)), and in the 16% Tris Tricine PAGE (Figure 2.10 (b)) in fractions B2-C3. The chromatogram shows the greatest detection at 220 nm (red) with multiple UV peaks. The 16% Tris Tricine PAGE (Figure 2.10 (b)) shows isolated ACP1 with the exception of fraction B5, where is a weaker band at ~17 kDa. This band could be a dimer peak, but further experimentation was not conducted. The final product of apo-ACP1 was prepared for NMR data collection with the reducing agent DTT.

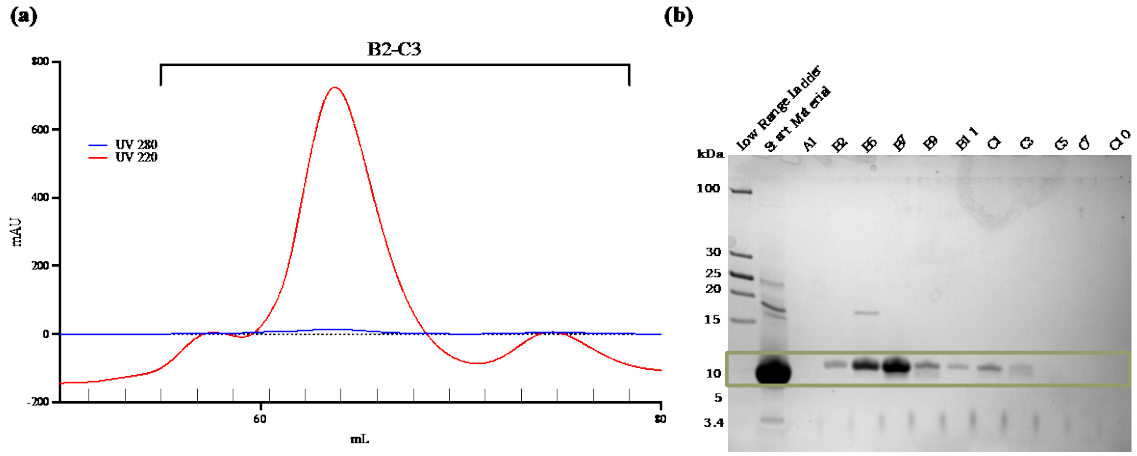

Figure 2.10 Example SEC ^{13}C, ^{15}N apo-ACP1 purification.
ÄKTA Pure 25 SEC with UV detection at 280 nm (blue) and 220 nm (red) show isolated ^{13}C, ^{15}N ACP1. In the **(a)** chromatogram and **(b)** 16% Tris-Tricine PAGEs, ACP can be in wells B2 - C3 in a 96-well block. These fractions pooled and stored for future use.

DTT studies were conducted using SEC on AcpH treated, apo-ACP1 and untreated (without AcpH) ACP1. There are dimer peaks in the 220 nm chromatogram eluting at 68 mL and 80 mL peaks in the untreated ACP1 (green) (Figure 2.11). The apo-ACP1 that was treated with AcpH and DTT (purple) only shows one peak reduced peak eluting at 64 mL. This confirms the form of apo-ACP1 that was used for NMR data collection and where the dimerization is occurring.

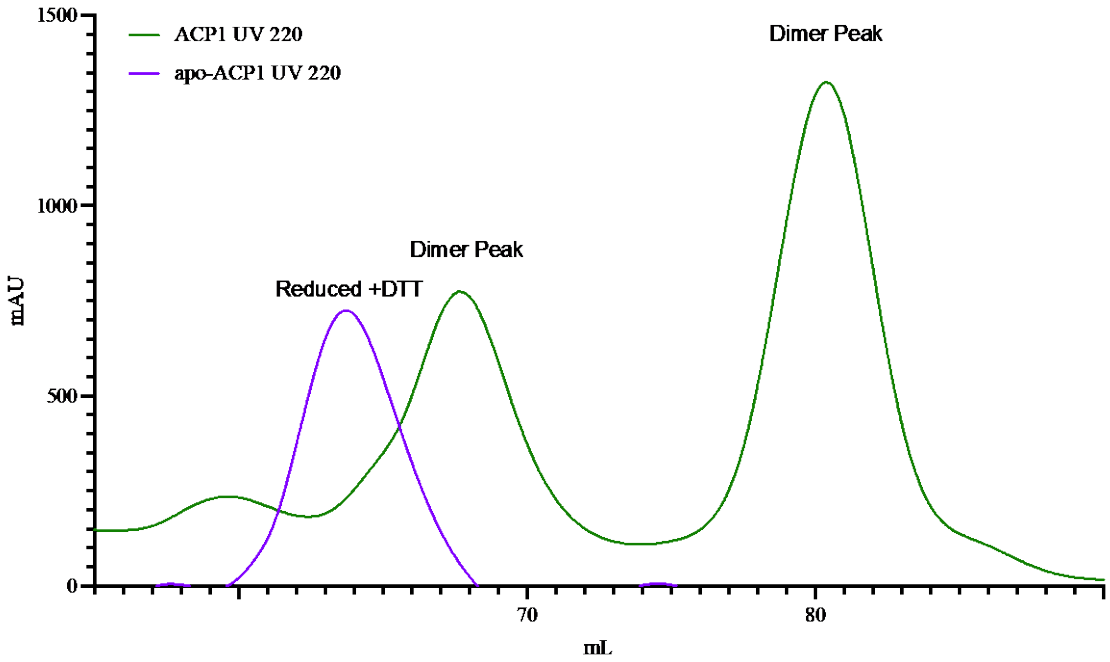

Figure 2.11 SEC peak multiplicity example.
ÄKTA Pure 25 SEC with UV detection at 280 nm (solid) and 220 nm (dashed) show untreated ^{13}C, ^{15}N ACP1 (green) prior to the AcpH reaction and AcpH treated ^{15}N apo-ACP1 (purple).

NMR chemical shift perturbations of apo-ACP1

The ^{1}H, ^{15}N HSQC NMR spectrum is the root spectrum from which the 3D spectra are mapped to assign backbone chemical shifts of a protein through peak picking, carbon linkages, amino acid linkages and finally assigning residues to spin systems. A spin system is defined as the ^{1}H, ^{15}N, $^{13}C\alpha$ and $^{13}C\beta$ chemical shifts for the *i* peaks of a protein. By determining the spin system types and linking them together with the *i* and the *i*-1 peaks from the HNCACB and CBCAcoNH, resonance assignments can be made by matching these connections into the protein sequence [12].

The spectra were processed with NMRPipe and analyzed with the CCPN Analysis 2.0 on the virtual server NMRBox [19, 20, 21]. Backbone assignments began with ^{1}H,

^{15}N-HSQC peak picking (which identifies the ^{1}H (y-axis) and ^{15}N (x-axis) of the 2D spectrum (Figure 2.12).

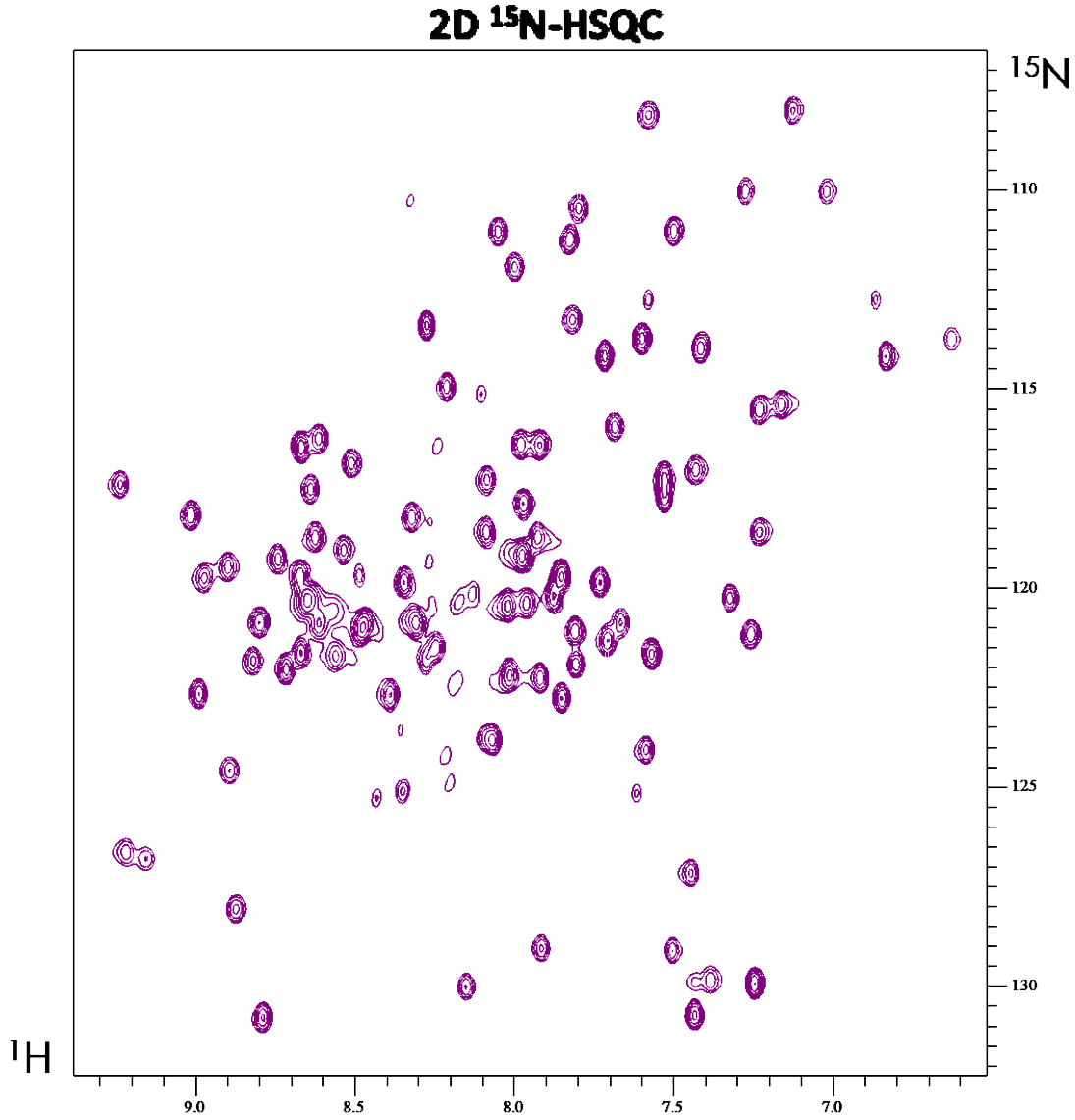

Figure 2.12 ^{1}H, ^{15}N HSQC spectrum of apo-ACP1.
^{15}N-HSQC spectra was processed through NMRPipe and analyzed with CCPN Analysis 2.0 on NMRBox [19, 20, 21].

The number of peaks in the HSQC spectrum, 111 peaks, were cross referenced with the number of residues provided from the sequence and Equation 2.1. The calculated number of peaks should be 100, leaving 11 peaks unaccounted for. A second

conformation (Conformation B) was constructed with 12 peaks. 12 residues were not able to be to identified in the spectrum, and contribute to the calculation error from the experimental data with 11 peaks that were not assigned.

Equation 2.1 $$\boldsymbol{number\ of\ peaks = number\ of\ residues + (side\ chain\ Arg + Asp + Gln) - \#\ of\ prolines}$$

^{13}Cα and ^{13}Cβ peaks were then identified for the HNCACB using positive (^{13}Cα; light pink) and negative (^{13}Cβ; maroon) contours (Figure 2.13) and CBCAcoNH spectra (Figure 2.14). These ^{13}Cα and ^{13}Cβ are the intra residues of the *i*-1 structure. Peaks from HNCACB and CBCAcoNH were then linked to the ^{15}N-HSQC spectrum based on corresponding ^{15}N and ^{1}H peaks.

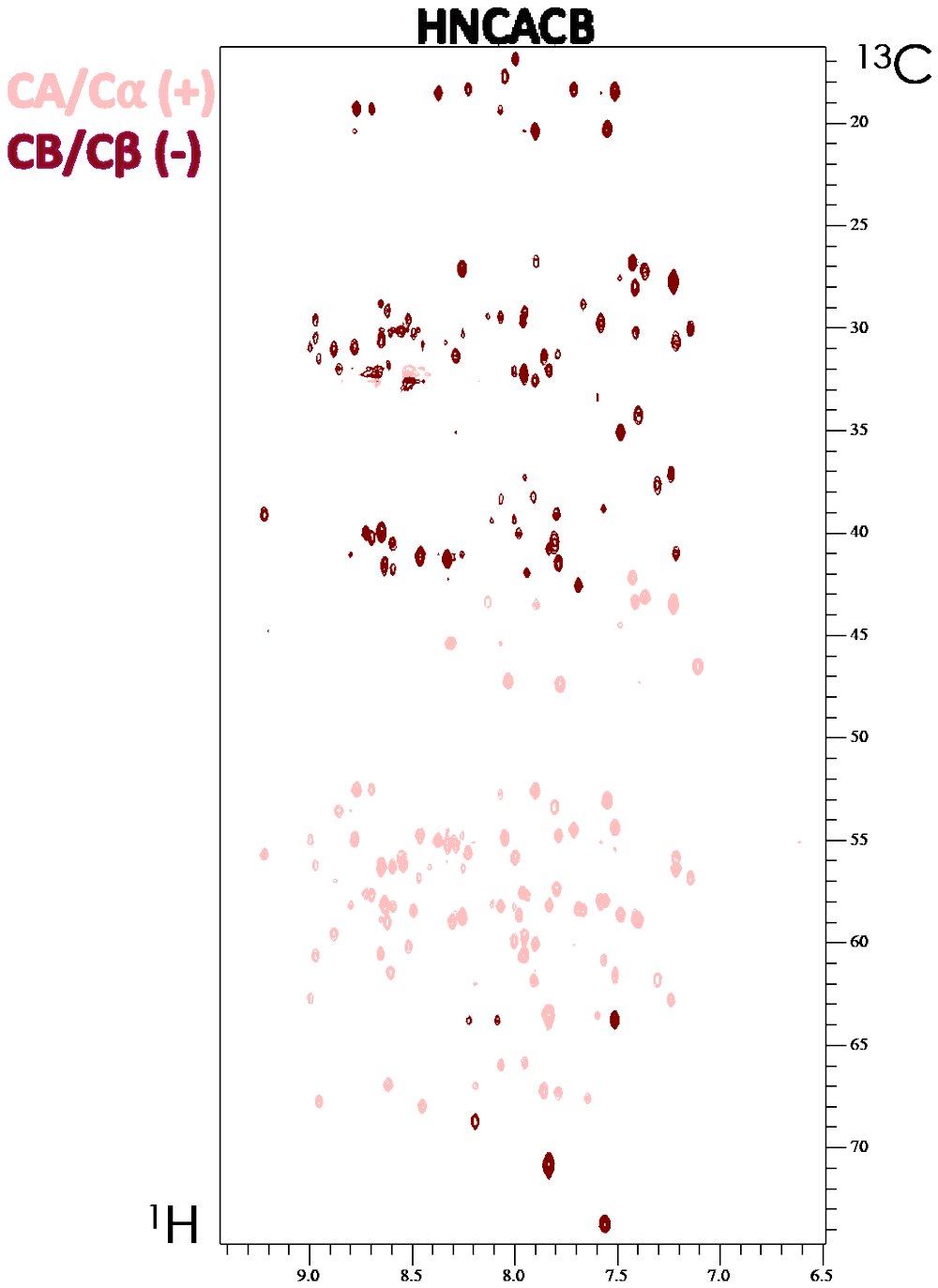

Figure 2.13 ^{1}H, ^{13}C, ^{15}N HNCACB spectrum of apo-ACP1.
HNCACB spectra was processed through NMRPipe and analyzed with CCPN Analysis 2.0 on NMRBox [19, 20, 21]. Positive peak contours (light pink) represent $^{13}C\alpha$ peaks, while negative peak contours (maroon) represent $^{13}C\beta$ peaks.

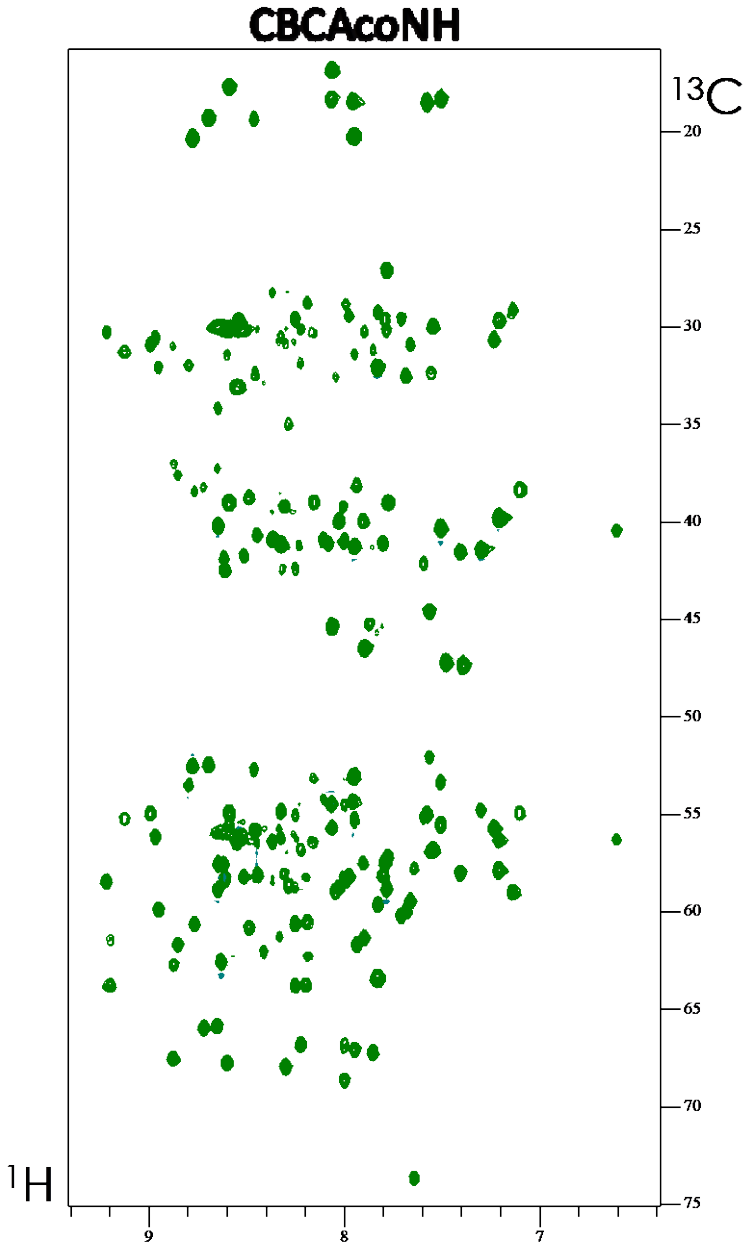

Figure 2.14 ^{1}H, ^{13}C, ^{15}N, CBCAcoNH spectrum of apo-ACP1.
The CBCAcoNH spectrum was processed with NMRPipe and analyzed with CCPN Analysis 2.0 on NMRBox [19, 20, 21].

C=O peaks were then identified for the HNCO (Figure 2.15). HNCO spectra can be used to validate the methods for spectra reconstruction and determining confidence regions of extracted parameters without using repeated measurements [28]. The reconstruction and parameters extracted can be used for 3D modeling and angle construction of the protein residues. This type of experimentation was used in this study because the homology modeling for ACP1 used a template to construct a 3D structure. Peaks were still identified for future use.

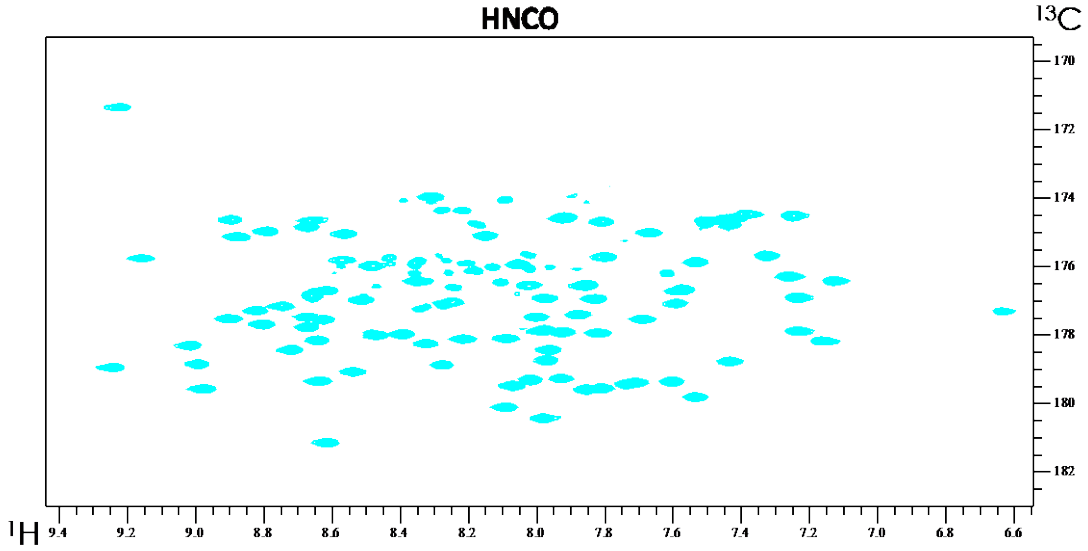

Figure 2.15 ^{1}H, ^{13}C, ^{15}N, HNCO spectrum of apo-ACP1.
The NHCO spectrum was processed with NMRPipe and analyzed with CCPN Analysis 2.0 on NMRBox [19, 20, 21].

After the peaks were assigned for ^{15}N HSQC, HNCACB, and CBCAcoNH spectra, assignments for HNCACB and CBCAcoNH were propagated, and the protein sequence was uploaded into the CCPN Analysis 2.0 software.

Protein sequence assignments use a ^{1}H, ^{13}C, ^{15}N (X, Y, Z) format with CBCAcoNH as a query window (HCN) and HNCACB as a stripped matching window (HCN strips). The CBCAcoNH spectra is also made visible on the stripped matching

window to ensure the HNCACB is not matched to the *i*-1 residues. Unassigned spin system residues are opened and analyzed to see which strip matches query window on horizontal markers. Once analyzed, a strip selection is made and the sequence link is created, linking the query window residue as a *i*+1 residue and the matching strip as a *i*-1 residue.

When all of the sequence residues are linked, the linkage is checked by a process known as "backbone walking." Backbone walking checks the matching of the $^{13}C\alpha$ and $^{13}C\beta$ from the *i* residue to the *i*-1 residues (Figure 2.16). Unmatched $^{13}C\beta$ are indicative of Gly residues with no $^{13}C\beta$ connection (17Gly, 34Gly, and 52Gly). Breaks in the backbone walking are from unidentified residues with the exception of 78Pro and 79Thr because proline (Pro) does not have visible peaks in the spectra. Prolines lack amine protons when they are in a polypeptide chain, and therefore cannot be detected in 2D ^{15}NH spectra [29].

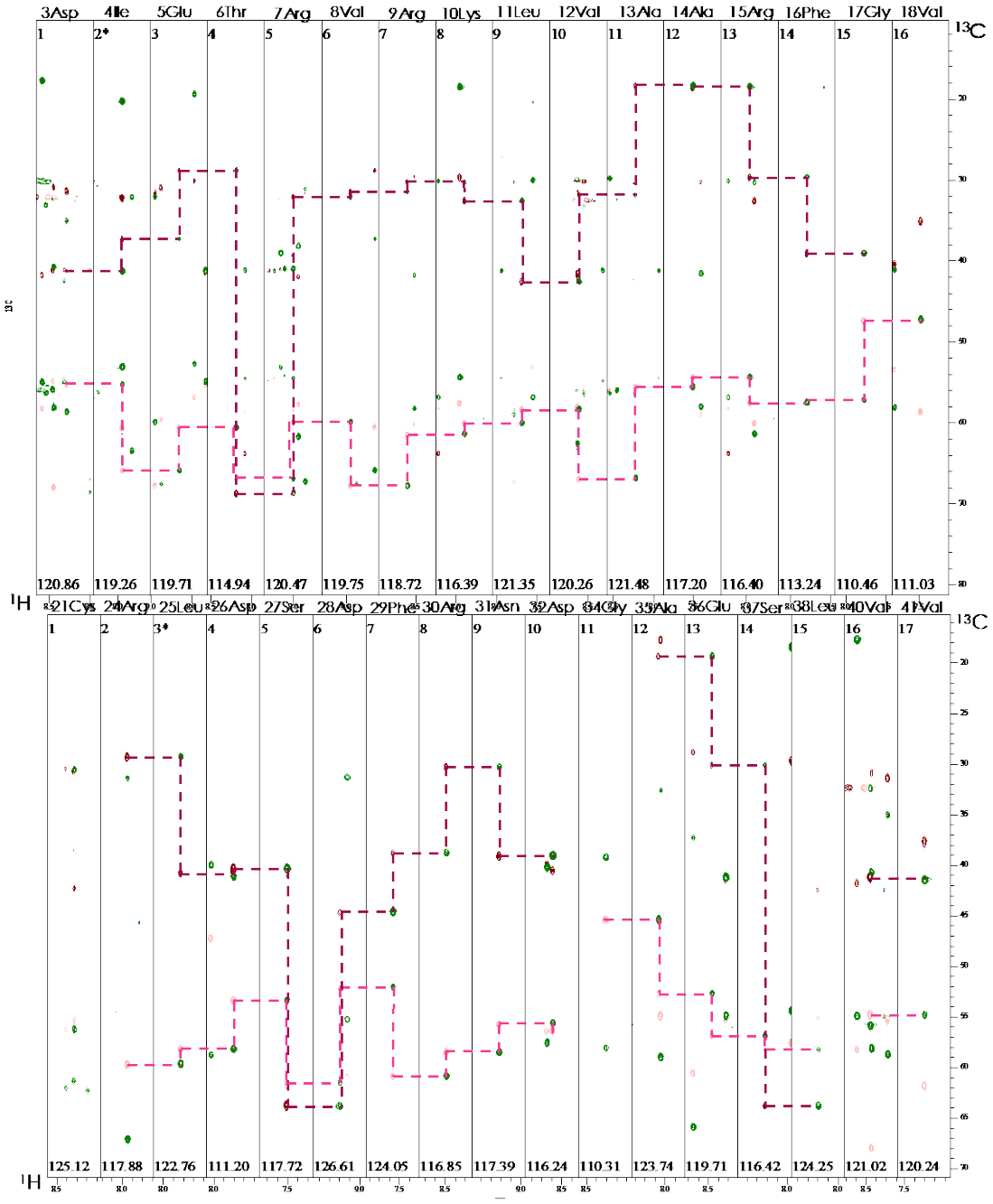
3Asp 4Ile 5Glu 6Thr 7Arg 8Val 9Arg 10Lys 11Leu 12Val 13Ala 14Ala 15Arg 16Phe 17Gly 18Val
120.86 119.26 119.71 114.94 120.47 119.75 118.72 116.39 121.35 120.26 121.48 117.20 116.40 113.24 110.46 111.03
21Cys 24Arg 25Leu 26Asp 27Ser 28Asp 29Phe 30Arg 31Asn 32Asp 34Gly 35Ala 36Glu 37Ser 38Leu 40Val 41Val
125.12 117.88 122.76 111.20 117.72 126.61 124.05 116.85 117.39 116.24 110.31 123.74 119.71 116.42 124.25 121.02 120.24
13C
1H

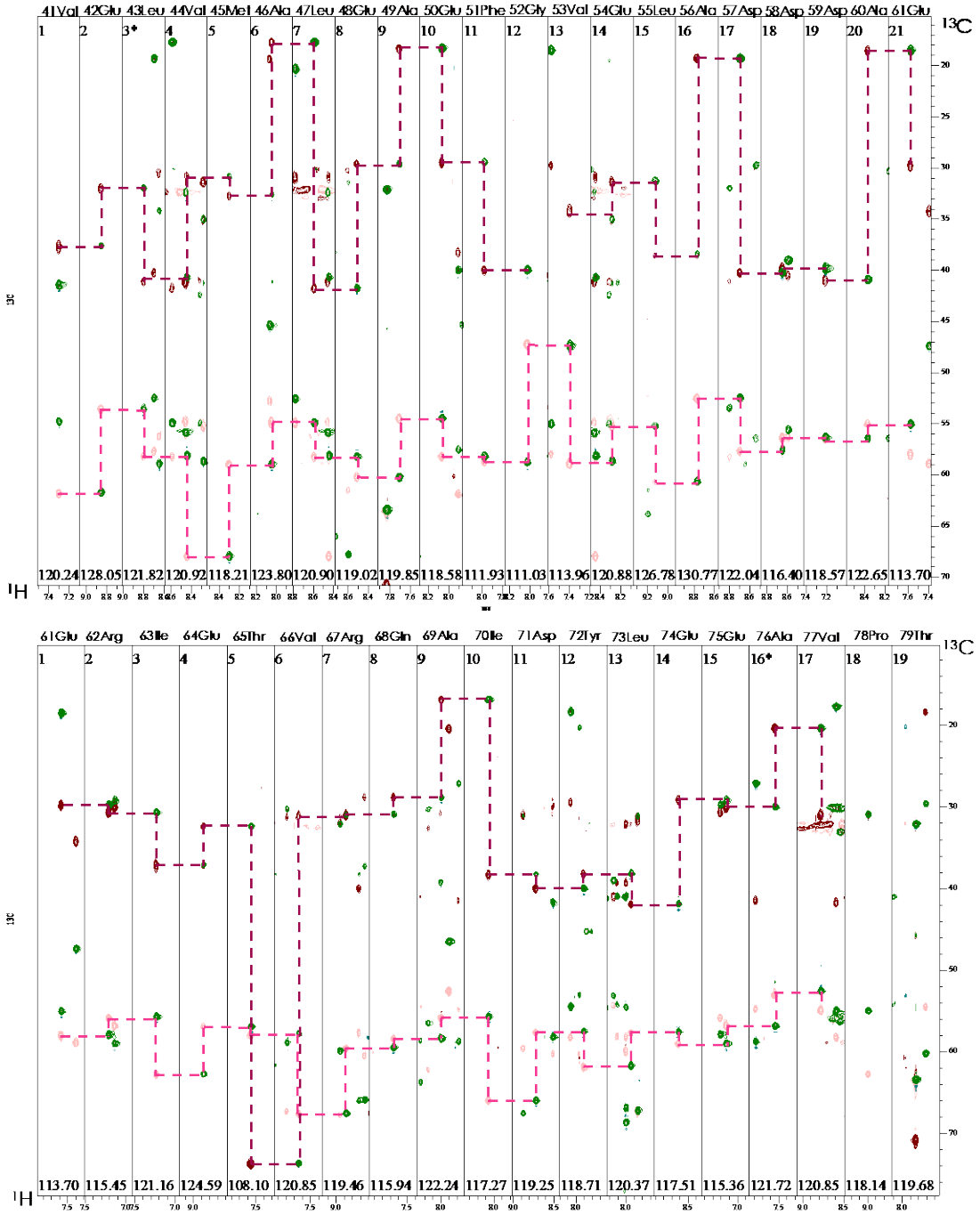

Figure 2.16 Backbone walking for apo-ACP1 sequence (Conformation A). Strip plots showing slices from CBCAcoNH (^{1}H, ^{13}C, ^{15}N; green peaks) and HNCACB (^{1}H, ^{13}C, ^{15}N; ^{13}Cα peaks [light pink], ^{13}Cβ peaks [maroon]) spectra are shown. The nitrogen dimension is noted at the bottom of each strip. Corresponding dashed lines indicate backbone walking on the ^{13}C axis. Unmatched ^{13}Cβ are indicative of Gly residues with no ^{13}Cβ connection (17Gly, 34Gly, and 52Gly). Breaks in the backbone walking are from unidentified resides with the exception of 78Pro and 79Thr [20].

All of the chemical shifts were then compared to the Reference Chemical Shift table provided by CCPN Analysis 2.0 (Figure 2.17) to validate the sequence [20]. Some chemical shifts are more easily identified than others because of the local diamagnetic shielding effect. For example, alanine (Ala) residues have a distinct ^{13}Cβ peak upfield between 16-23 ppm because it does not have any deshielding sidechains and behaves like a methyl group. Serine (Ser) and threonine (Thr) amino acids also have distinct ^{13}Cβ peak that are seen downfield, in the typical ^{13}Cα range, between 62-66 ppm and 68-72 ppm respectively. The ^{13}Cβ of both residues are highly deshielded by the hydroxyl group on the sidechains. The ^{13}Cβ of Thr is even further downfield due to a combined desheilding effect from local diamagnetic desheilding and the hydroxyl group. Glycine (Gly) is another defining residue because it has only an alpha carbon, and therefore only one ^{13}Cα peak between 43-48 ppm [11, 20, 30].

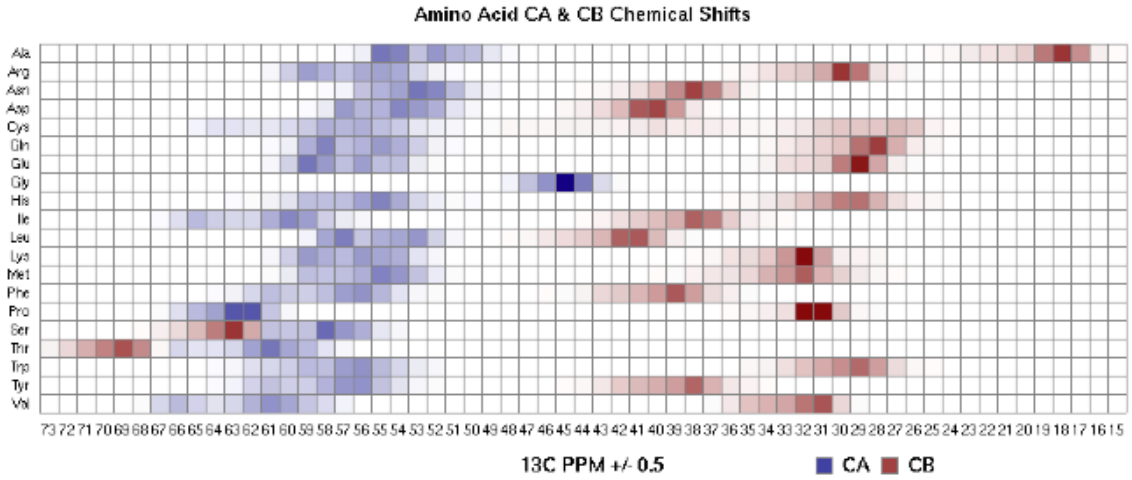

Figure 2.17 Reference Chemical Shifts for protein Cα and Cβ.
^{13}Cα and ^{13}Cβ reference chemical shift table provided by CCPN Analysis 2.0 [20].

In the sequence for apo-ACP1, there are nine alanine's, two serine's, three threonine's, and three glycine's [31]. These peaks are identified as residue types based on

their distinct chemical shifts and then assigned to a sequence number with respect to their neighboring residues. This process aided in the identification of a secondary conformation (Conformation B) in part of the ACP1 protein. There are ten spin systems that are consistent with alanine's chemical shifts in the spectra and evidence of two Ala-Gly (alanine *i* peak and glycine *i*-1 peak) connections with this only one (34Gly, 35Ala) occurring in the sequence. Additionally, three serine peaks were also identified in the spectra, with only two seen in the sequence. The third Ser can be seen at 27Ser based on the sequence conformation's (27Ser-30Arg) connection to 31Asn in the original Conformation A (Figure 2.18). A comparison Conformation B in comparison to Conformation A (Figure 2.16) is seen in Figure 2.19.

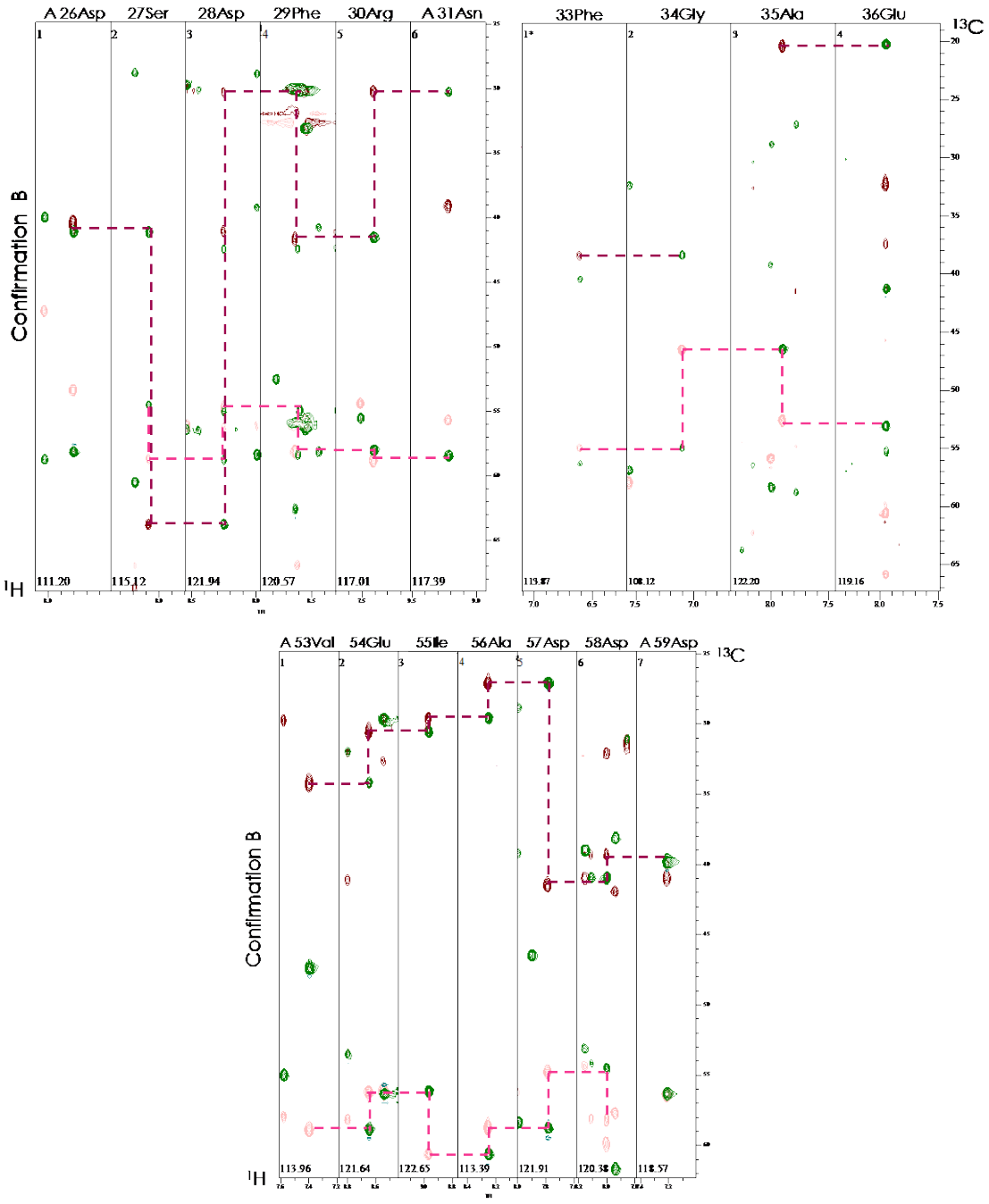

Figure 2.18 Backbone walking for an alternate sequence of apo- ACP1 (Conformation B).

CBCAcoNH (^{1}H, ^{13}C, ^{15}N; green peaks) and HNCACB (^{1}H, ^{13}C, ^{15}N; ^{13}Cα peaks [light pink], ^{13}Cβ peaks [maroon]) spectra with corresponding dashed lines to indicate backbone walking on the ^{13}C axis. Corresponding dashed lines were not drawn if carbon atoms did not match. An "A" was placed in front of a residue if Conformation B corresponded to a residue from Conformation A.

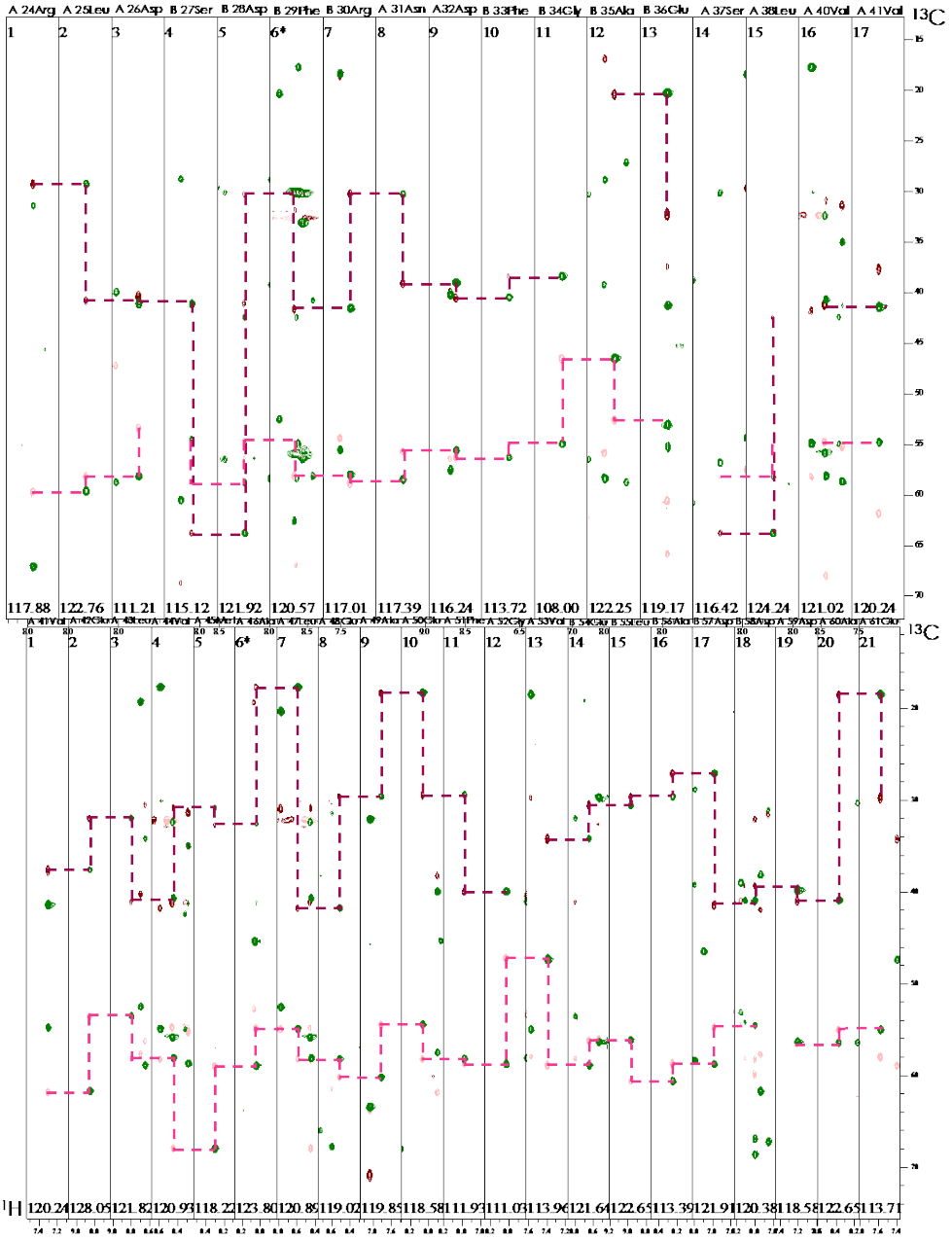

Figure 2.19 Backbone walking for apo-ACP1 with Conformations A and B. Strip plots showing slices from CBCAcoNH (^{1}H, ^{13}C, ^{15}N; green peaks) and HNCACB (^{1}H, ^{13}C, ^{15}N; ^{13}Cα peaks [light pink], ^{13}Cβ peaks [maroon]) spectra are shown. The nitrogen dimension is noted at the bottom of each strip. Corresponding dashed lines indicate backbone walking on the ^{13}C axis. Unmatched ^{13}Cβ are indicative of Gly residues with no ^{13}Cβ connection (34Gly, and 52Gly). Breaks in the backbone walking are from unidentified resides (40Glu) or disconnections between Conformations A and B[20].

When a protein experiences at least two conformational states (Conformations A and B), the chemical exchange between the two states can directly alter the primary NMR observables [32]. Slow exchange is when the change in chemical shifts is much greater than the exchange between the two conformational states. In this case, signals from both states are observed reflecting their distinct chemical shifts, intensities and linewidths. For fast exchange, the exchange between the conformational states is greater than the change in chemical shift, and only one signal is observed reflecting the population-weighted averages of chemical shift, intensity and linewidth. Intermediate exchange, where the exchange between the conformational states is approximately equal to the change in chemical shift, only one signal is observed with intermediate chemical shift. In this case, the linewidth is increased because of "exchange broadening," which can lead to undetectable signals [30]. The peak volumes of the apo-ACP1 HSQC spectra indicate conformational exchange because of the decreased peak volumes of some assigned residues (Figure 2.20). These peak volume decreases are mostly observed at residues 33Phe, 34Gly, 37Ser, 38Leu, 72Glu and 73Thr. Unidentified residues are displayed without a peak volume, and are blank. Some of these decreases (33Phe and 34Gly) correspond to an identified secondary conformation (Conformation B). The remaining peaks (45Ser, 46Leu, 64Glu and 65Thr) could be some of the unidentified peaks and could link the Conformation B sequence 41Phe-44Glu to Conformation A.

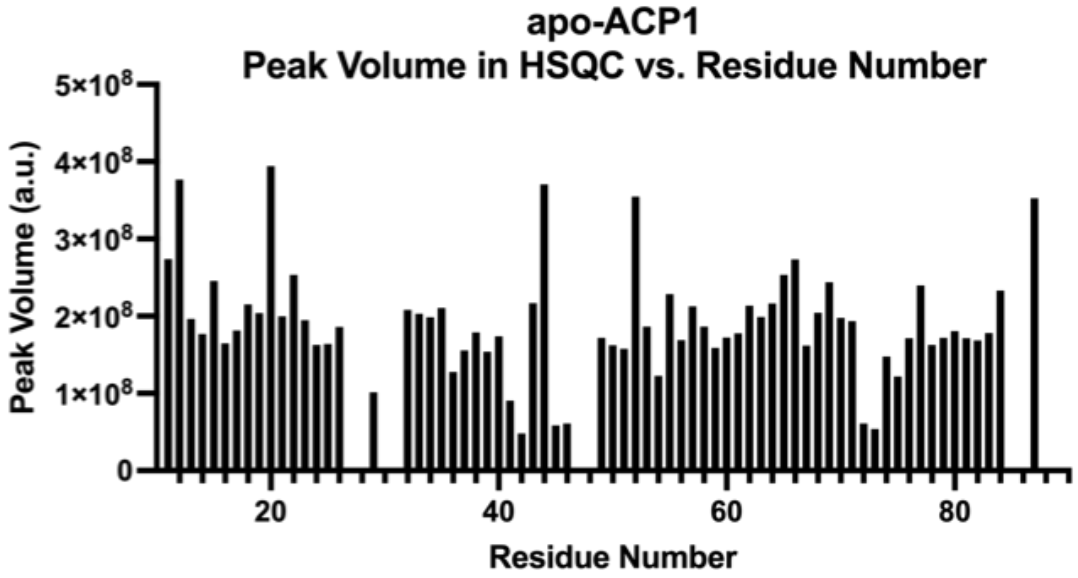

Figure 2.20 Protein backbone peak heights for apo-ACP1.
A bar graph using labeled residue sequence numbers from the ^{15}N-HSQC spectra (^{1}H, ^{15}N) as the x-axis and peak volume/height as the y-axis to visualize peak strength [20]. Decreased peak values for individual residues indicate intermediate exchange and possible confirmational changes. Peak values of zero are unassigned residues.

Figure 2.21 is a homology model of apo-ACP1 with the regions of conformational change (Conformation B) highlighted in grey. This figure shows that most of the secondary conformations are in the loops, which are susceptible to change due to their flexibility [33].

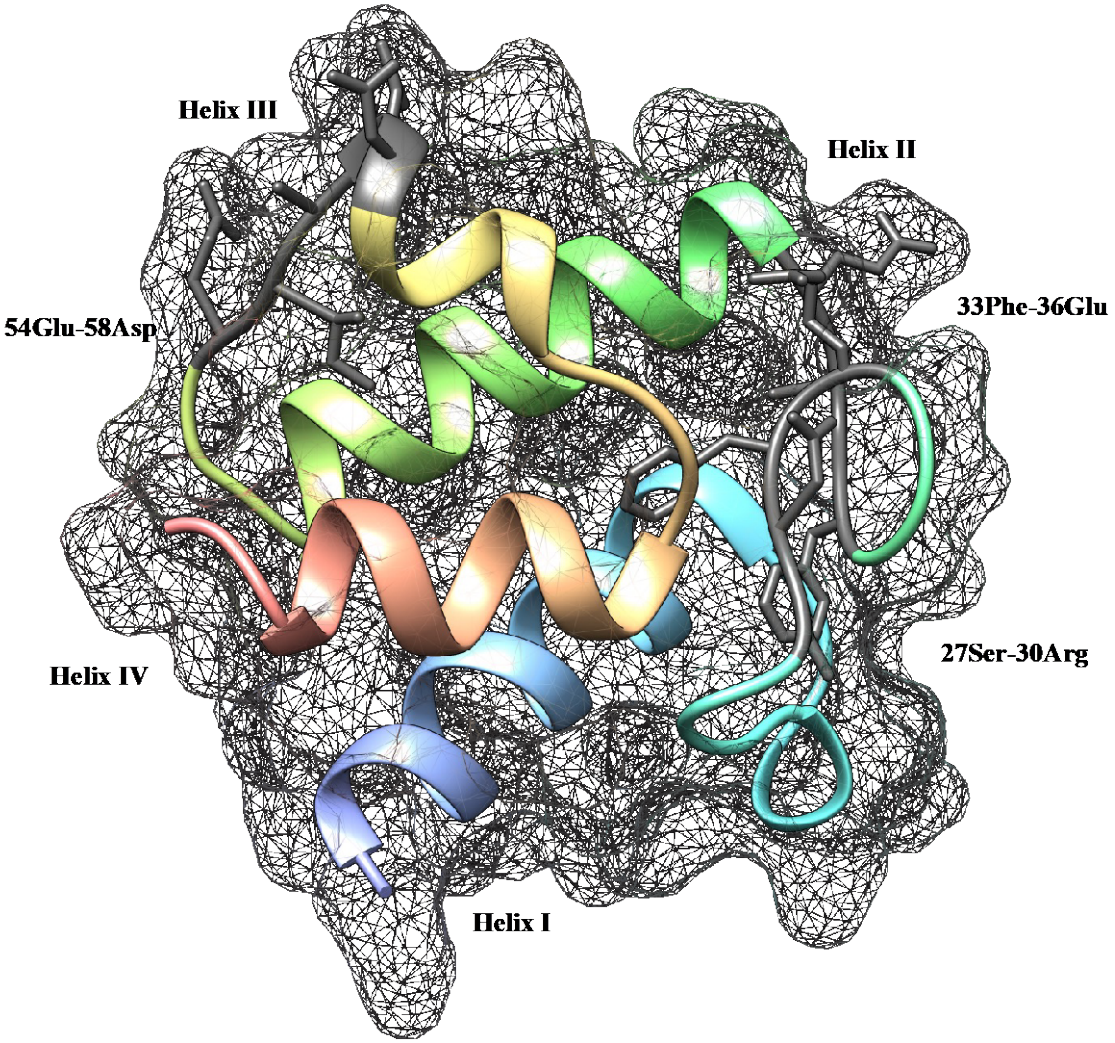

Figure 2.21 Apo-ACP1 with secondary conformational change highlighted. Four helices of apo-ACP1 with residues 34Asp-39Asn, 42Gly-43Glu, and 61Val-67Asp highlighted in grey [5, 6, 7].

The final residue assignments of the apo-ACP1 ^{15}N-HSQC spectra were assigned with the original conformation (Conformation A) structure (Figure 2.22 and secondary conformation (Conformation B; Figure 2.23). Not all peaks were identified in the protein backbone (Figure 2.22 and Figure 2.23). Some of the rouge peaks are arginine (Arg) sidechains in the bottom right-hand corner (black rectangle). The matching rouge peaks in the top right-hand corner (black connecting lines) are asparagine (Asn) and glutamine (Gln) sidechains **(**Figure 2.22, Figure 2.23, and Figure 2.24). These peaks are identifiable

as sidechains because there are no *i*-1 (green) peaks associated with the ^{15}N-HSQC peaks (purple) (Figure 2.24).

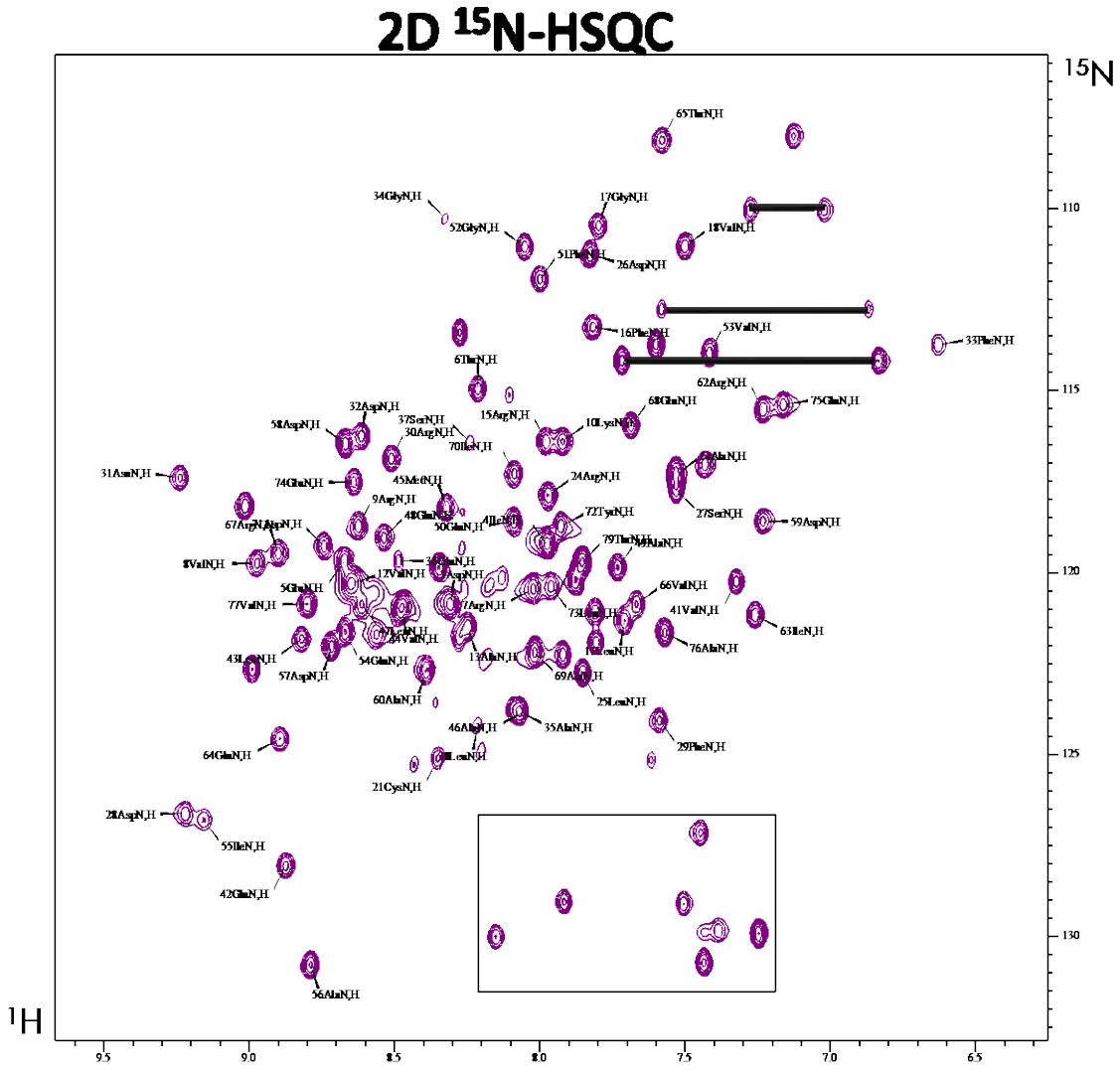

Figure 2.22 Protein backbone assignments for apo-ACP1.
^{15}N-HSQC spectra (^{1}H, ^{15}N) with labeled residue peaks of Conformation A [20]. The black rectangle indicates Arg sidechains and the black connecting lines indicate matching Asn and Gln sidechains.

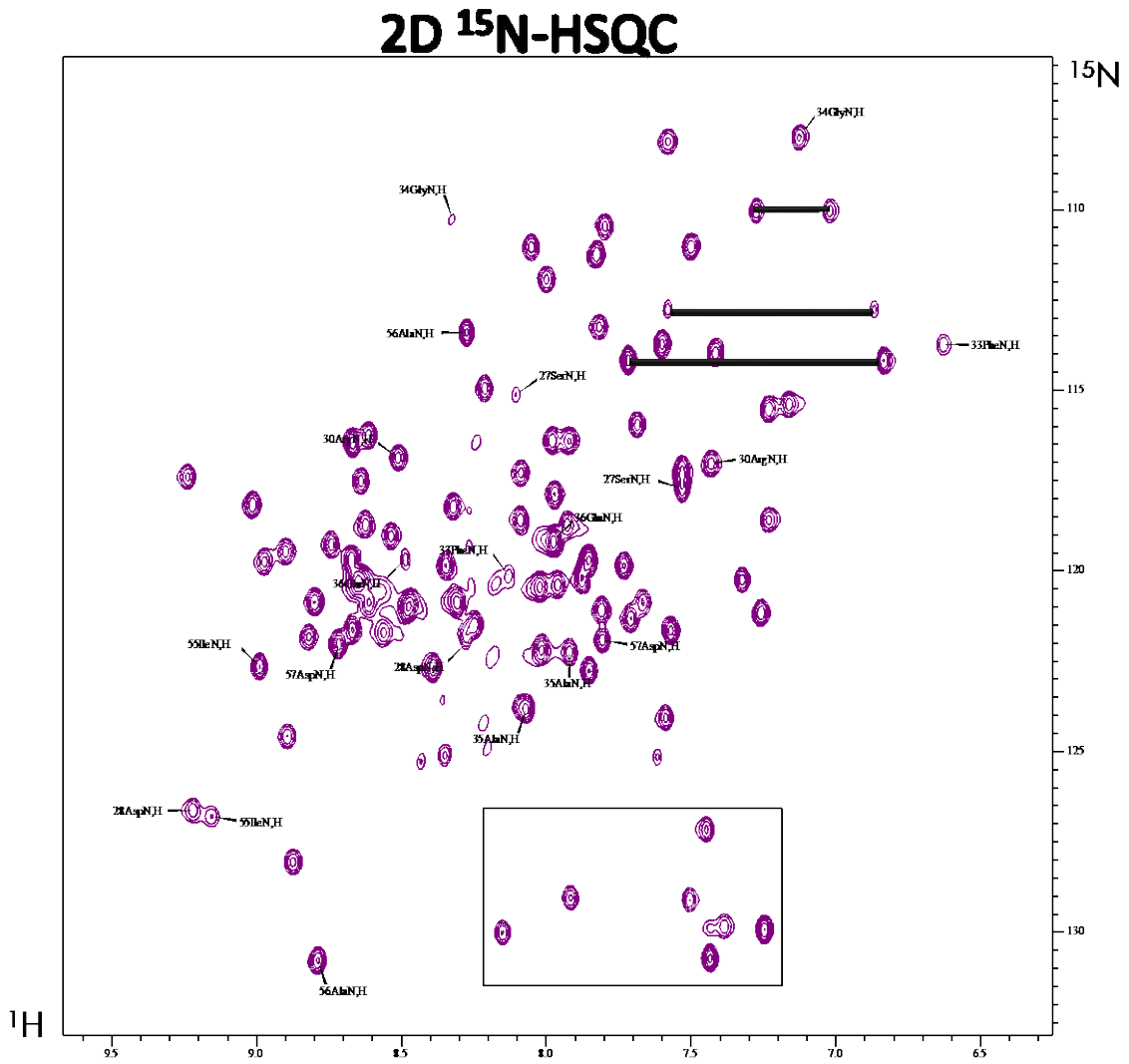

Figure 2.23 Protein backbone assignments for apo-ACP1.
^{15}N-HSQC spectra (^{1}H, ^{15}N) with labeled residue peaks of Conformation B with the duplicates from Conformation A [20]. The black rectangle indicates Arg sidechains and the black connecting lines indicate matching Asn and Gln sidechains.

Sidechain peaks are identifiable because there are no *i*-1 (green) peaks associated with the ^{15}N-HSQC peaks (purple) (Figure 2.24). Asn and Gln appear with matching peaks (indicated with black connecting lines) because both residues have sidechains that share the same nitrogen atom but have two non-equivalent hydrogen atoms, making the

proton atom appear twice on the ^{1}H plane (x-axis) and align on the ^{15}N plane (y-axis) [11, 20, 30].

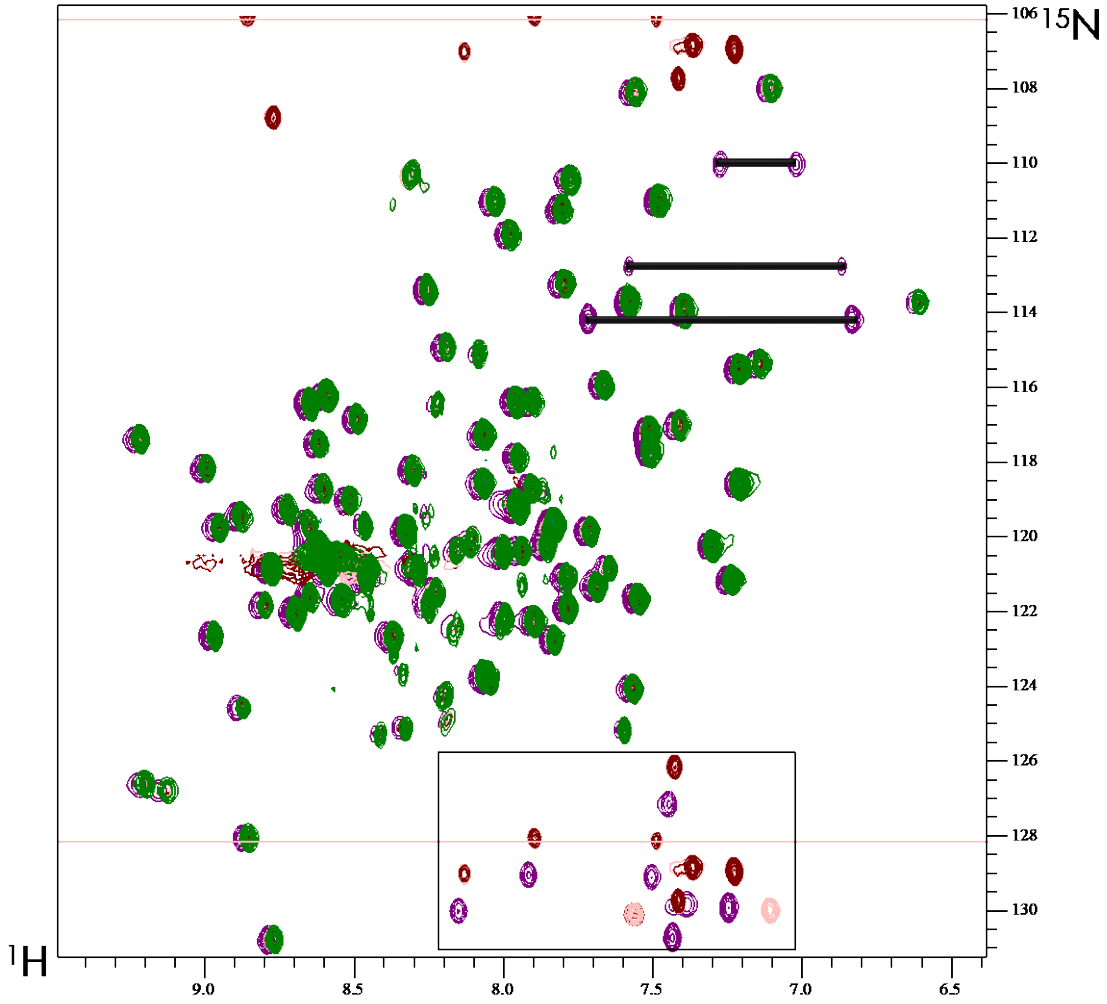

Figure 2.24 ^{15}N-HSQC, CBCAcoNH, and HNCACB spectra for apo-ACP1. ^{15}N-HSQC spectra (purple peaks), CBCAcoNH (green peaks), and HNCACB ($^{13}C\alpha$ peaks [light pink], $^{13}C\beta$ peaks [maroon]) spectra (^{1}H, ^{15}N, ^{13}C) with labeled ^{15}N-HSQC spectra residues. Arg side chains are outlined with a black rectangle and Asn and Gln sidechains have black connecting lines [20].

Homology Modeling

A homology model for ACP1 was generated for this study to accurately display the protein structure of ACP1 and for future use with 3D protein-enzyme interactions. The sequence used was sequenced from ACP1, but did not include the His_6 tag (HMDDIETRVRKLVAARFGVEECDIRLDSDFRNDFGAESLEVVELVMALEAEFGV EIADDDAERIETVRQAIDYLEEAVPT). The crystal structure for malonyl-ACP from *bacillus subtilis* (2x2b.1.A) was used as a template model to assemble the protein structure angles and residue interactions. The resulting homology model was constructed using the online workspace SWISS-MODEL [5, 6]. The provided sequence was ingested into the SWISS-MODEL workspace as a target sequence before the program could build the model. Once the sequence was processed, a protein data bank (.pbd) file could be downloaded, and ingested into the work spaces Chimera and ChemDraw 21.0.0 [7 - 8]. The quality of the model is rated based off of the global model quality estimation (GMQE) with a rating of 0.68. An alternative structure 2ehs.1.A (GMQE: 0.70) was not used because it is an acyl carrier protein from *Aquifex aeolicus*, and *P. aeruginosa* is a type of bacillus [34]. SWISS-MODEL conducts a quality check for models with an associated Ramachandran Plot, residue specific quality reports, and quality estimates of the model in comparison (Figure 2.25). A Ramachandran plot associated with ACP1 predicts the accuracy of a predicted protein based on stereochemical parameters of the protein (Figure 2.25 (a)) [35]. Based on the Ramachandran plot, the predicted proteins (red/purple circles) are mostly favored, with most structures falling in the most favorable structural region (dark green), and a few structures falling in a moderately favorable region (light green). Figure 2.25 (b) shows the predicted model's template alignment with

ACP from *bacillus subtilis* (2x2b.1.A). Matching residues are outlined with a box with a purple/pink quality mean score above each individual residue. The closer the score is to the solid gray line (QMEAN), the higher the quality of the residues structure. The Figure 2.25 (c) is the quality estimate of the model compared with other non-redundant sets of PDB structures from the software. The red star is the generated model, which is plotted within the mean quality scores for its protein size.

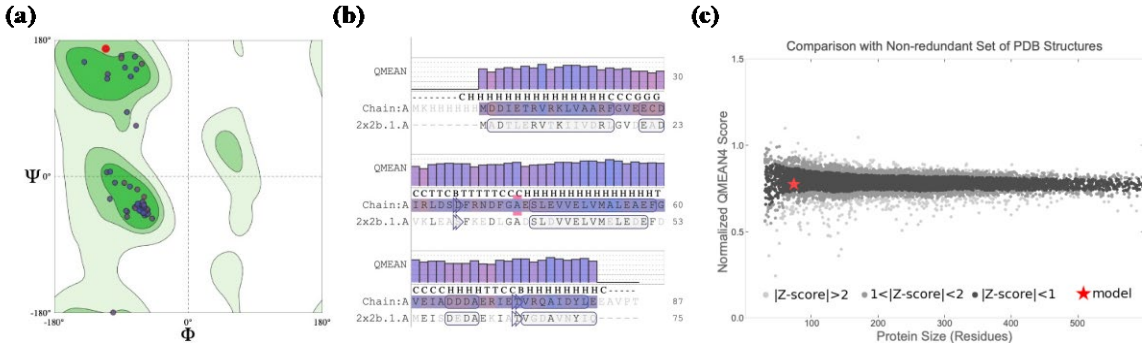

Figure 2.25 Homology modeling estimates of ACP1.
ACP1 was modeled using sequencing data from ATUM, and ingesting this it and a common crystal structure (2x2b.1.A) into the SWISS-MODEL workspace [5, 6]. **(a)** Ramachandran Plot associated with the ACP1 model, **(b)** is model-template alignment comparison, and **(c)** is the quality estimate of the model compared to the PDB.

CHAPTER THREE: C4I-ACP1 PROTEIN BACKBONE ASSIGNMENTS

Introduction

Naturally, acyl-ACP is produced in the FAB cycle with coenzyme A (CoA) [4]. Synthetically, the desired cargo must first be synthesized with alkyl-CoA, resulting in acyl-CoA. Acyl-CoA then reacts with apo-ACP and the enzyme surfactin phosphopantetheinyl transferase (Sfp), to load the desired cargo on to apo-ACP, are the production of acyl-ACP. Cargo synthesis, cargo loading and NMR data collection for acyl-ACP from *P. aeruginosa* (C4I-ACP1) was also collected prior to this study. This study only analyzed the ^{15}N HSQC of C4I-ACP1 with minimal chemical shift perturbations. This information will be used in future studies for chemical shift perturbation analysis and to define the ACP1-RhlI axis.

Materials and Methods

Cargo Synthesis and Purification

C4I acyl cargo was synthesized overnight from an alkyl-CoA reaction. In a round bottom (RB) flask, 65 μmol of powder CoA was dissolved in 1 mL nanopure water. Then, the pH is adjusted to ~8.5 with K_2CO_3 prior to adding 65 μmol TCEP, another 1 mL Nanopure water, 1 mL dimethylformamide, and 120.2 μmol 1-bromobutane. Nitrogen gas passed over the RB flask to remove air and left overnight. The following day, 2 mL of water was added prior to washing the solution with 4 mL of diethylether three times. The aqueous layer was kept and filtered before loading onto a semi-prep

UHPLC column for purification and fractionation. For this study, C4I cargo was not synthesized, but was previously provided for apo-ACP cargo loading.

Cargo-Loaded ACP Ligands

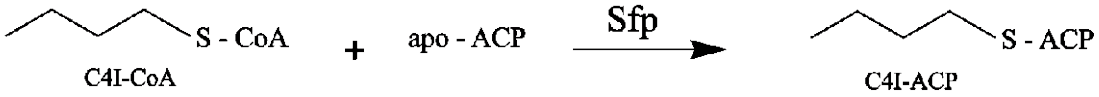

Figure 3.1 Cargo loading reactions to make acyl-ACP.
C4I-CoA reacts with apo- ACP and the enzyme Sfp to produce acyl-ACP or C4I-ACP1 [8].

Synthesized C4I cargo was loaded onto apo-ACP1 with the enzyme Sfp by incubating 500 μM of apo-ACP1 at 37 °C in acyl-CoA buffer (acyl-CoA 625 μM, Sfp 1 μM, $MgCl_2$ 10 mM, TCEP 1 mM, Tris/HCl pH 6.8 50 mM). The UHPLC instrument measuring UV at 280 nm was used to check the reaction. When the sample reached 75% saturation, ammonium sulfate was added. The mixture was then stirred at 4 °C for 1 hour before separating any precipitate through centrifugation at 13,000×g for 15 minutes. The supernatant was then concentrated using a 6 mL sartorius Vivapin centrifuge tubes with a membrane containing a 3,000 MWCO. Aliquots were flash frozen in liquid nitrogen and stored at -80 °C before use. This study only analyzed previously produced C4I-ACP1, and did not cargo load apo-ACP.

Nuclear Magnetic Resonance Methods

This study only analyzed previously acquired spectra provided by Oregon State University. NMR data was obtained on a Bruker AVANCE III 800 MHz spectrometer equipped with a cryogenically cooled TCI cryoprobe. 1D ^{1}H, 2D ^{1}H, ^{15}N HSQC, and non-uniform sampling 3D HNCO, HNCA, HNCACB, and CBCAcoNH NMR spectra

were collected, processed with NMRPipe and analyzed with the CCPN Analysis 2.0 on NMRBox [19, 20, 21].

Results and Discussion

NMR chemical shift perturbations of C4I-ACP1

The spectra were processed with NMRPipe and analyzed with the CCPN Analysis 2.0 on NMRBox [19, 20, 21]. The initial ^{15}N-HSQC spectrum for C4I-ACP1 (Figure 3.2) can be seen in Figure 3.2.

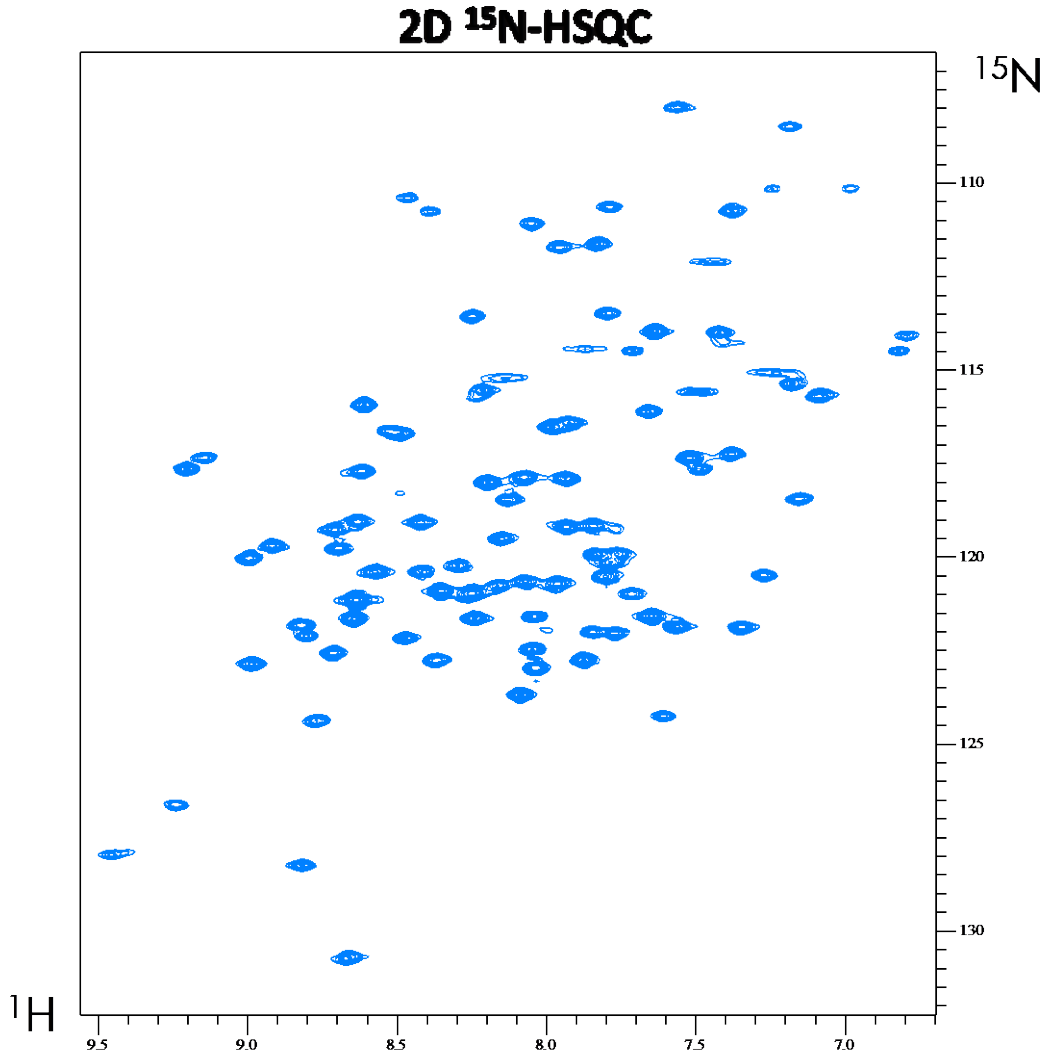

Figure 3.2 ^{1}H, ^{15}N HSQC spectrum of C4I-ACP1.
^{15}N-HSQC spectra process through NMRPipe and analyzed with CCPN Analysis 2.0 on NMRBox [19, 20, 21].

Full assignments for the spectra were not completed, but ^{15}N HSQC assignments were made for C4I-ACP based on minimal chemical shift perturbations from apo-ACP1 assignments, with 76 of C4I-ACP peaks assigned. (Figure 3.3).

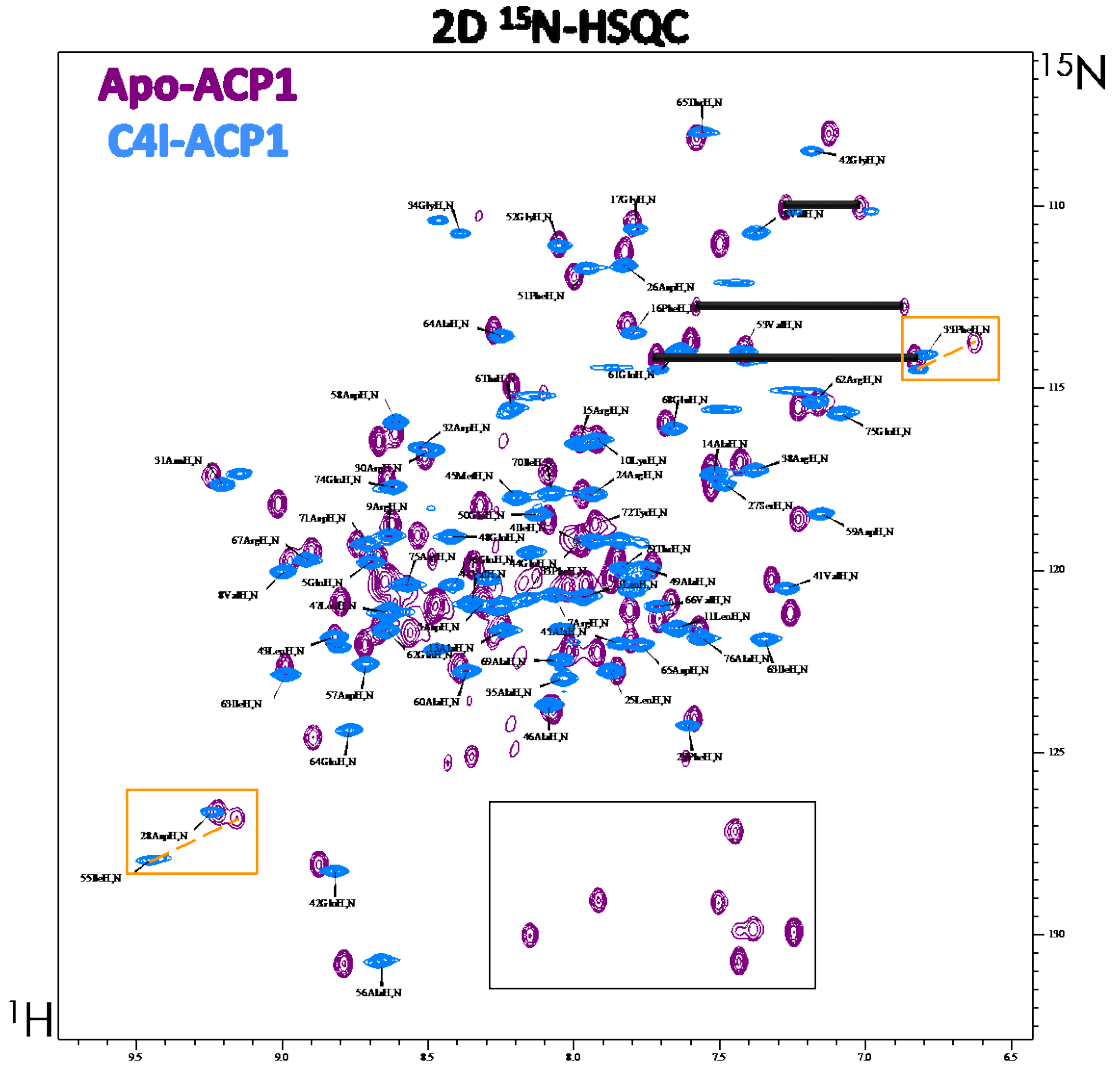

Figure 3.3 Compared ^{15}N-HSQC for apo-ACP1 and C4I-ACP1 protein backbone assignments.

^{15}N-HSQC spectra (^{1}H, ^{15}N) with labeled residue peaks for apo-ACP1 (purple) and C4I-ACP1 (blue). C4I-ACP1 assignments are based on minimal chemical shift perturbations. Chemical shifts have been identified with an orange box and dashed line. Arg side chains from the apo-ACP1 HSQC spectra are outlined with a black rectangle and Asn and Gln sidechains have black connecting lines [20].

Of the 76 peaks, 8 were secondary conformational change (Conformation B) peaks from the original apo-ACP1 structure (28Asp, 30 Arg, 34Gly-36Glu, 55Ile-57Asp). All of these residues asigned in the C4I-ACP1 spectra are a part of a loop construct and have flexibility to their structure. Because of the processing, sidechain peaks were not confirmed without the CBCAcoNH spectra. Some presumed Arg peaks were seen with flattened peaks instead of spherical peaks. For example, the peak at 7.5 ppm, 112 ppm (^{1}H, ^{15}N) is most likely a sidechain peak. Larger chemical shift perturbations have been identified with an orange box and matching dashed line. These prominent shifts correlate with Conformation B (55Ile and 33Phe) from the original apo-ACP1 structure.

Additional assignments would be able to identify rouge peaks such as the two additional peaks near 34Gly (8.6 ppm, 110 ppm). These peaks could be chemical shifts or unidentified residues from the Conformation A of the apo-ACP1. These peaks are most likely not from the acyl group or phosphopantetheine linker because only the apo-ACP1 carbons we isotopically enriched. Complete assignments will need to be conducted to identify new conformational structures and additional chemical shift perturbations.

CHAPTER FOUR: CONCLUSION AND FINAL THOUGHTS

The protein backbone assignments for apo-ACP1 and possible conformational changes are the first steps towards understanding the broader interaction between acyl-ACP and AHLS enzymes.

Research will continue by using the protein expression and purification optimizations outlined in APPENDIX A to produce the proteins and enzymes used for quorum sensing in *P. aeruginosa,* and eventually other bacterial strains. First more ^{15}N apo-ACP1, ^{15}N C4I-ACP1, ^{15}N C6I-ACP1, His_6MBP-RhlI, and His_6MBP tag production is required for NMR data collection on enzymatic titrations. Once enough protein and enzymes are produced, the His_6MBP-RhlI can be titrated with different cargo loaded ACP1, showing NMR chemical shift perturbations during the enzymatic reaction for AHL synthesis.

After the NMR data from the titrations is obtained, the ^{13}C, ^{15}N apo-ACP1 NMR data and assigned protein backbone can be used as a template to identify chemical shift perturbations or conformational shifts during the enzymatic reaction for cargo loaded ACP1. If these chemical shift perturbations can define the axis between ACP1 and RhlI for *P. aeruginosa*, then this concept can be applied to other ACP's and AHLS enzymes for other bacterial strains.

Drug development for inhibition of quorum sensing of multiple bacterial strains will working towards a novel antibiotic resistance solution, where bacterial cells are not destroyed, but their communication is limited.

REFERENCES

(1) Miller, M. B.; Bassler, B. L. Quorum Sensing in Bacteria. *Annu Rev Microbiol* **2001**, *55*, 165–199. https://doi.org/10.1146/annurev.micro.55.1.165.

(2) Preda, V. G.; Săndulescu, O. Communication Is the Key: Biofilms, Quorum Sensing, Formation and Prevention. *Discoveries (Craiova) 7* (3), e100. https://doi.org/10.15190/d.2019.13.

(3) Smith, R. S.; Harris, S. G.; Phipps, R.; Iglewski, B. The Pseudomonas Aeruginosa Quorum-Sensing Molecule N-(3-Oxododecanoyl)Homoserine Lactone Contributes to Virulence and Induces Inflammation in Vivo. *J Bacteriol* **2002**, *184* (4), 1132–1139. https://doi.org/10.1128/jb.184.4.1132-1139.2002.

(4) Gullett, J. M.; Rock, C. O. Fatty Acid and Phospholipid Biosynthesis in Prokaryotes. In *Biochemistry of Lipids, Lipoproteins and Membranes*; Elsevier, 2021; pp 85–120. https://doi.org/10.1016/B978-0-12-824048-9.00007-9.

(5) Waterhouse, A.; Bertoni, M.; Bienert, S.; Studer, G.; Tauriello, G.; Gumienny, R.; Heer, F. T.; de Beer, T. A. P.; Rempfer, C.; Bordoli, L.; Lepore, R.; Schwede, T. SWISS-MODEL: Homology Modelling of Protein Structures and Complexes. *Nucleic Acids Res* **2018**, *46* (W1), W296–W303. https://doi.org/10.1093/nar/gky427.

(6) Martinez, M. A.; Zaballa, M.-E.; Schaeffer, F.; Bellinzoni, M.; Albanesi, D.; Schujman, G. E.; Vila, A. J.; Alzari, P. M.; de Mendoza, D. A Novel Role of Malonyl-ACP in Lipid Homeostasis. *Biochemistry* **2010**, *49* (14), 3161–3167. https://doi.org/10.1021/bi100136n.

(7) Pettersen, E. F.; Goddard, T. D.; Huang, C. C.; Couch, G. S.; Greenblatt, D. M.; Meng, E. C.; Ferrin, T. E. UCSF Chimera--a Visualization System for Exploratory Research and Analysis. *J Comput Chem* **2004**, *25* (13), 1605–1612. https://doi.org/10.1002/jcc.20084.

(8) *ChemDraw - PerkinElmer Informatics*. https://perkinelmerinformatics.com/products/research/chemdraw (accessed 2022-09-14).

(9) Zhang, W.; Li, C. Exploiting Quorum Sensing Interfering Strategies in Gram-Negative Bacteria for the Enhancement of Environmental Applications. *Front. Microbiol.* **2016**, *6*. https://doi.org/10.3389/fmicb.2015.01535.

(10) Raychaudhuri, A.; Jerga, A.; Tipton, P. A. Chemical Mechanism and Substrate Specificity of RhlI, an Acylhomoserine Lactone Synthase from *Pseudomonas Aeruginosa*. *Biochemistry* **2005**, *44* (8), 2974–2981. https://doi.org/10.1021/bi048005m.

(11) Williamson, M. P. Using Chemical Shift Perturbation to Characterise Ligand Binding. *Progress in Nuclear Magnetic Resonance Spectroscopy* **2013**, *73*, 1–16. https://doi.org/10.1016/j.pnmrs.2013.02.001.

(12) Victoria A. Higman. Visualising 3D Spectra, 2012. https://www.protein-nmr.org.uk/solution-nmr/assignment-theory/visualising-3d-spectra/.

(13) Fricke, P.; Chevelkov, V.; Zinke, M.; Giller, K.; Becker, S.; Lange, A. Backbone Assignment of Perdeuterated Proteins by Solid-State NMR Using Proton Detection and Ultrafast Magic-Angle Spinning. *Nat Protoc* **2017**, *12* (4), 764–782. https://doi.org/10.1038/nprot.2016.190.

(14) Sztain, T.; Bartholow, T. G.; Lee, D. J.; Casalino, L.; Mitchell, A.; Young, M. A.; Wang, J.; McCammon, J. A.; Burkart, M. D. Decoding Allosteric Regulation by the Acyl Carrier Protein. *Proc. Natl. Acad. Sci. U.S.A.* **2021**, *118* (16), e2025597118. https://doi.org/10.1073/pnas.2025597118.

(15) *Protein NMR Spectroscopy: Principles and Practice*, 2nd ed.; Cavanagh, J., Ed.; Academic Press: Amsterdam ; Boston, 2007.

(16) Kay, L. E.; Ikura, M.; Tschudin, R.; Bax, A. Three-Dimensional Triple-Resonance NMR Spectroscopy of Isotopically Enriched Proteins. *Journal of Magnetic Resonance (1969)* **1990**, *89* (3), 496–514. https://doi.org/10.1016/0022-2364(90)90333-5.

(17) Grzesiek, S.; Bax, A. An Efficient Experiment for Sequential Backbone Assignment of Medium-Sized Isotopically Enriched Proteins. *Journal of Magnetic Resonance (1969)* **1992**, *99* (1), 201–207. https://doi.org/10.1016/0022-2364(92)90169-8.

(18) Miller, J. H. *Experiments in Molecular Genetics*; Cold Spring Harbor Laboratory: Cold Spring Harbor, N.Y., 1972.

(19) Delaglio, F.; Grzesiek, S.; Vuister, GeertenW.; Zhu, G.; Pfeifer, J.; Bax, A. NMRPipe: A Multidimensional Spectral Processing System Based on UNIX Pipes. *J Biomol NMR* **1995**, *6* (3). https://doi.org/10.1007/BF00197809.

(20) Vranken, W. F.; Boucher, W.; Stevens, T. J.; Fogh, R. H.; Pajon, A.; Llinas, M.; Ulrich, E. L.; Markley, J. L.; Ionides, J.; Laue, E. D. The CCPN Data Model for NMR Spectroscopy: Development of a Software Pipeline. *Proteins* **2005**, *59* (4), 687–696. https://doi.org/10.1002/prot.20449.

(21) Maciejewski, M. W.; Schuyler, A. D.; Gryk, M. R.; Moraru, I. I.; Romero, P. R.; Ulrich, E. L.; Eghbalnia, H. R.; Livny, M.; Delaglio, F.; Hoch, J. C. NMRbox: A Resource for Biomolecular NMR Computation. *Biophysical Journal* **2017**, *112* (8), 1529–1534. https://doi.org/10.1016/j.bpj.2017.03.011.

(22) Mdonnell. UV Spectrum Comparisons, 2004. https://department.monm.edu/chemistry/chemistry330/fall2004/mdonnell/GFP%20Project/Characterization/uv_spectrum_comparisons.htm.

(23) Valle, A.; Pérez-Socas, L. B.; Canet, L.; Hervis, Y. de la P.; de Armas-Guitart, G.; Martins-de-Sa, D.; Lima, J. C. B.; Souza, A. C. B.; Barbosa, J. A. R. G.; de Freitas, S. M.; Pazos, I. F. Self-Homodimerization of an Actinoporin by Disulfide Bridging Reveals Implications for Their Structure and Pore Formation. *Sci Rep* **2018**, *8* (1), 6614. https://doi.org/10.1038/s41598-018-24688-2.

(24) Barbuddhe, S. B.; Vergis, J.; Rawool, D. B. Immunodetection of Bacteria Causing Brucellosis. In *Methods in Microbiology*; Elsevier, 2020; Vol. 47, pp 75–115. https://doi.org/10.1016/bs.mim.2019.11.003.

(25) Scheuermann, S.; Hambsch, B.; Hesse, L.; Stumm, J.; Schmidt, C.; Beher, D.; Bayer, T. A.; Beyreuther, K.; Multhaup, G. Homodimerization of Amyloid Precursor Protein and Its Implication in the Amyloidogenic Pathway of Alzheimer's Disease. *Journal of Biological Chemistry* **2001**, *276* (36), 33923–33929. https://doi.org/10.1074/jbc.M105410200.

(26) Bunkoczi, G.; Pasta, S.; Joshi, A.; Wu, X.; Kavanagh, K. L.; Smith, S.; Oppermann, U. Mechanism and Substrate Recognition of Human Holo ACP Synthase. *Chem Biol* **2007**, *14* (11), 1243–1253. https://doi.org/10.1016/j.chembiol.2007.10.013.

(27) Bob Bickler. *What is the Chemistry Behind Reversed-Phase Flash Chromatography?*. Biotage. https://selekt.biotage.com/blog/what-is-the-chemistry-behind-reversed-phase-flash-chromatography.

(28) Mayzel, M.; Ahlner, A.; Lundström, P.; Orekhov, V. Y. Measurement of Protein Backbone 13CO and 15N Relaxation Dispersion at High Resolution. *J Biomol NMR* **2017**, *69* (1), 1–12. https://doi.org/10.1007/s10858-017-0127-4.

(29) Felli, I. C.; Bermel, W.; Pierattelli, R. *Exclusively Heteronuclear NMR Experiments for the Investigation of Intrinsically Disordered Proteins: Focusing on Proline Residues*; preprint; Liquid-state NMR/Pulse-sequence development, 2021. https://doi.org/10.5194/mr-2021-37.

(30) Kleckner, I. R.; Foster, M. P. An Introduction to NMR-Based Approaches for Measuring Protein Dynamics. *Biochimica et Biophysica Acta (BBA) - Proteins and Proteomics* **2011**, *1814* (8), 942–968. https://doi.org/10.1016/j.bbapap.2010.10.012.

(31) *The Proteomics Protocols Handbook*; Walker, J. M., Ed.; Humana Press: Totowa, NJ, 2005. https://doi.org/10.1385/1592598900.

(32) Fischer, P. D.; Chowdhury, A. S.; Bartholow, T.; Basu, S.; Baggs, E.; Cox III, H. S.; Matosin, S.; Burkart, M.; Warner, L.; Nagarajan, R.; Arthanari, H. Carrier Protein Mediated Cargo Sensing in Quorum Signal Synthases. *Chem. Commun.* **2022**, 10.1039.D2CC03551K. https://doi.org/10.1039/D2CC03551K.

(33) Subramani, A.; Floudas, C. A. Structure Prediction of Loops with Fixed and Flexible Stems. *J Phys Chem B* **2012**, *116* (23), 6670–6682. https://doi.org/10.1021/jp2113957.

(34) Prince, A. S. 155 - Pseudomonas Aeruginosa. In *Principles and Practice of Pediatric Infectious Diseases (Fourth Edition)*; Long, S. S., Ed.; Elsevier: London, 2012; pp 842-846.e2. https://doi.org/10.1016/B978-1-4377-2702-9.00157-4.

(35) Agnihotry, S.; Pathak, R. K.; Singh, D. B.; Tiwari, A.; Hussain, I. Protein Structure Prediction. In *Bioinformatics*; Elsevier, 2022; pp 177–188. https://doi.org/10.1016/B978-0-323-89775-4.00023-7.

(36) Chung, J.; Goo, E.; Yu, S.; Choi, O.; Lee, J.; Kim, J.; Kim, H.; Igarashi, J.; Suga, H.; Moon, J. S.; Hwang, I.; Rhee, S. Small-Molecule Inhibitor Binding to an N-Acyl-Homoserine Lactone Synthase. *Proc Natl Acad Sci U S A* **2011**, *108* (29), 12089–12094. https://doi.org/10.1073/pnas.1103165108.

(37) Latifi, A.; Winson, M. K.; Foglino, M.; Bycroft, B. W.; Stewart, G. S. A. B.; Lazdunski, A.; Williams, P. Multiple Homologues of LuxR and LuxI Control Expression of Virulence Determinants and Secondary Metabolites through Quorum Sensing in Pseudomonas Aeruginosa PAO1. *Mol Microbiol* **1995**, *17* (2), 333–343. https://doi.org/10.1111/j.1365-2958.1995.mmi_17020333.x.

(38) Kosa, N. M.; R. W. Haushalter; A. R. Smith; M. D. Burkart. Reversible Chemoenzymatic Labeling of Native and Fusion Carrier Protein Motifs. Nat Methods 9, 981–984 (2012)., 2012.

(39) Podracky, C. J.; An, C.; DeSousa, A.; Dorr, B. M.; Walsh, D. M.; Liu, D. R. Laboratory Evolution of a Sortase Enzyme That Modifies Amyloid-β Protein. *Nat Chem Biol* **2021**, *17* (3), 317–325. https://doi.org/10.1038/s41589-020-00706-1.

(40) Barbe, V.; Cruveiller, S.; Kunst, F.; Lenoble, P.; Meurice, G.; Sekowska, A.; Vallenet, D.; Wang, T.; Moszer, I.; Médigue, C.; Danchin, A. From a Consortium Sequence to a Unified Sequence: The Bacillus Subtilis 168 Reference Genome a Decade Later. *Microbiology* **2009**, *155* (6), 1758–1775. https://doi.org/10.1099/mic.0.027839-0.

APPENDIX A

Protein Purification And Expression Optimizations

Introduction

Optimization studies for the the key players in quorum sensing (ACP1, RhlI, and C4-AHL for *P. aeruginosa*), and the enzymes used to produce these proteins (Sfp and AcpH) were conducted for titration studies. These proteins will be used in NMR data collection, visualizing the chemical shifts of ACP1 in complex with the AHLS enzyme RhlI for *P. aeruginosa*.

Introduction to Key Enzymes: RhlI, AcpH and Sfp

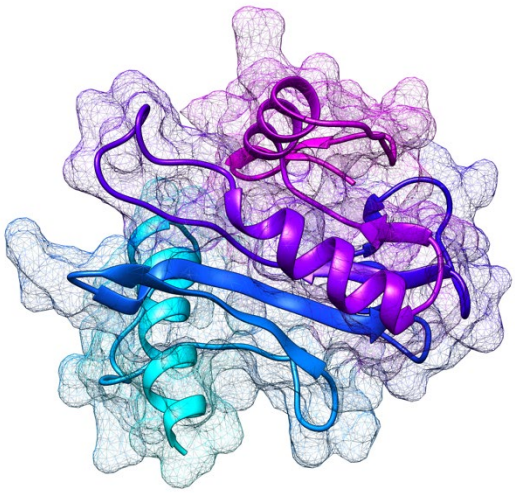

Figure A.1 Structural representation of the AHLS enzyme RhlI. RhlI is the natural AHLS enzyme for *P. aeruginosa* and ACP1. The purchased RhlI from ATUM contains a ~42.5 kDa His_6MBP tag connected by 3C that is not included in the model **[**5, 6, 7, 36].

RhlI is the natural AHLS enzyme for *P. aeruginosa* and ACP1, and aids in the production of AHL molecules. The MW for RhlI is ~22.5 kDa naturally, but the purchased construct of the enzyme from ATUM contains a His_6MBP tag (~42.5 kDa) connected by 3-chymotrypsin (3C) that was not included in the model above (Figure A.1). The total molecular weight of His_6MBP-RhlI enzyme is 67.97 kDa, and attempts to cleave the His_6MBP tag were made for NMR data collection.

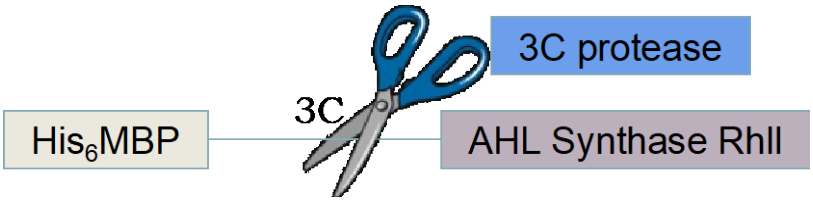

Figure A.2 Structural representation of the AHLS enzyme RhlI. RhlI is ~22.5 kDa enzyme naturally [37]. The purchased RhlI from ATUM contains a ~42.5 kDa His6MBP tag connected by 3C. Attempts to cleave the His_6MBP tag were made with 3C protease in this study, but ultimately was unsuccessful. A His6MBP tag control was used for NMR analysis.

The purchased construct of RhlI from ATUM contains a His_6MBP tag connected by 3-chymotrypsin (3C) (Figure A.2). To reproduce a natural environment for ACP1 and RhlI, an attempt to remove the His_6MBP tag by cleaving the 3C linkage with 3C protease was made, but ultimately was unsuccessful. His_6MBP tag was therefore isolated to be used as a control for the natural reaction of ACP1 and RhlI. The control His_6MBP tag will be titrated into with ACP1 to confirm there is no adverse reaction to the tag.

AcpH and Sfp are the enzymes used to convert apo-ACP1 to holo-ACP1 and vice versa. Sfp is also used for cargo loading acyl groups onto apo-ACP [8]. Production optimization was conducted for these enzymes, but the enzyme used in Chapter Two were previously provided.

Materials and Methods

Expression and Purification of His_6MBP-RhlI

Escherichia coli BL21 (DE3) cells were transformed with pD441-NH plasmid (ATUM) encoding the RhlI protein from *P. aeruginosa* with a His_6MBP tag. Cells were plated on Luria-Bertani (LB)-agar with 1 mM kanamycin selection. Several colonies were used to inoculate 5 mL of LB supplemented with 1 mM kanamycin and grown overnight at 37 °C, shaking at 250 rpm. The 5 mL culture was then inoculated into a larger 1 L LB

broth culture with 1mM kanamycin. The 1 L culture incubated at 37 °C, 250 rpm and left to grow until reaching an OD_{600} = 0.6-0.8. A pre-induced sample was collected for SDS-PAGE analysis. The remaining culture was induced with 0.5 mM IPTG and left to incubate overnight at 30 °C, 250 rpm. A 1 mL induced sample was collected for SDS-PAGE analysis. The remaining induced cells were harvested through centrifugation, and frozen for at least 30 min prior to lysing. The harvested pellets were lysed with B-PER complete, 1 mM lysozyme, 1 mM DNase and ½ tablet Pierce™ protease inhibitor and left to incubate at room temperature for 30 min before centrifugation for 45 min at 20,000×g. The protein filled supernatant was filtered with a 0.45 μm polyethersulfone syringe filter and was purified using affinity chromatography (MBPTrap™ HP 5 mL column) on an ÄKTA Start instrument (Cytiva). The column was equilibrated before sample loading and was washed with 10 CV of amylose column A buffer (20 mM Tris HCl, 200 mM NaCl, 1 mM EDTA, pH 7.4) before the sample was eluted off the column into 5 mL fractions with 10 CV of amylose elution B buffer (20 mM Tris HCl, 200 mM NaCl, 1 mM EDTA, 10 mM maltose pH 7.4). Fractions containing the desired protein from the purification can be seen using the UV visual chromograph measured at 280 nm and confirmed using a 12% sodium dodecyl sulfate–polyacrylamide gel electrophoresis (SDS PAGE). Fractions containing purified protein were pooled, concentrated using a 10,000 MWCO centrifugal concentrator (Sartorius) and aliquoted (Figure A.3). Aliquots were flash frozen in liquid nitrogen and stored at -80°C before enzymatic reactions.

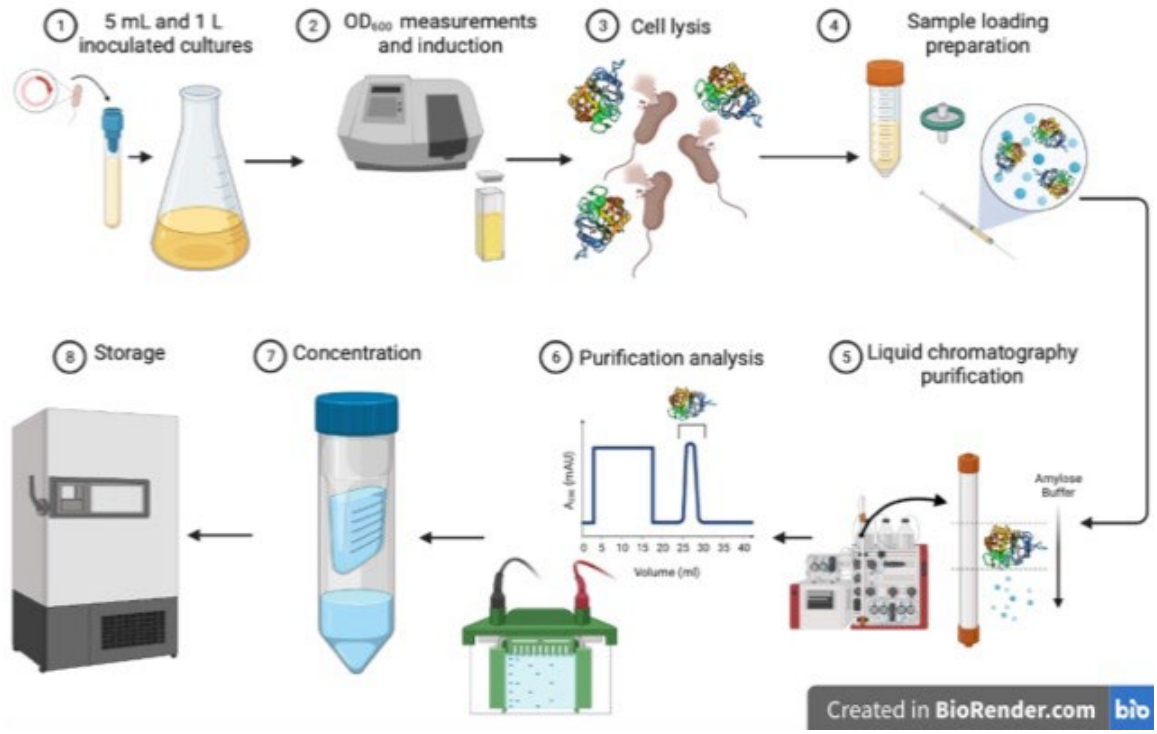

Figure A.3 Protein expression and purification for RhlI.

1) Plasmid encoding RhlI was transformed and inoculated into LB culture until 2) the culture reached an OD_{600} between 0.5-0.8 and was induced. 3) Cells are then lysed and 4) clarified prior to 5) affinity chromatography purification. 6) Protein is then analyzed before 7) concentration and 8) storage. [Adapted from "Protein Overexpression and Purification from Bacteria", by BioRender.com (2020). Retrieved from https://app.biorender.com/biorender-templates].

Optimization of 3C Cleavage of His_6MBP-RhlI

Optimization for the His_6MBP tag cleavage of His_6MBP-RhlI used human rhinovirus (HRV) 3C protease. Cleavage optimization tested the need for dialysis into a HRV 3C buffer, purchased vs. produced 3C protease products, pH levels, incubation temperature and time, and the concentration of 3C protease in the sample. Results indicated that cleavage of the His_6MBP tag from His_6MBP-RhlI promotes the enzyme to precipitate, and that cleaved His_6MBP needed to be used as a control for NMR data analysis. Cleavage for the His_6MBP tag was perceived to be optimized at 30 °C in D-HRV-3C buffer at pH 7.4 at least overnight. These results also indicate that removal of

the His_6MBP will most likely not reach completion and His_6MBP-RhlI will remain in the reaction, requiring further purification.

Expression and Purification of AcpH

E. coli BL21 (DE3) cells were transformed with pET29b-AcpH (ATUM) using an individual colony for growth. Transformed cells were preserved in a glycerol cell stock before the expression and purification process. Cells were grown to saturation in a 5 mL LB broth at 37 °C, 250 rpm, and inoculated into a larger 1 L LB culture under the same conditions until OD_{600} = 0.5-0.8 was reached. The culture was then induced using 1 mM IPTG before incubating overnight at 16 °C, 250 rpm. Cells were harvested through centrifugation, and frozen for at least 30 min prior to lysing. The harvested pellets were resuspended with lysis buffer (50 mM Tris HCl, 100 mM NaCl, 5% glycerol, 5 mM BME, and 1 mM Imidazole) mixed with 1 mM lysozyme, 1 mM DNase, and ½ tablet Pierce™ protease inhibitor. Sonication was used for lysis with a Fisherbrand™ Model 705 Sonic Dismembrator (Fisher Scientific), alternating pulses for 9 min in 30 sec on/off steps (total 18 min). The protein was separated from cell debris through centrifugation before filtration with a 0.45 μm polyethersulfone syringe and purification using immobilized nickel affinity chromatography (HisTrap™ HP 1 mL column on an ÄKTA Start instrument [Cytiva]) and imidazole. The affinity chromatography column was washed with 10 CV of I20 buffer before the sample was eluted off the column into 1.5 mL fractions with 10 CV of I200 buffer. Fractions containing the desired protein from the purification can be seen using the Ultra-Violet (UV) chromogram measured at 280 nm and confirmed using a 12% SDS PAGE. Fractions containing purified protein pooled and concentrated using a 10,000

MWCO centrifugal concentrator (Sartorius) before further purification using size SEC on a HiLoad™ Superdex™ 75 pg (Cytiva) (Figure A.4).

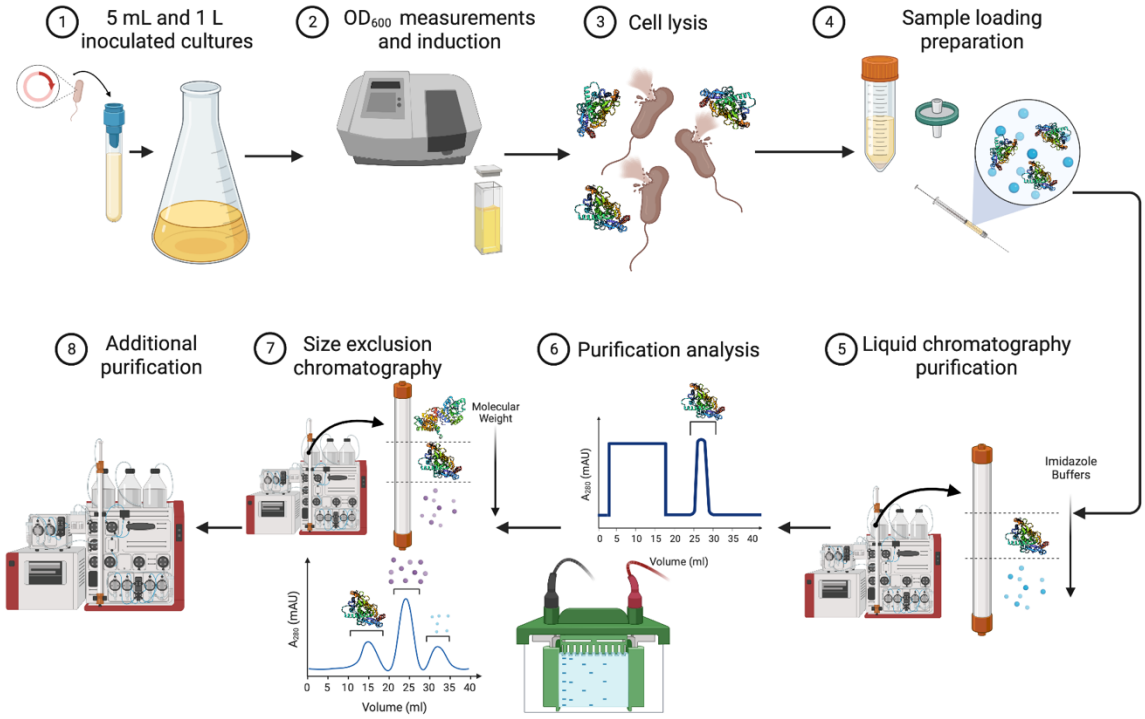

Figure A.4 Protein expression and purification for AcpH.

1) Plasmid encoding AcpH was transformed and inoculated into LB culture until 2) the culture reached an OD_{600} between 0.5-0.8 and was induced. 3) Cells are then lysed with sonication and 4) clarified prior to 5) affinity chromatography purification. 6) Protein is then analyzed before 7) being further purified using size exclusion chromatography (SEC). 8) Additional purifications are required to clean the sample before concentration. [Adapted from "Protein Overexpression and Purification from Bacteria", by BioRender.com (2020). Retrieved from https://app.biorender.com/biorender-templates].

Fractions containing purified protein were again identified using 12% SDS PAGE, pooled, and concentrated using a 10,000 MWCO centrifugal concentrator (Sartorius). Aliquots were stored in a 4°C for future use.

Expression and Purification of Sfp

Transformed *E. coli* BL21 (DE3) cells encoding the Sfp enzyme for *B. subtilis* was provided by BURKART [38]. Transformed cells were preserved in a glycerol cell stock before the expression and purification process. Cells were grown to saturation in a 5 mL LB broth at 37 °C, 250 rpm, and inoculated into a larger 1 L LB culture under the same conditions until OD_{600} = 0.5-0.8 was reached. The culture was then induced using 0.5 mM IPTG, grown for 3 hours at 37 °C and harvested through centrifugation and frozen for at least 30 min prior to lysing. The harvested pellets were resuspended with lysis buffer mixed with 1 mM lysozyme, 1 mM DNase, and ½ tablet Pierce™ protease inhibitor. Sonication was used for lysis with a Fisherbrand™ Model 705 Sonic Dismembrator (Fisher Scientific), alternating pulses for 9 min in 30 sec on/off steps (total 18 min). The protein was separated from cell debris through centrifugation before filtration with a 0.45 μm polyethersulfone syringe and purification using immobilized nickel affinity chromatography (HisTrap™ HP 1 mL column on an ÄKTA Start instrument [Cytiva]) and imidazole. The affinity chromatography column was washed with 10 CV of I20 buffer before the sample was eluted off the column into 1.5 mL fractions with 10 CV of I200 buffer. Fractions containing the desired protein from the purification can be seen using the Ultra-Violet (UV) chromogram measured at 280 nm and confirmed using a 12% SDS PAGE. Fractions containing purified protein pooled and concentrated using a 10,000 MWCO centrifugal concentrator (Sartorius) before further purification using size SEC on a HiLoad™ Superdex™ 75 pg (Cytiva) (Figure A.5).

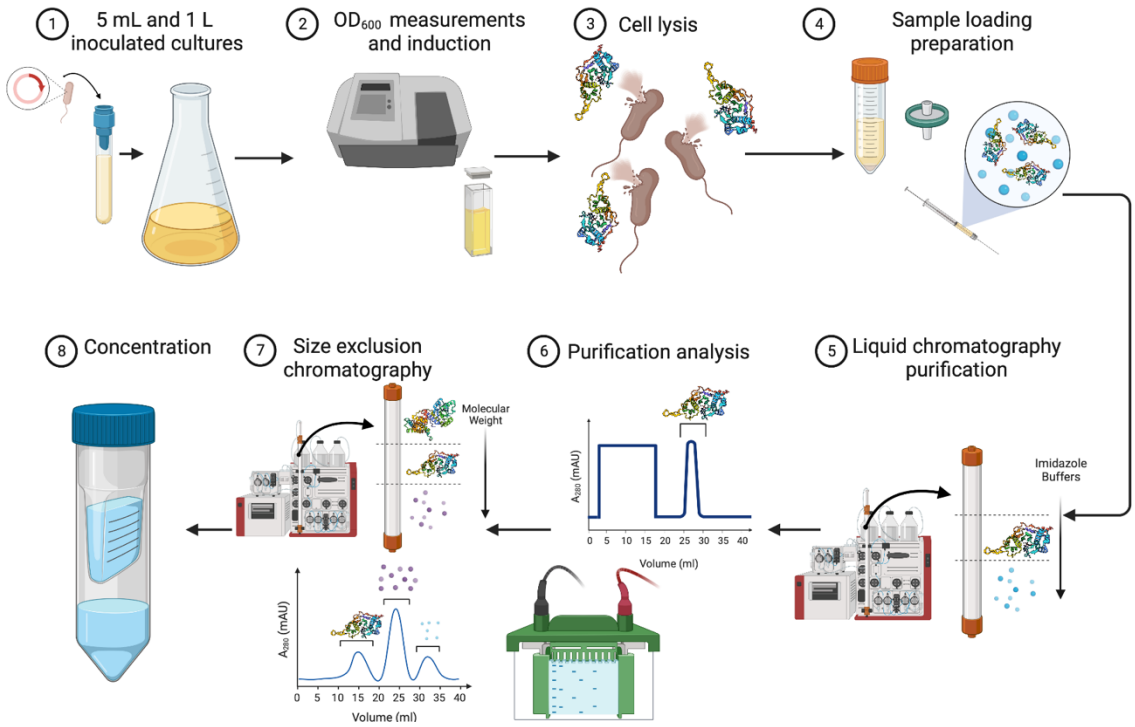

Figure A.5 Protein expression and purification for Sfp.

1) Plasmid encoding Sfp was transformed and inoculated into LB culture until 2) the culture reached an OD_{600} between 0.5-0.8 and was induced. 3) Cells are then lysed with sonication and 4) clarified prior to 5) affinity chromatography purification. 6) Protein is then analyzed before 7) being further purified using size exclusion chromatography (SEC) and 8) concentrated. [Adapted from "Protein Overexpression and Purification from Bacteria", by BioRender.com (2020). Retrieved from https://app.biorender.com/biorender-templates].

Fractions containing purified protein were again identified using 12% SDS PAGE, pooled, and concentrated using a 10,000 MWCO centrifugal concentrator (Sartorius). Aliquots were stored in a 4°C for future use.

Expression and Purification of ^{15}N ACP1

Expression and purification of isotope enriched proteins for NMR studies in an *E. coli* platform requires growth of the bacteria and expression in a defined medium. M9 medium is a salt based medium derived from the laboratory manual provided by Miller et. al. [18]. The medium is used to isotopically enrich atoms in proteins such as ^{2}H, ^{13}C,

and ^{15}N by preparing the medium with isotopes as the sole source. ^{15}N ACP1 production used ^{15}N-ammonium chloride as an enriched medium and the sole source nitrogen to isotopically enrich the ACP1 protein. Isotopic enrichment is necessary for NMR studies because ^{14}N are not magnetically active, and signals are not strong enough for the NMR instrument [15]. Single isotopes of ^{15}N vs. ^{13}C, ^{15}N enriched proteins are used for titrations because only the ^{15}N HSQC spectra is required for to see chemical shift perturbations. The previously assigned spectra will be used for peak assignments based on minimal chemical shift perturbations.

Several batches of ^{15}N ACP1 were produced for future titrations of apo-ACP1, C4I-ACP1, C6I-ACP1, and both C4I-ACP1 and C6I-ACP1 in complex with RhlI. ^{15}N ACP1 was expressed and purified using the same methods and materials as ^{13}C, ^{15}N ACP1, with the exception of the M9 minimal media broth. The 1 L isotopically labeled ^{15}N M9 minimal media broth contained 20% Glucose, 0.5 g/L ^{15}N-ammonium chloride, 0.5 g/L ^{15}N-isogro, 1 mM magnesium sulfate, 0.3 mM calcium chloride, 1 mM biotin,1 mM thiamin, 10 mL 100×trace element, 100 mL 10×M9 salt, 1 mM kanamycin.

Results and Discussion

Expression and Purification of His_6MBP-RhlI Results

His_6MBP-RhlI can be a sensitive protein to grow and express. Previous research showed that the ideal temperature for induction was 30 °C overnight with 0.5 mM IPTG. Several batches were used for this research and a representative chromograph and 12% SDS PAGE gel image is used as an example (Figure A.6). All of the batch figures can be found in APPENDIX : His6MBP-RhlI. All of the batches have similar chromatograms as Figure A.6 (a) and 12% SD PAGE images as Figure A.6 (b). Figure A.6 (a) shows the

loading of the sample as a block at the beginning of the UV measurements (280 nm). Then a singular peak is seen following which is indicative of the protein elution. In Figure A.6 (a) the sample is loaded at 37 mL to 73 mL and eluted at 118 mL or the end of fraction 2. The protein is confirmed in Figure A.6 (b) with the strongest bands of RhlI (67.97 kDa) seen in fractions 2 and 3. For this sample, fractions 2-4 were pooled and concentrated. Additional bands near the 40 kDa mark are most likely His_6MBP, which is ~42.5 kDa alone [37].

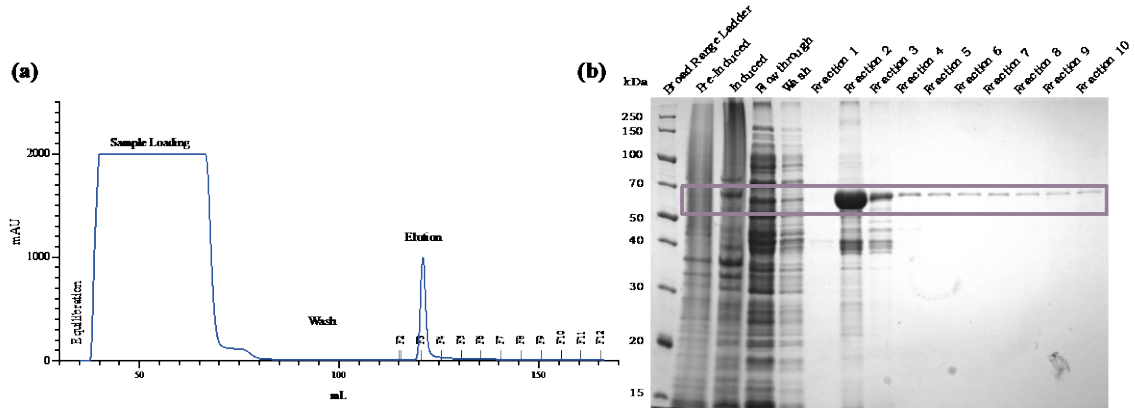

Figure A.6 Example Affinity Column Chromatography His_6MBP-RhlI purification.

ÄKTA Start Affinity Column (MBPTrap™) Chromatography is used to purify His_6MBP-RhlI (67.97 kDa), and can be seen in the **(a)** chromatogram and **(b)** 12% SDS PAGE mostly in fractions 2 – 4.

Optimization and 3C Cleavage of His_6MBP-RhlI Results

A portion of the purified His_6MBP-tagged RhlI was used to optimize the 3C cleavage reaction with HRV 3C protease. Figure A.7 (a) tested the need for dialysis from the amylose buffer after affinity chromatography, into a D-HRV-3C (0.05 mM Tris HCL, 300 mM NaCl, 1 mM DIT and pH 7.5) and the quality of an "in-house" 3C protease (~35.4 kDa) vs. a store bought 3C protease (~47.8 kDa). Glutathione S-transferase (GST) was used as a control to test the quality of in-house vs. store bought cleavage. The results for

pre- and post-dialysis into the D-HRV-3C buffer were the same, indicating there is no need for dialysis. The in-house 3C protease cleaved more RhlI with weaker bands where the whole His_6MBP-RhlI (67.97 kDa) protein should be. Figure A.7 (b)-(c) tested the optimal pH level of the 3C protease reactions, ranging from pH 6.6-8.0. Control without 3C protease (- 3C) was used to compare with reactions contained 3C protease (+ 3C). Lower pH levels show stronger bands for the His_6MBP tag at ~42.5 kDa. A pH of 7.4 was considered ideal for constancy from the amylose buffer and is comparable to 7.2, 7.0, 6.8 and 6.6 pH levels. Figure A.7 (d) examines the time required for 3C protease reaction to occurs with samples taken after 6 hrs and overnight (O/N) at lower pH levels. While 6-hour reactions are ideal with stronger bands for the His_6MBP tag at ~42.5 kDa, overnight show evidence of 3C cleavage with ~42.5 kDa bands. Figure A.7 (e) reviewed the concentration of 3C protease to see if the reaction could reach completion. Larger quantities of 3C protease did not have an effect on the reaction, implying the reaction will not reach completion with more 3C protease. Figure A.7 (f) is an example reaction of the ideal 7.4 pH at a lower temperature of 30 °C. This reaction shows there is 3C cleavage at lower temperatures with a band ~42.5 kDa.

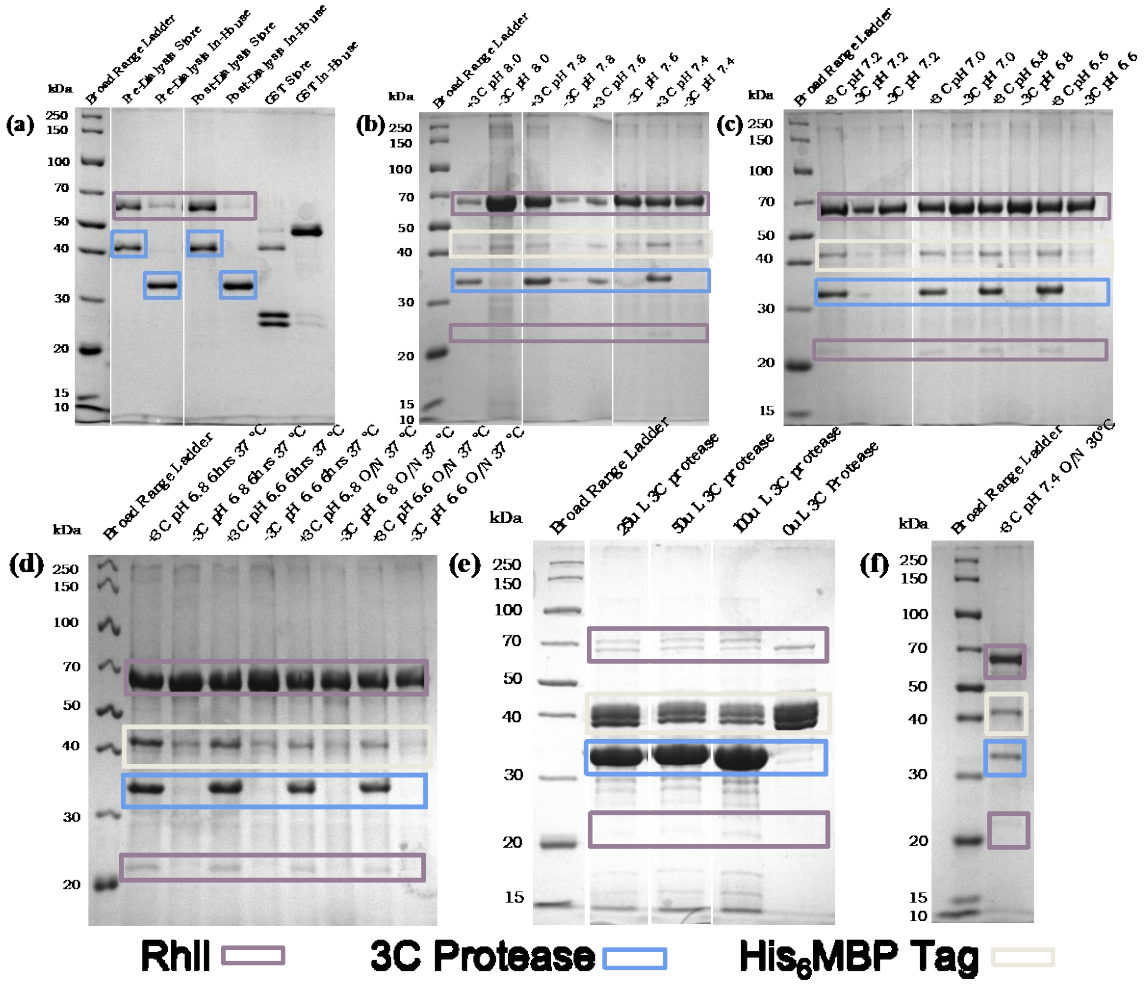

Figure A.7 Optimization of His_6MBP-RhlI/3C protease reaction. His_6MBP-RhlI as a whole is 67.97 kDa, RhlI alone is ~22.5 kDa and His_6MBP alone is ~42.5 kDa [37]. **(a)** His_6MBP-RhlI dialysi optimization and quality test of 3C protease produced in-house. **(b)** and **(c)** D-HRV-3C buffer pH level optimization. **(d)** 3C protease rection time optimization **(e)** Saturation of 3C protease for reaction completion optimization **(f)** His_6MBP-RhlI/3C protease reaction with pH 7.4 D-HRV-3C buffer overnight at 30 °C.

3C Cleavage of the His_6MBP Tag Results

For 3C cleavage of the His_6MBP tag, 280 µL of 76 µM His_6MBP-RhlI was mixed with 2 mL D-HRV-3C buffer and 100 µL of 1.49 mM 3C protease made in-house. This was left to incubate in a 34 °C water bath for ~48 hours before a 12% SDS PAGE gel was used to confirm cleavage. Cleavage can be seen in a band at ~42.5 kDa in Figure A.8.

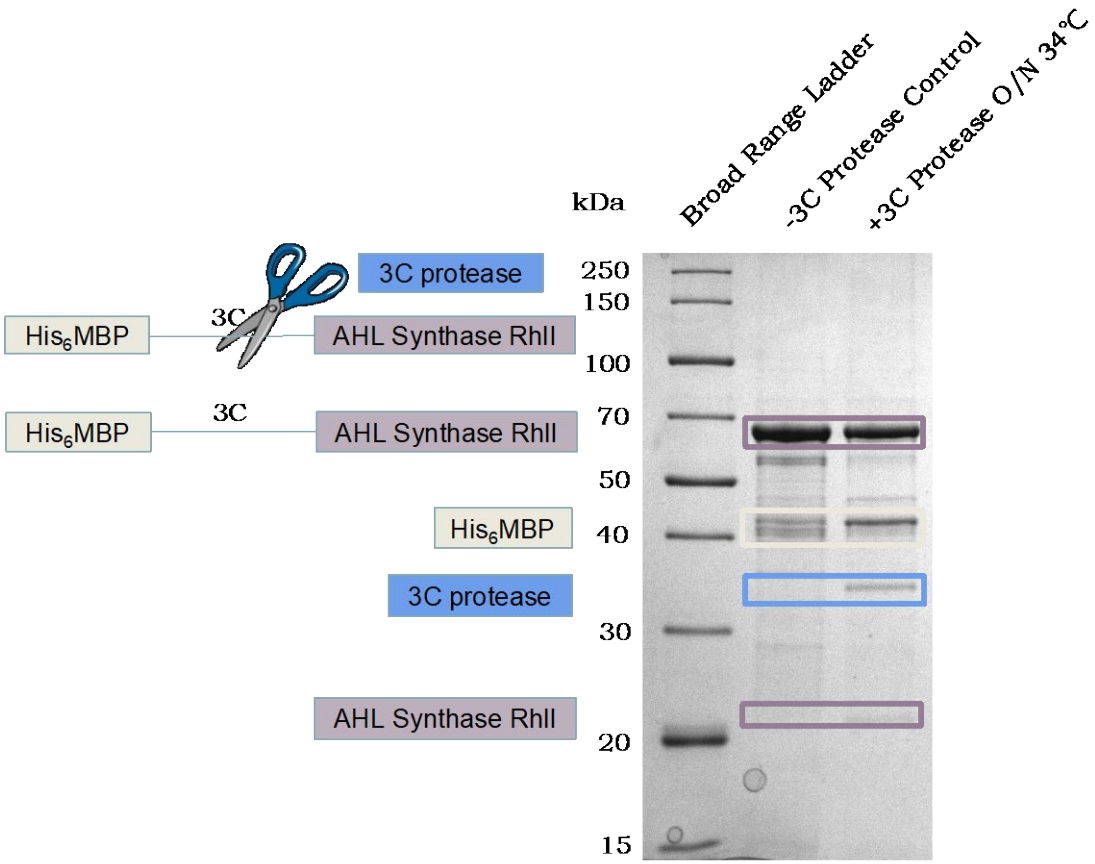

Figure A.8 Example His_6MBP-RhlI/3C protease reaction.
This is an example of the optimized His_6MBP-RhlI/3C protease reaction with D-HRV-3C buffer at pH 7.4 and at 30 °C overnight. The His_6MBP-RhlI as a whole is 67.97 kDa and RhlI alone is ~22.5 kDa as outlined in purple. His_6MBP alone is ~42.5 kDa and can be seen in the beige outline [37]. The in-house made 3C protease is 35.4 kDa and is outlined in blue.

After ~36 hours, the 3C reaction was loaded onto a 1 mL Ni-NTA HisTrap™ column on an ÄKTA Start instrument with 10 CV I20 buffer and eluted with 10 CV of I200 buffer. The chromatogram of this purification and resulting 12% SDS PAGE can be seen in Figure A.9 (a)-(b). The chromatogram with UV measurements at 280 nm showed unusual loading peaks because the concentration of the sample was low (76 µM before the reaction). The elution peak of the chromatogram was also unusual because the peak did not return to the baseline UV, but remained high. The 12% SDS PAGE was used to confirm

the elution fractions from the column. The His_6MBP tag can be seen in fractions 2-4 from the purification at ~42.5 kDa. There fractions were pooled and dialyzed out of the I200 buffer and into the ACP NMR buffer.

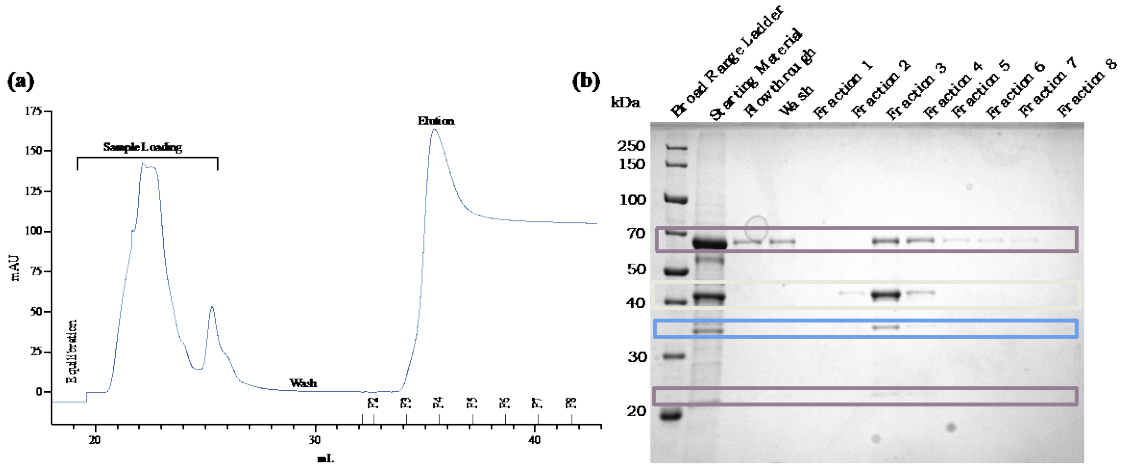

Figure A.9 Example Nickel Column Chromatography His_6MBP tag purification. His_6MBP tags are cleaved from His_6MBP-RhlI to be used as a control for NMR data analysis. ÄKTA Start Nickel Column (HisTrap™) Chromatography is used to purify the His_6MBP tags after the 3C protease reaction. Tags can be seen in the **(a)** chromatogram and **(b)** 12% SDS PAGE as a first step of purification.

Because of the remaining whole His_6MBP-RhlI in the fractions, SEC on a HiLoad™ Superdex™ 75 pg (Cytiva) was used to separate the 67.97 kDa His_6MBP-RhlI from the cleaved ~42.5 kDa His_6MBP tag (Figure A.10). The chromatogram from the SEC shows a smaller peak from fractions B5-B10. In accordance with the 12% SDS PAGE (Figure A.10 (b)), the smaller fraction contains the His_6MBP tag with the same ~42.5 kDa bands in fractions B5-B10. The larger peak is most likely the 3C protease because it is smaller in size, but is not visualized in the 12% SDS PAGE image. Fractions containing purified tag pooled, and concentrated using a 10,000 MWCO centrifugal concentrator (Sartorius). Aliquots were flash frozen in liquid nitrogen and stored at -80°C before enzymatic reactions.

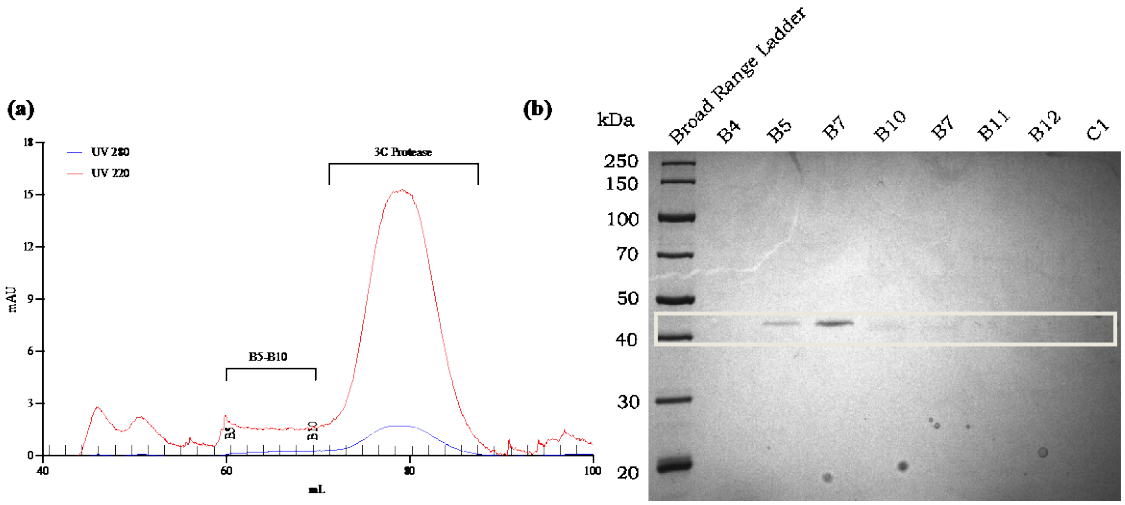

Figure A.10 Example SEC His_6MBP tag purification.
ÄKTA Pure 25 SEC with UV detection at 280 nm (blue) and 220 nm (red) show isolated His_6MBP tags in the **(a)** chromatogram and **(b)** 12% SDS PAGE were used as a second method of purification for the His_6MBP tags and to separate the tags from the retained His_6MBP-RhlI.

Expression and Purification of AcpH Results

AcpH was purified as described above, with fractions visually displayed using 12% SDS PAGE. The chromatogram for the affinity column was measured at 280 nm and shows sample loading from 11 mL to 54 mL Figure A.11 (a). A strong elution peak at 62 mL and fraction 3, corresponds to Figure A.11 (b). Figure A.11 (b) has the strongest bands overall in this fraction and bands at ~67 kDa. Bands at ~67 kDa can be seen in all of the fractions, along with several other bands, indicating the need for a second round of purification.

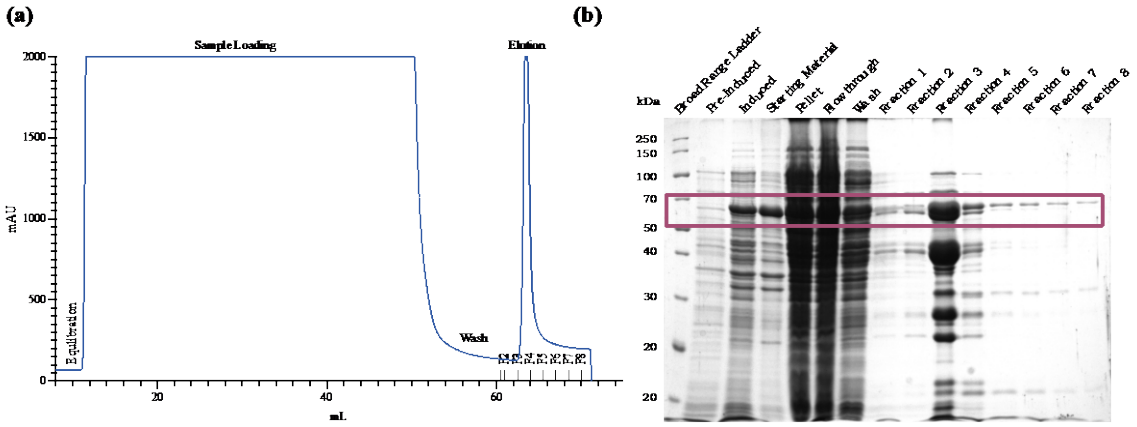

Figure A.11 AcpH affinity chromatography purification.
AcpH purification used ÄKTA Start Nickel Column (HisTrap™) Chromatography **(a)** chromatogram and corresponding **(b)** 12% SDS PAGE. AcpH is ~67 kDa and can be found mostly in fractions 1 through 8 from the chromogram and gel image.

All fractions were pooled for a more purification using SEC (Figure A.12). The SEC chromatogram (Figure A.12 (a)) shows serval peaks measured at 220 nm. The first, smallest peak has weaker bands at ~67 kDa, but the second middle peak shows stronger bands at ~67 kDa, (Figure A.12 (b)). This indicates the protein are in are in both peaks or fractions A8-B6. Because the sample is still impure, the two peaks and delay in elution could be from other impurities. The last, largest peak are smaller imidazole molecules and other small impurities according to the corresponding 12% SDS PAGE. Because of the impurities in the fractions, fractions containing the AcpH protein were pooled and stored for further purification and optimization experiments. Likely, the protein will be purified again using immobilized nickel affinity chromatography.

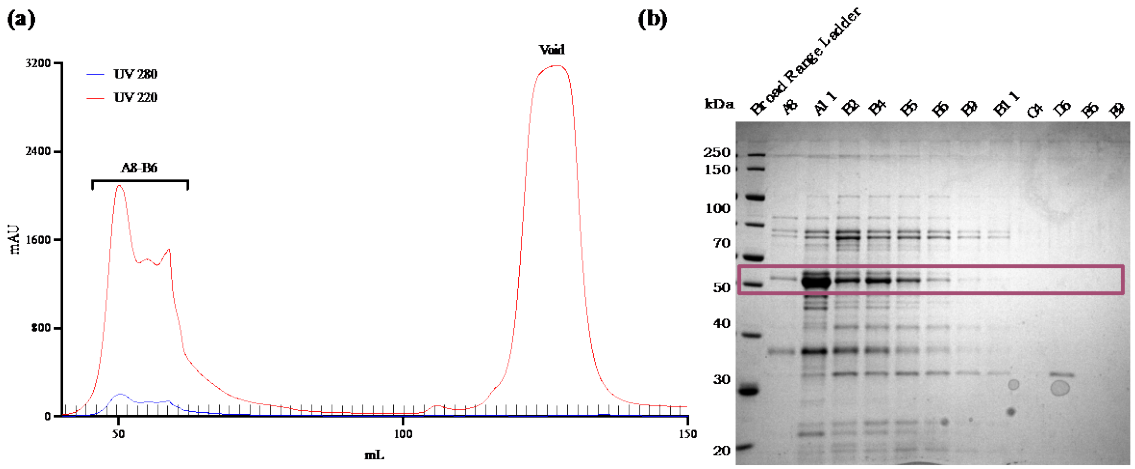

Figure A.12 SEC AcpH purification.
ÄKTA Pure 25 SEC with UV detection at 280 nm (blue) and 220 nm (red) show impure AcpH. In the **(a)** chromatogram and **(b)** 12% SDS PAGE, AcpH are in wells A8 - B6 in a 96-well block.

Expression and Purification of Sfp Results

Sfp was purified as described above, and the final concentration for Sfp was calculated with a thermo scientific NanoDrop One, using the protein analysis A280 program. The extinction coefficient and molecular weight used for calculation was 27.22 Ɛ/1000 and 26.10 kDa [39 - 40], with the final concentration of 30mM. The chromatogram from the affinity chromatography column shows sample loading from 11 mL to 54 mL (Figure A.13 (a)). There are two elution peaks because the sample wash and fractions 1 and 2 were combined (first peak) before the fractionation occurred (second peak). Figure A.13 (b) show strong Sfp bands at 26.10 kDa in the wash + fractions 1—2 and fractions 3-8. These fractions and the wash we pooled and concentrated for purification to remove impurities.

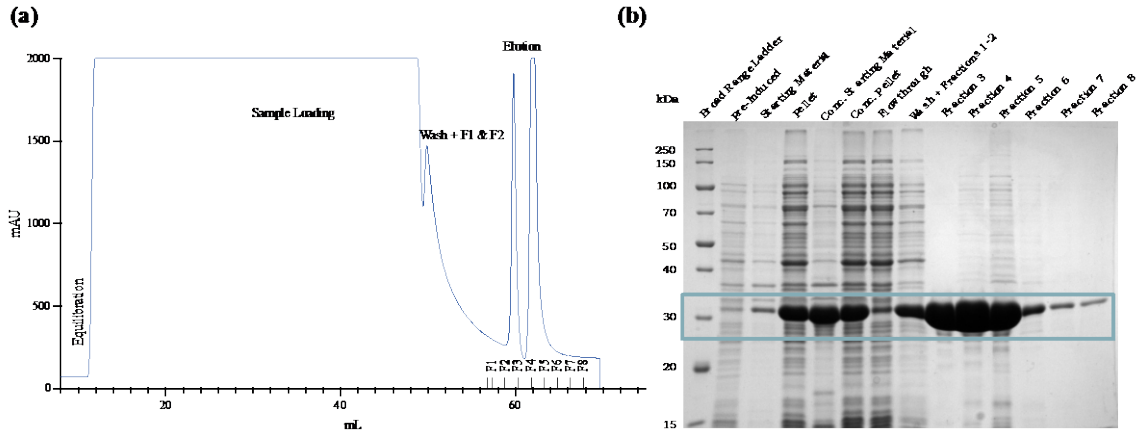

Figure A.13 Sfp affinity chromatography purification.
Sfp purification used ÄKTA Start Nickel Column (HisTrap™) Chromatography **(a)** Chromatogram and corresponding **(b)** 12% SDS PAGE. Sfp is 26.10 kDa and can be found mostly in the wash with fractions 1-2 and in fractions 3-8 from the chromograph and gel image.

Figure A.14 (a) shows the chromatogram for the SEC. There are three peaks at fractions A6-A11, fractions B7-C3 and fraction D8-E12. The first two peaks contain bands at 26.10 kDa. It appears that some Sfp protein elutes in the smaller peak, and the elutes even further in the middle peak. This delay in elution could be from the formation of dimers or binding of contaminant proteins, but further research would need to be conducted. The largest peak from D8-E12 are smaller impurities.

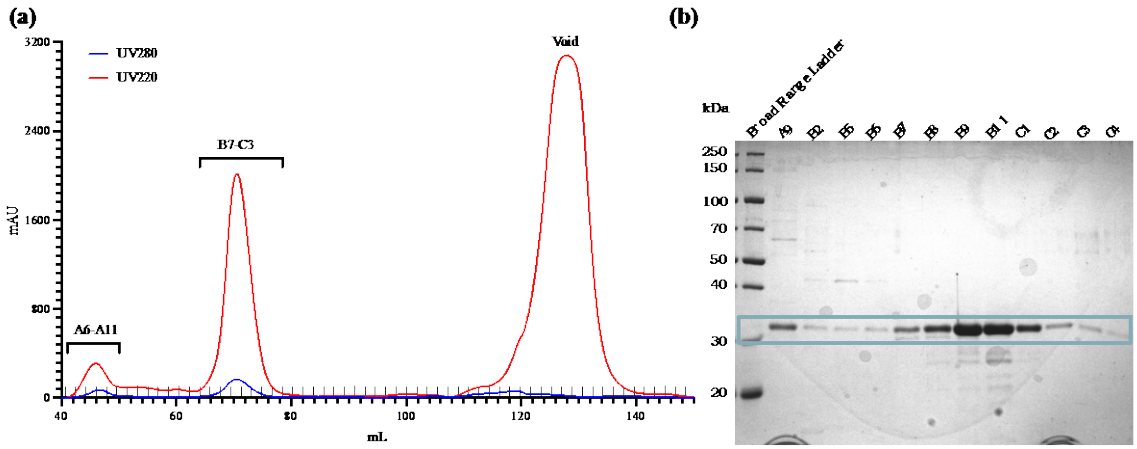

Figure A.14 SEC Sfp purification.
ÄKTA Pure 25 SEC with UV detection at 280 nm (blue) and 220 nm (red) show isolated Sfp. In the **(a)** chromatogram and **(b)** 12% SDS PAGE, Sfp can be seen in fractions A6-A11 and B7-C3 from the 96-well block. These fractions were pooled and stored for future use.

Expression and Purification of Single Labeled ACP1 Results

Several batches of ^{15}N ACP1 were produced. Additional figures for all ^{15}N ACP1 can be found in APPENDIX : Single Labeled ACP1 ^{15}N. An example figure for immobilized nickel affinity chromatography (Figure A.15) and ÄKTA Pure 25 SEC (Figure A.16) are used to describe the production of ^{15}N ACP1. Figure A.15 (a) shows the UV 280 nm chromatogram from the ^{15}N ACP1 affinity chromatography. The sample is loaded onto the column from 22 mL to 54 mL, and a small elution peak is seen at 64 mL or fraction 3. This sample had instrumentation difficulties, where the sample was not completely loaded, and had to manually be loaded onto the column. This is why there is a dip in the sample loading peak. The elution peak is smaller in size and shows the concentration is probably lower than the typical purification. The elution peak corresponds to the 16% Tris Tricine PAGE (Figure A.15 (b)) with the strongest ~10 kDa peak for ACP1 seen in fractions 3. Weaker bands can be seen on fractions 2 and 4, and we pooled for further purification.

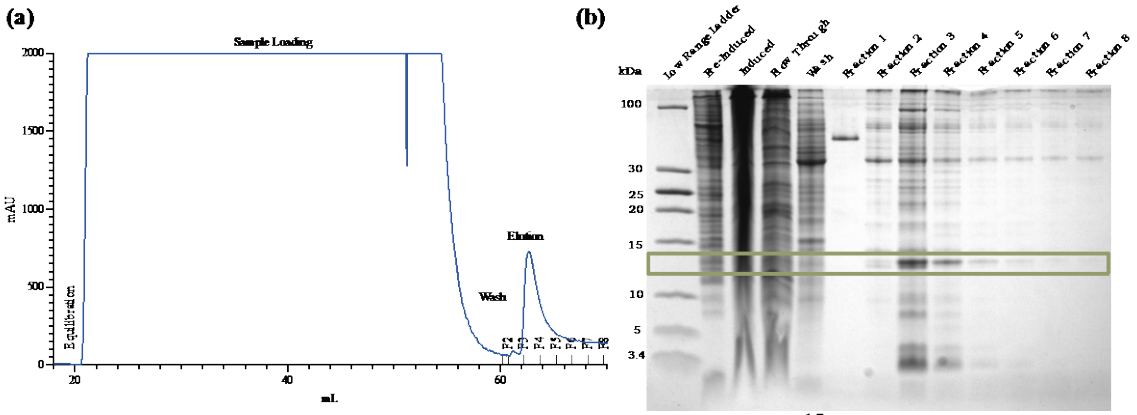

Figure A.15 Example Nickel Column Chromatography ^{15}N ACP1 purification. An example ÄKTA Start Nickel Column (HisTrap™) Chromatography **(a)** Chromatogram and corresponding **(b)** 16% Tris Tricine Gel for single labeled ACP1. ACP1 is ~10 kDa and can be found mostly in fractions 2 - 4 from the chromograph and gel image.

Figure A.16 (a) shows the UV 220 nm (red) chromatogram from SEC. Multiple peaks can are shown with larger impurities eluting from fractions A7-B5 and smaller impurities eluting from fractions E3-E9. The ACP1 protein is found in the peak from fractions B7-C1 according the 16% Tris Tricine PAGE Figure A.16 (b), with isolated bands at ~10 kDa. There is a weaker peak from fractions C2-C8, but the 16% Tris Tricine PAGE shows a weak ~10 kDa in the C7 fraction. This peak was not included in the sample before apo-ACP1 conversion. The multiple peaks suggest dimers of ACP1 form by disulfide bridges from the sulfur atoms on the cystine (21Cys) residues [23].

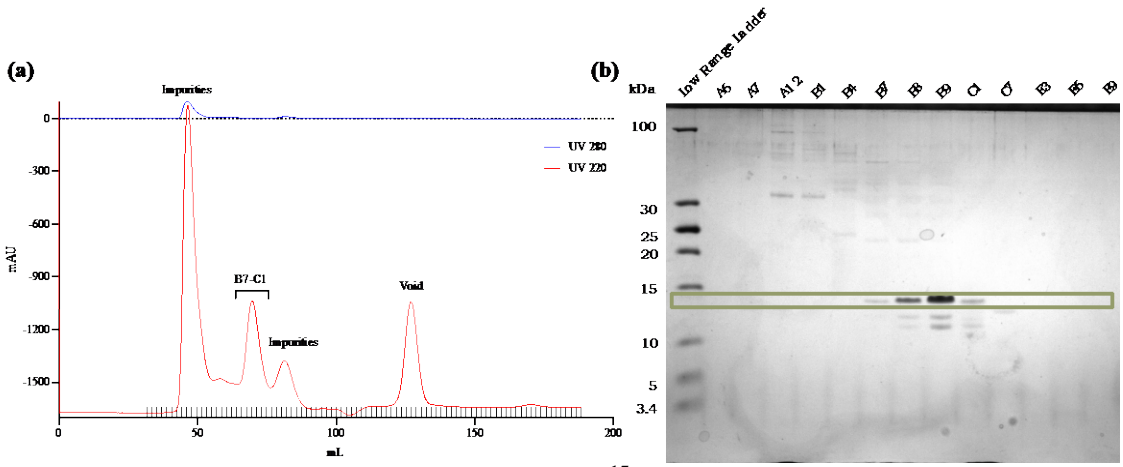

Figure A.16 Example SEC ^{15}N ACP1 purification.
ÄKTA Pure 25 SEC with UV detection at 280 nm (blue) and 220 nm (red) show isolated ^{15}N ACP1 in holo- and apo- form. In the **(a)** chromatogram and **(b)** 16% Tris-Tricine PAGE, ACP can be in wells B7 - C1 in a 96-well block. These fractions were pooled and stored for future use.

Batch 1 of the ^{15}N labeled ACP1 was produced as above. Batches 2-4 were made together and combined during SEC. Batches 2-4 also had difficulty growing and required 24 hours of growth to reach a range of OD_{600} measurements (0.897, 1.19, and 0.519 respectively) before induction. During purification of batch 4 on an ÄKTA Start instrument (Cytiva), the instrument relayed pressured errors and product was lost in the process. Batches 2-4 were pooled to get for SEC for a combined volume of 5mL. To accommodate for the large sample volume, the sample was loaded onto the column twice ~2.5 mL each time. Batches 5-7 were grown at the same time, but kept separated until SEC. During purification of batch 5, the instrument relayed pressured errors and product was lost in the process. The product appeared to elute in the fraction and with a final wash with 6 mL of I200. All fractions from the batch 5 purification were pooled and combined with factions 2-4 from batches 6 and 7 for SEC.

Holo- and Apo-ACP1 Conversion and Purification of ^{15}N ACP1 Results

Initial results from the UHPLC data suggested that the ^{15}N ACP1 produced was already significantly in apo-ACP1 form (Figure A.17) because of the retention times for all peaks appear after the 10 min mark.

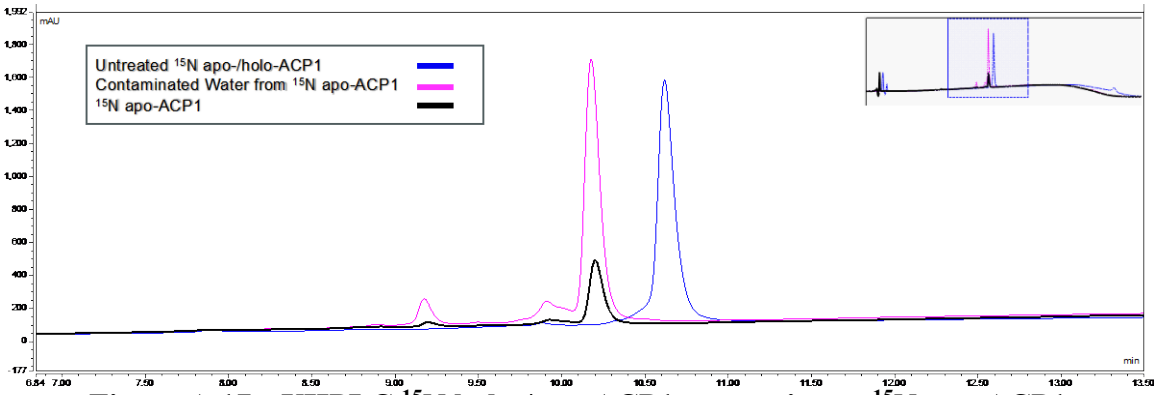

Figure A.17 UHPLC ^{15}N holo-/apo-ACP1 conversion to ^{15}N apo-ACP1 chromatograms.
An untreated ^{15}N holo-/apo-ACP1 UHPLC chromatogram (blue) compared to AcpH treated ^{15}N apo-ACP1 UHPLC chromatogram (black). Peak retention appears around the 10 min 40 sec mark for ^{15}N holo-/apo-ACP1 and around the 10 min 15 sec mark for ^{15}N apo-ACP1.

The AcpH and Sfp experiments conducted for conversion show that holo-ACP1 should release at lower retention times vs apo-ACP1 at higher retention times. This also suggests that the untreated ACP1 is mostly in apo- form. Prior studies have indicated that ACP1 grown in M9 minimal media can result in > 95% apo-ACP form. (Data not shown).

All ACP1 samples were still treated with AcpH to ensure protein conversion and purified using SEC. An example of the SEC chromatogram and corresponding 16% Tris Tricine PAGE can be seen in Figure A.18. Several peaks are seen in the 220 nm chromatogram with smaller impurities eluting in fractions D2-D8. Two large peaks are seen from fractions B4-B12 and fractions C1-C7. The multiple peaks suggests dimers of

ACP1 form by disulfide bridges from the sulfur atoms on cystine (21Cys) residues [23]. The 16% Tris Tricine PAGE (Figure A.18 (b)) confirms the apo-ACP1 protein is in fractions B4-C7 with weak ~10 kDa bands at their respective peak edges, and strong bands in the middle of the peaks.

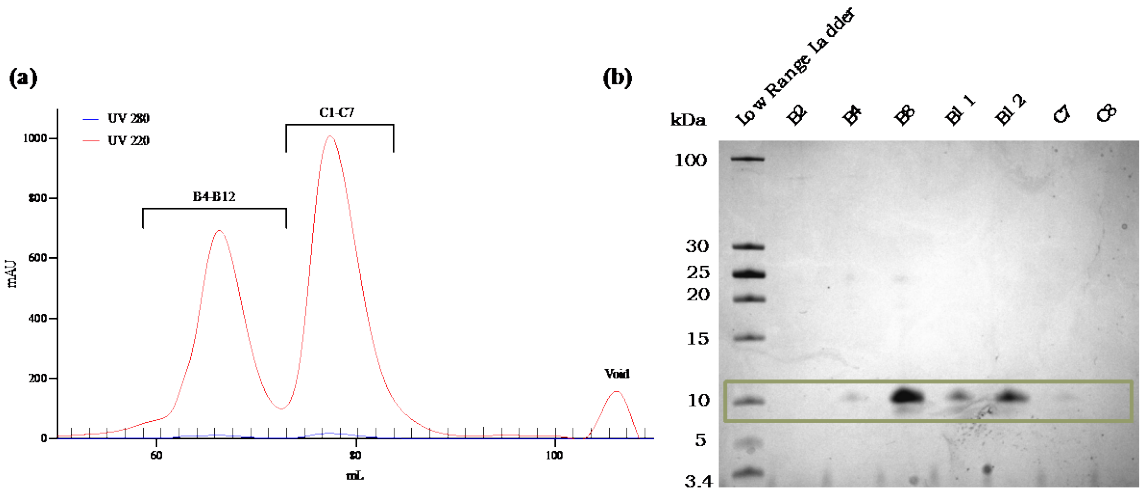

Figure A.18 Example SEC ^{15}N apo-ACP1 purification.
ÄKTA Pure 25 SEC with UV detection at 280 nm (blue) and 220 nm (red) show isolated ^{15}N ACP1 in holo- and apo- form. In the **(a)** chromatogram and **(b)** 16% Tris-Tricine PAGEs, ACP can be in wells B4–C7 in a 96-well block. These fractions were kept isolated based on the first (apo-) and last (holo-) peaks and stored for future use.

The final product of ^{15}N apo-ACP1 was prepared for cargo loading, but cargo loading was unsuccessful. One possibility could be from the dimerization of the proteins and inhibiting enzyme binding. To test this theory, the apo-ACP1 should be treated with a reducing agent to preserve the protein as a monomer.

Homology Modeling

A homology model for RhlI was generated using the sequence from RhlI sequencing, but did not include the His_6MBP tag from protein expression and purification (MIELLSESLEGLSAAMIAELGRYRHQVFIEKLGWDVVSTSRVRDQEFDQFDHPQ

TRYIVAMSRQGICGCARLLPTTDAYLLKDVFAYLCSETPPSDPSVWELSRYAASA
ADDPQLAMKIFWSSLQCAWYLGASSVVAVTTTAMERYFVRNGVILQRLGPPQK
VKGETLVAISFPAYQERGLEMLLRYHPEWLQGVPLSMAV). The crystal structure of TofI in a ternary complex with an inhibitor and MTA was used as a temple model for protein angles and ingested into the online workspace SWISS-MODEL [5, 6, 7, 36]. The provided sequence was ingested into the SWISS-MODEL workspace as a target sequence before the program could build the model. Once the sequence was processed, a .pbd file could be downloaded, and again ingested into the work spaces Chimera and ChemDraw 21.0.0 [7, 8]. The quality of the model is rated base off of the global model quality estimation (GMQE) with a rating of 0.60. SWISS-MODEL conducts a quality check for models with an associated Ramachandran Plot, residue specific quality reports, and s quality estimate of the model in comparison (Figure A.19). The Ramachandran plot associated with RhlI predicts the accuracy of a predicted protein based on the stereochemical parameters of the protein (Figure A.19 (a)) [35]. Based on the Ramachandran plot, the predicted protein structures for RhlI (red circle/purple circles) are favorable falling in the most favorable structural regions (dark green). Figure A.19 (b) shows the models template alignment with TofI (3p2h.1.A). Matching residues are outlined with a box with a purple/pink quality mean score above each individual residue. The closer the score is to the solid gray line (QMEAN), the higher the quality of the residues structure. There are several dips in the score quality seen in the sequence such as the dip near residue 40. These residues are associated with loops and are susceptible to change [33]. There are also blanks where a QMEAN could not be calculated. Figure A.19 (c) is shows a quality estimate of the model compared with other non-redundant sets of

PDB structures from the software. The red star is the generated model, which is plotted just outside of the mean quality scores for its protein size. This is most likely from the dips in quality mean score from Figure A.19 (b). This model was created to accurately depict the RhlI protein for this study and for future modeling with 3D protein-enzyme interactions.

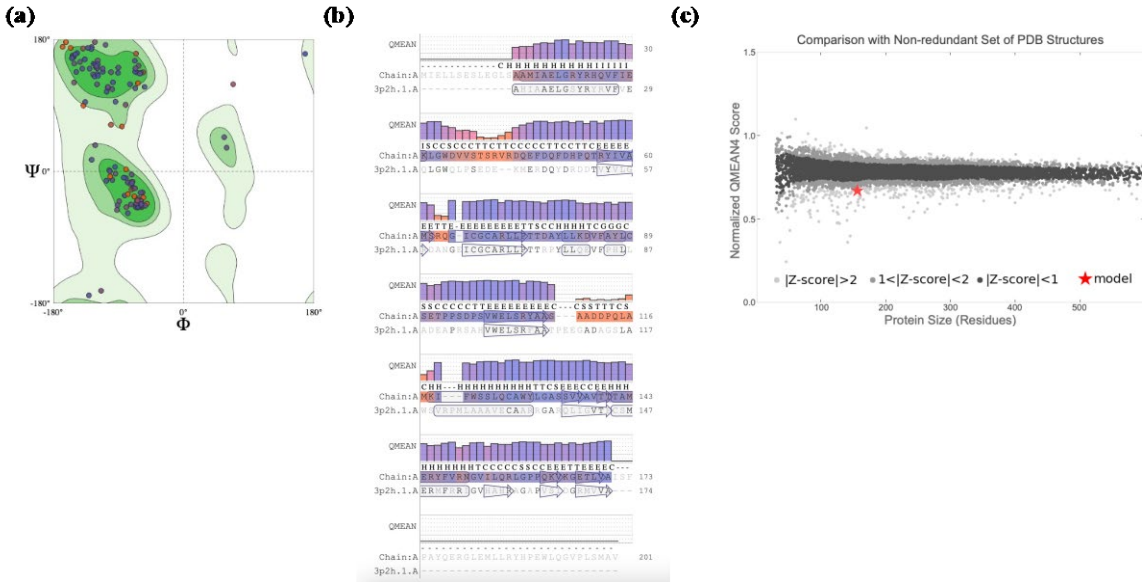

Figure A.19 Homology modeling estimates of RhlI.
RhlI was modeled using sequencing data from ATUM, and ingesting this it and a common crystal structure (3p2h.1.A) into the SWISS-MODEL workspace [5, 36]. **(a)** Ramachandran Plot associated with the RhlI model, **(b)** is model-template alignment comparison, and **(c)** is the quality estimate of the model compared to the PDB

APPENDIX B

Compilation of Additional Figures

$\underline{His_6MBP\text{-}RhlI}$

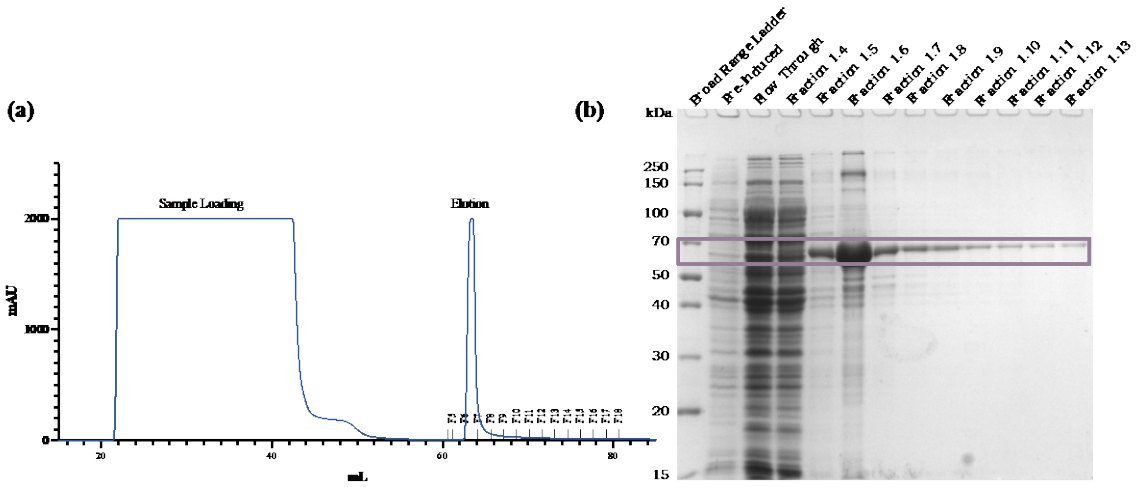

Figure B.1 Batch 1 Affinity Column His_6MBP-RhlI purification.
ÄKTA Start Affinity Column (MBPTrap™) Chromatography is used to purify His_6MBP-RhlI (67.97 kDa) and can be seen in the **(a)** chromatogram and **(b)** 12% SDS PAGE mostly in fractions 1.5 - 1.9.

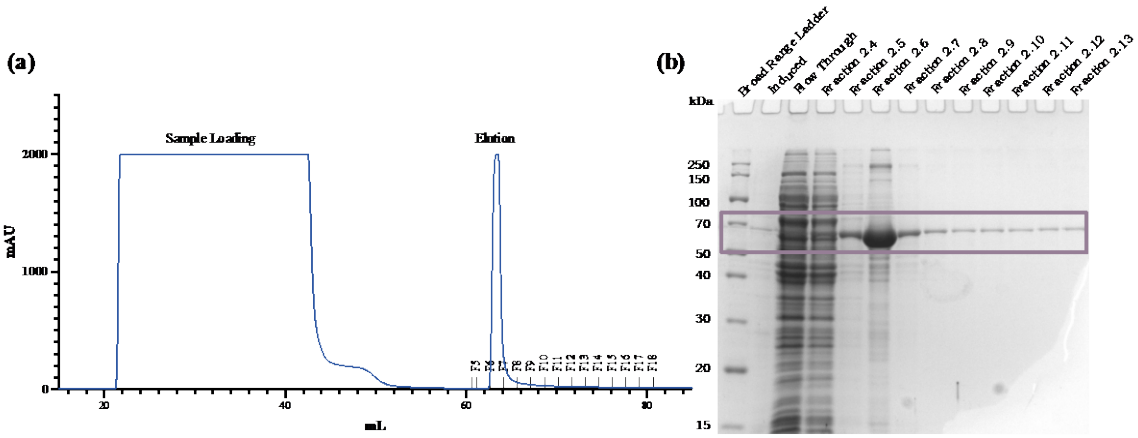

Figure B.2 Batch 2 Affinity Column His_6MBP-RhlI purification.
ÄKTA Start Affinity Column (MBPTrap™) Chromatography is used to purify His_6MBP-RhlI (67.97 kDa), and can be seen in the **(a)** chromatogram and **(b)** 12% SDS PAGE mostly in fractions 2.5 - 2.7.

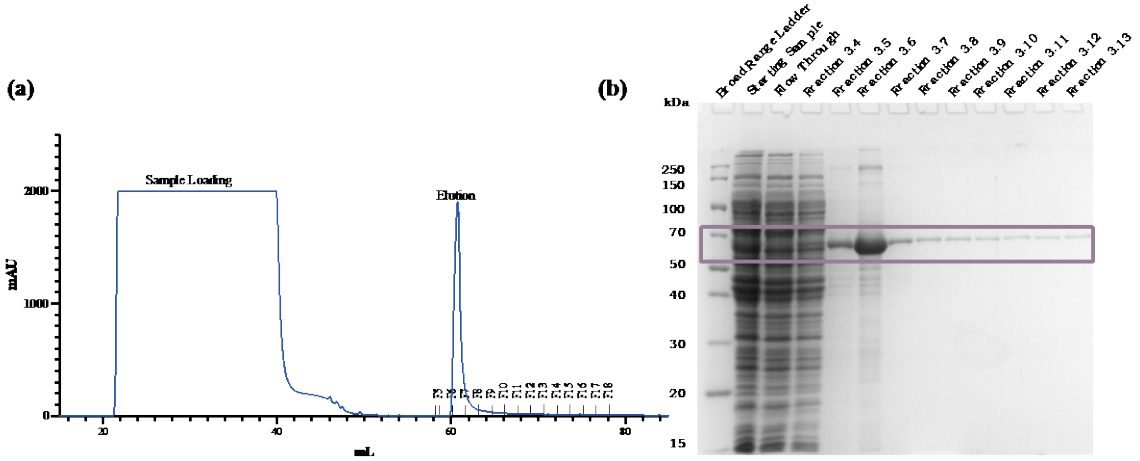

Figure B.3 Batch 3 Affinity Column His_6MBP-RhlI purification.
ÄKTA Start Affinity Column (MBPTrap™) Chromatography is used to purify His_6MBP-RhlI (67.97 kDa), and can be seen in the **(a)** chromatogram and **(b)** 12% SDS PAGE mostly in fractions 3.5 - 3.7.

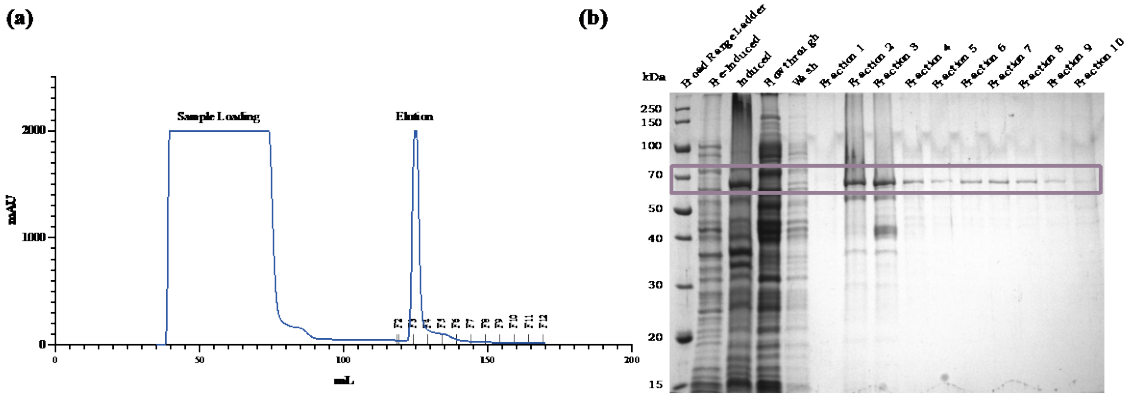

Figure B.4 Batch 4 Affinity Column His_6MBP-RhlI purification.
ÄKTA Start Affinity Column (MBPTrap™) Chromatography is used to purify His_6MBP-RhlI (67.97 kDa), and can be seen in the **(a)** chromatogram and **(b)** 12% SDS PAGE mostly in fractions 2 - 8.

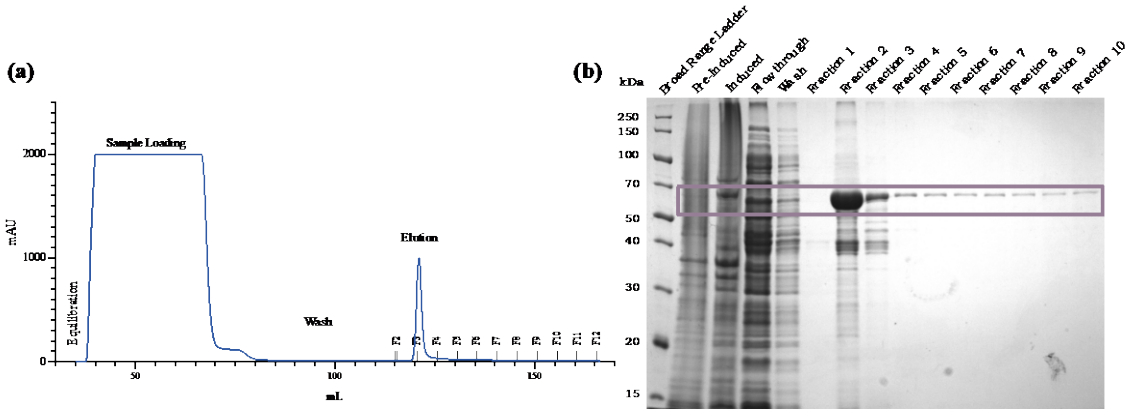

Figure B.5 Batch 5 Affinity Column His_6MBP-RhlI purification.

ÄKTA Start Affinity Column (MBPTrap™) Chromatography is used to purify His_6MBP-RhlI (67.97 kDa), and can be seen in the **(a)** chromatogram and **(b)** 12% SDS PAGE mostly in fractions 2 – 3.

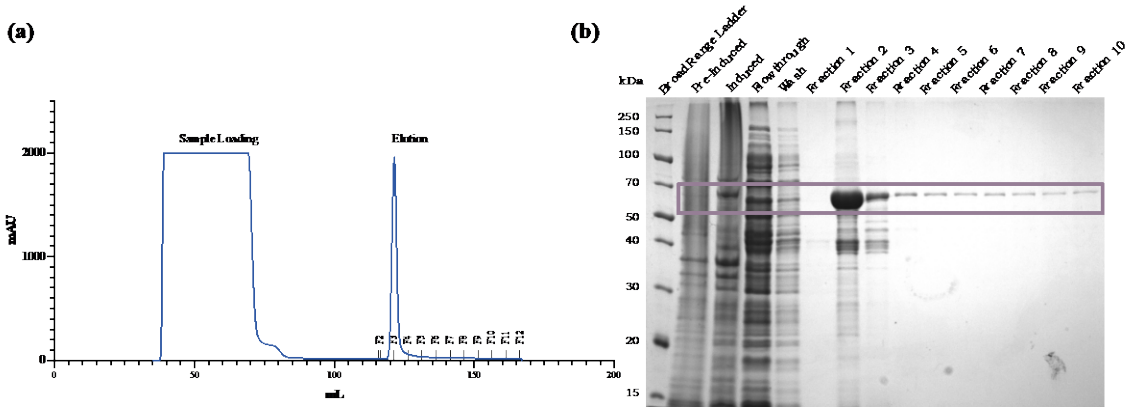

Figure B.6 Batch 6 Affinity Column His_6MBP-RhlI purification.

ÄKTA Start Affinity Column (MBPTrap™) Chromatography is used to purify His_6MBP-RhlI (67.97 kDa), and can be seen in the **(a)** chromatogram and **(b)** 12% SDS PAGE mostly in fractions 2 – 4.

Single Labeled ACP1 ^{15}N

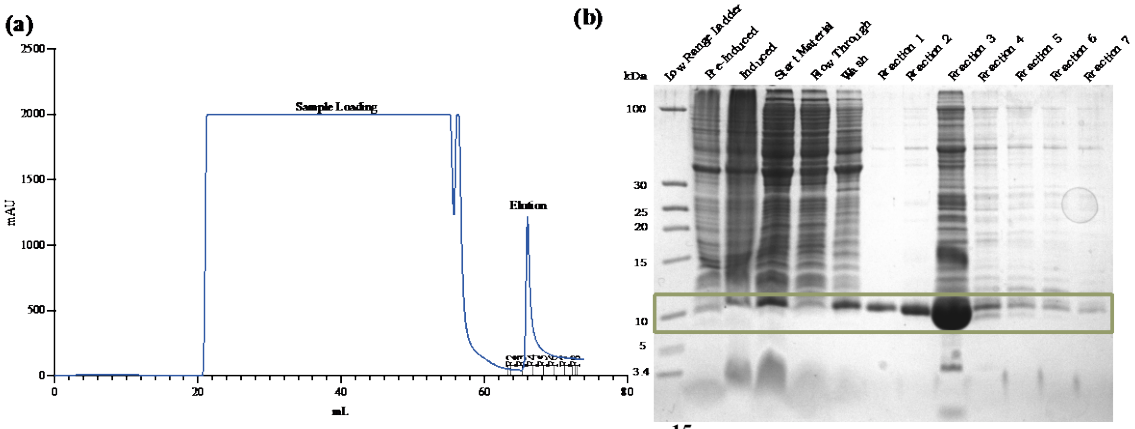

Figure B.7 Batch 1 Nickel Column ^{15}N ACP1 purification.

ÄKTA Start Nickel Column (HisTrap™) Chromatography **(a)** Chromatogram and corresponding **(b)** 16% Tris Tricine Gel for single labeled ACP1. ACP1 is 10 kDa and can be found mostly in fractions 1 - 4 from the chromograph and gel image.

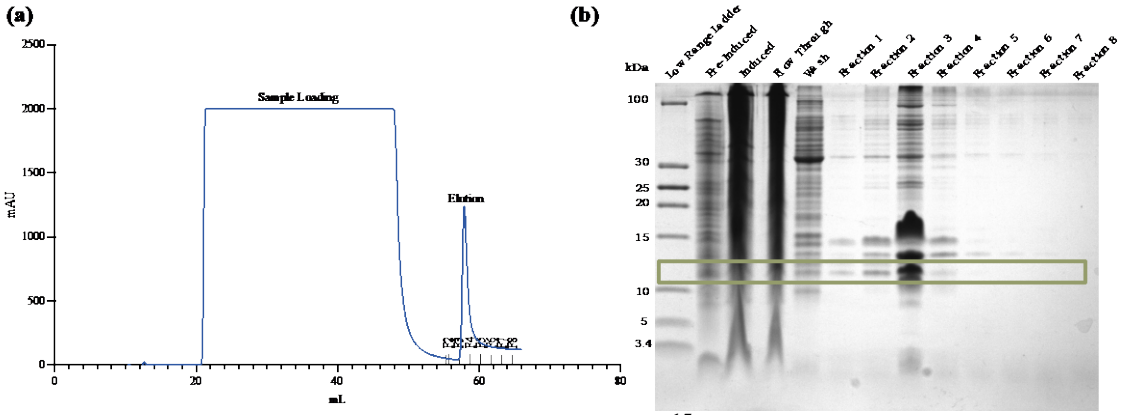

Figure B.8 Batch 2 Nickel Column ^{15}N ACP1 purification.

ÄKTA Start Nickel Column (HisTrap™) Chromatography **(a)** Chromatogram and corresponding **(b)** 16% Tris Tricine Gel for single labeled ACP1. ACP1 is 10 kDa and can be found mostly in fractions 1 - 4 from the chromograph and gel image.

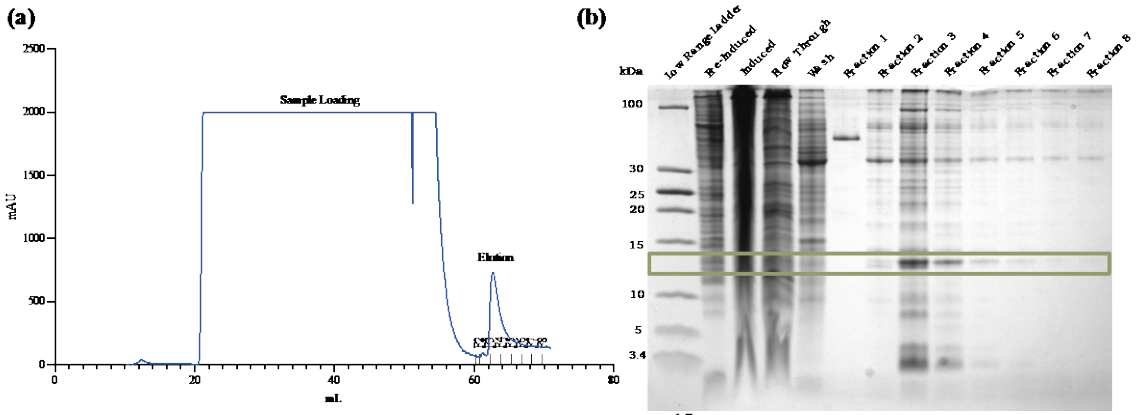

Figure B.9 Batch 3 Nickel Column ^{15}N ACP1 purification.

ÄKTA Start Nickel Column (HisTrap™) Chromatography **(a)** Chromatogram and corresponding **(b)** 16% Tris Tricine Gel for single labeled ACP1. ACP1 is 10 kDa and can be found mostly in fractions 3 - 4 from the chromograph and gel image.

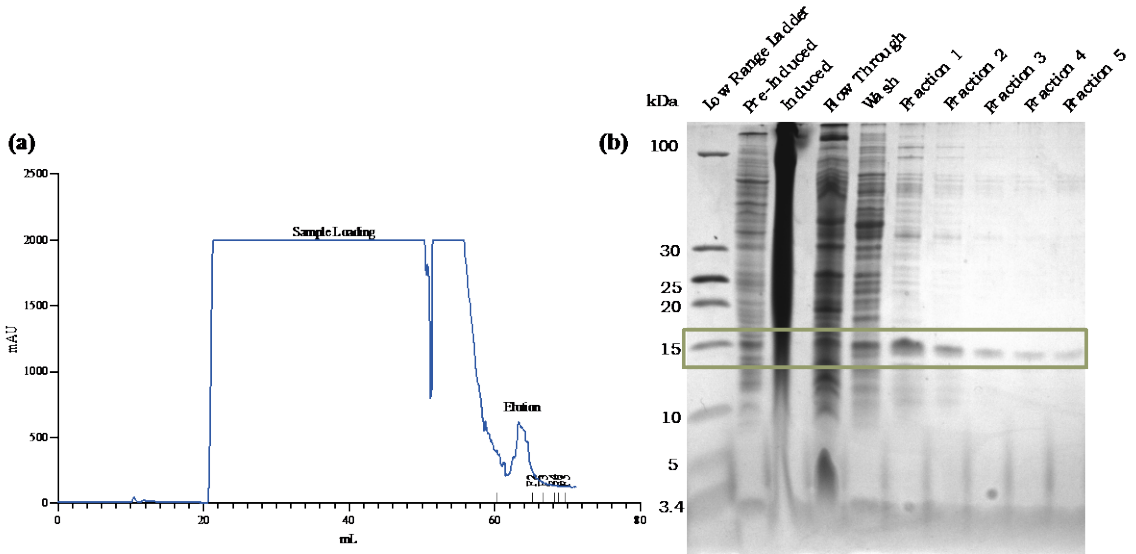

Figure B.10 Batch 4 Nickel Column ^{15}N ACP1 purification.

ÄKTA Start Nickel Column (HisTrap™) Chromatography **(a)** Chromatogram and corresponding **(b)** 16% Tris Tricine Gel for single labeled ACP1. ACP1 is 10 kDa and can be found mostly in fractions 1 - 3 from the chromograph and gel image.

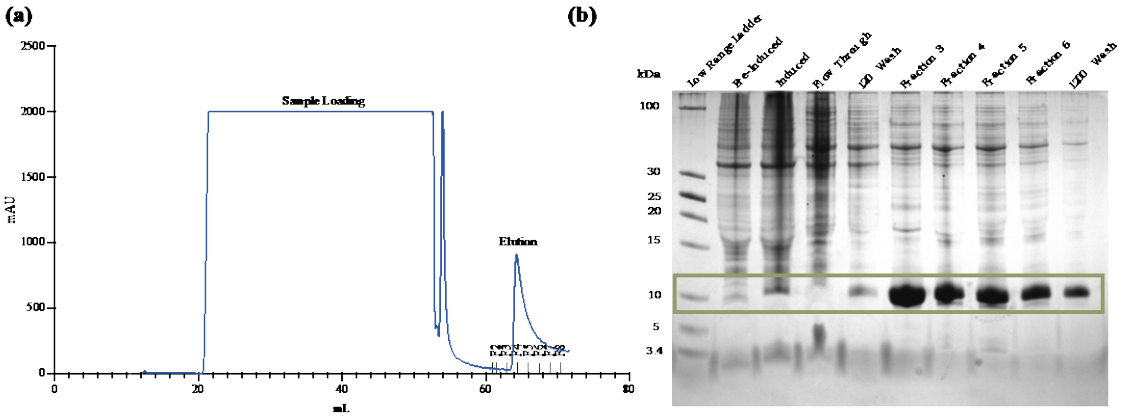

Figure B.11 Batch 5 Nickel Column ^{15}N ACP1 purification.
ÄKTA Start Nickel Column (HisTrap™) Chromatography **(a)** Chromatogram and corresponding **(b)** 16% Tris Tricine Gel for single labeled ACP1. ACP1 is 10 kDa and can be found mostly in fractions 3 - 6 and in a 1200 wash through from the chromograph and gel image.

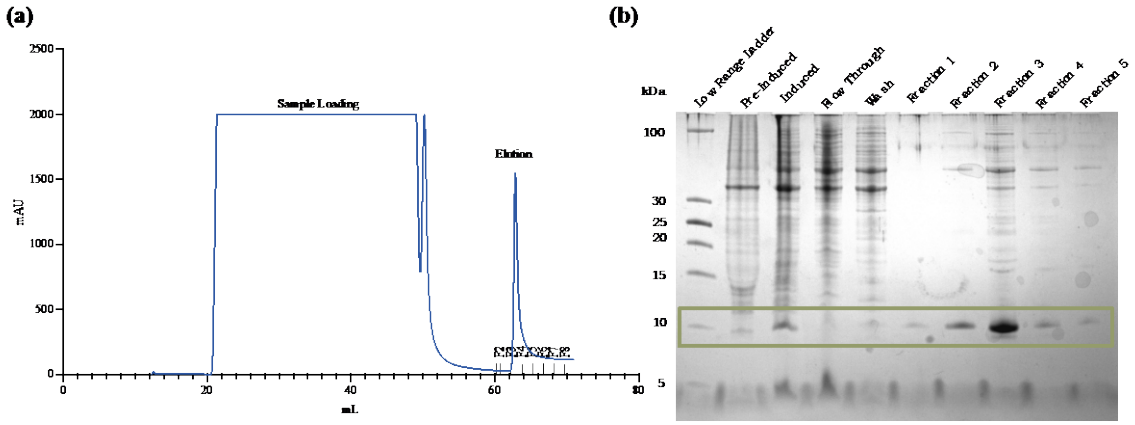

Figure B.12 Batch 6 Nickel Column ^{15}N ACP1 purification.
ÄKTA Start Nickel Column (HisTrap™) Chromatography **(a)** Chromatogram and corresponding **(b)** 16% Tris Tricine Gel for single labeled ACP1. ACP1 is 10 kDa and can be found mostly in fractions 2 - 4 from the chromograph and gel image.

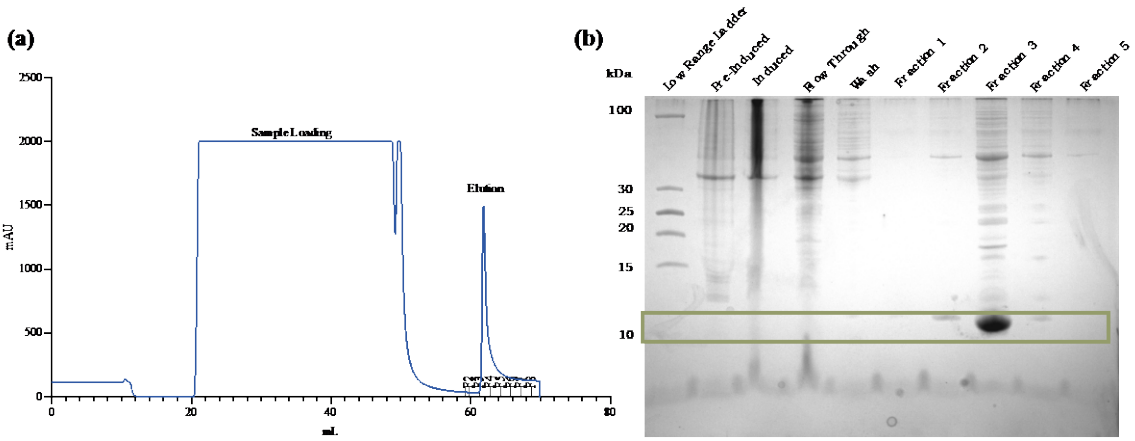

Figure B.13 Batch 7 Nickel Column ^{15}N ACP1 purification.
ÄKTA Start Nickel Column (HisTrap™) Chromatography **(a)** Chromatogram and corresponding **(b)** 16% Tris Tricine Gel for single labeled ACP1. ACP1 is 10 kDa and can be found mostly in fraction 3 from the chromograph and gel image.

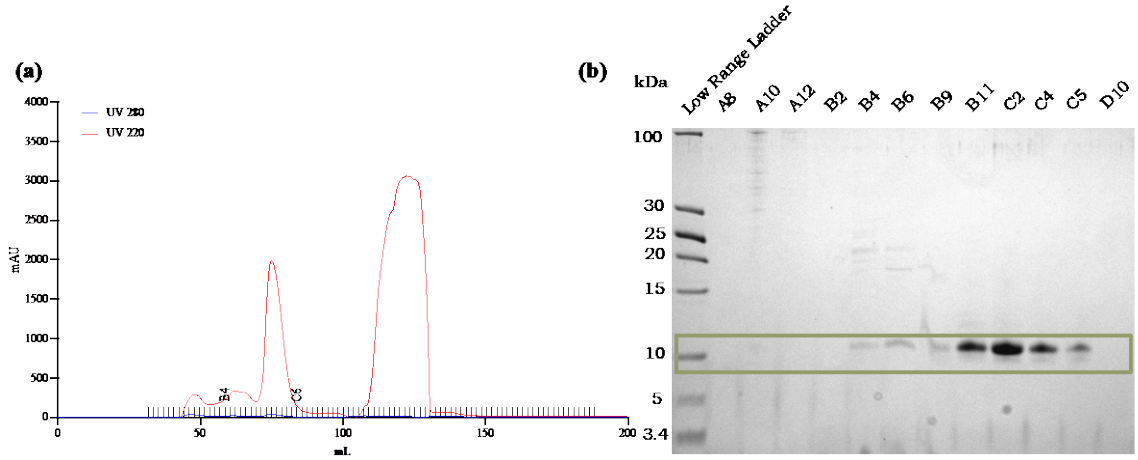

Figure B.14 Batch 1 SEC 15N ACP1 purification.
ÄKTA Pure 25 SEC with UV detection at 280 nm (blue) and 220 nm (red) show isolated ^{15}N ACP1 in holo- and apo- form. In the (a) chromatogram and (b) 16% Tris-Tricine PAGE, ACP (10 kDa) can be in wells B4-C6 in a 96-well block.

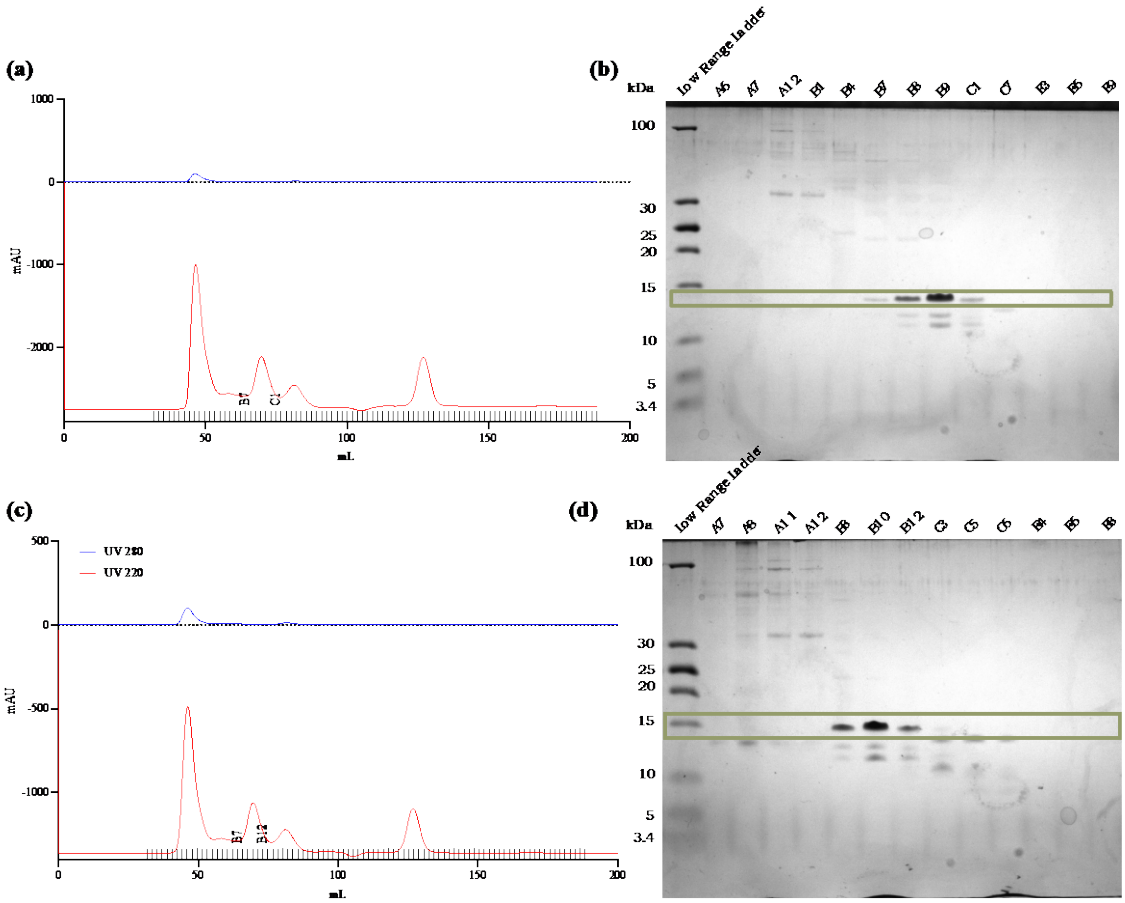

Figure B.15 Batches 2-4 SEC 15N ACP1 purification.
ÄKTA Pure 25 SEC with UV detection at 280 nm (blue) and 220 nm (red) show isolated ^{15}N ACP1 in holo- and apo- form. In the (a), (c) chromatograms and (b), (d) 16% Tris-Tricine PAGEs, ACP can be in wells B7-C1 and B7-B12 of the 96-well blocks.

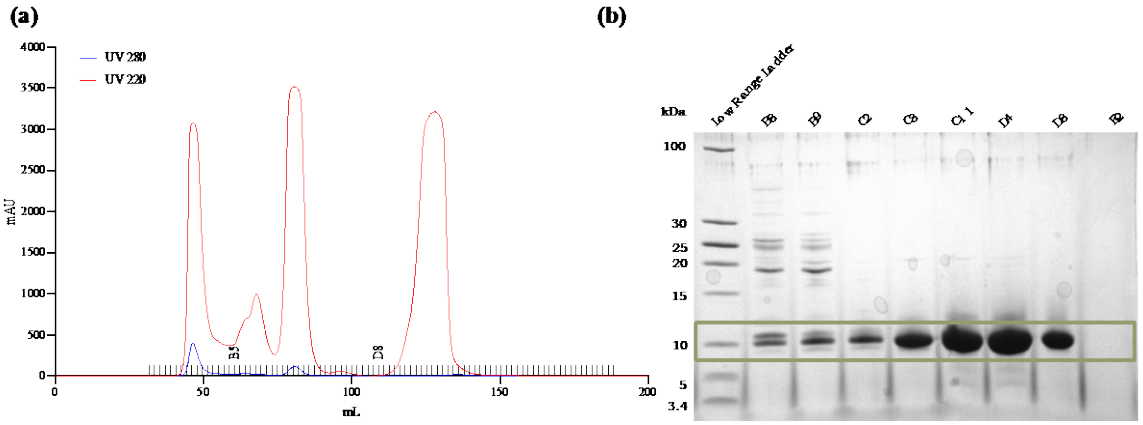

Figure B.16 Batches 5-7 SEC 15N ACP1 purification.
ÄKTA Pure 25 SEC with UV detection at 280 nm (blue) and 220 nm (red) show isolated ^{15}N ACP1 in holo- and apo- form. In the (a) chromatogram and (b) 16% Tris-Tricine PAGE, ACP can be in wells B5-D10 in a 96-well block.

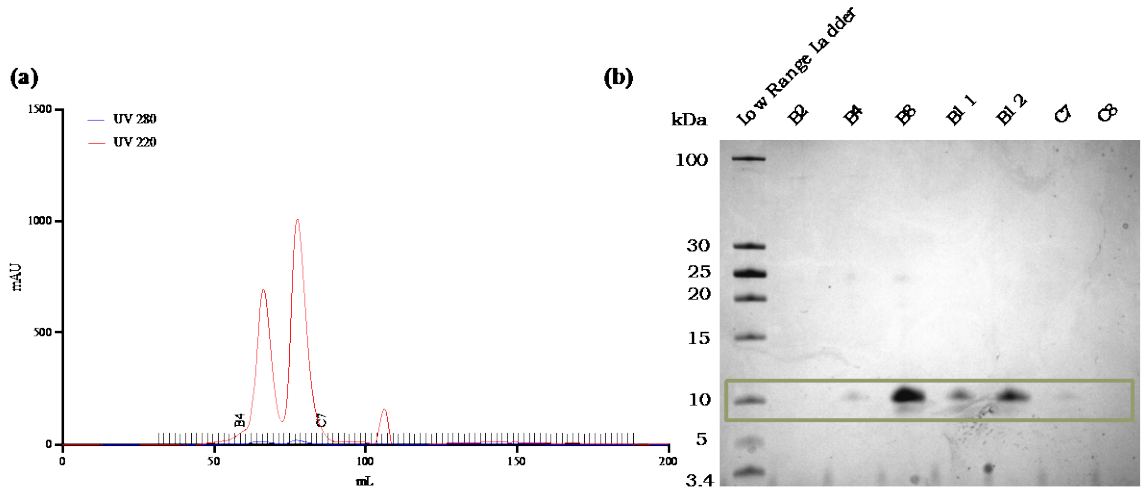

Figure B.17 Batch 1 SEC ^{15}N apo-ACP1 purification.
ÄKTA Pure 25 SEC with UV detection at 280 nm (blue) and 220 nm (red) show isolated ^{15}N ACP1 in apo- form. In the **(a)** chromatogram and **(b)** 16% Tris-Tricine PAGE, ACP can be in wells B4-C7 in a 96-well block.

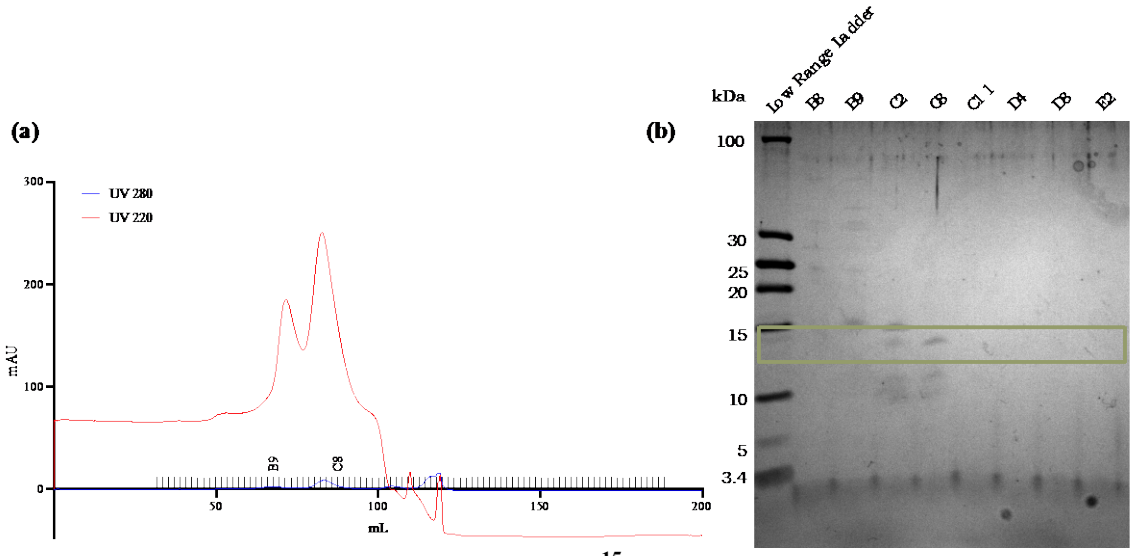

Figure B.18 Batches 2-4 SEC ^{15}N apo-ACP1 purification.
ÄKTA Pure 25 SEC with UV detection at 280 nm (blue) and 220 nm (red) show isolated ^{15}N ACP1 in apo- form. In the **(a)** chromatogram and **(b)** 16% Tris-Tricine PAGE, ACP can be in wells B9-C8 in a 96-well block.

Batches 5-7 SEC ^{15}N ACP1 was not converted to apo-ACP1 because of UHPLC holo-/apo- experiments.

NMR Parameters

Table B.1 ^{13}C, ^{15}N apo-ACP1 NMR spectra parameters.
Spectra collected for protein backbone assignments and the respective parameters used for data collection.

Filename	Experiment	B_0	sw	sw1	sw2	ni	ni2	np	ns	dl
Y:\lwarner\13C15N ACP1-apo_05172022\4	hsqcfpf3gpphwg	600.132	16.0221	45	N/A	150	N/A	2048	8	1
Y:\lwarner\13C15N ACP1-apo_05172022\6	hncogpwg3d	600.132	14.0263	26	15	40	128	2048	16	1
Y:\lwarner\13C15N ACP1-apo_05172022\8	hncagp3d	600.132	16.0221	26	30	40	128	2048	16	1
Y:\lwarner\13C15N ACP1-apo_05172022\12	hncacbgpwg3d	600.132	16.0221	22	80	40	128	2048	32	1
Y:\lwarner\13C15N ACP1-apo_05172022\15	cbcaconhgpwg3d	600.132	16.0221	26	80	40	128	2048	44	1

B_0 – static magnetic field strength in MHz

np – number of complex points in t_2 (or t_3)

ni – number of complex points in t_1

sw – acquisition sweep width (ppm)

sw1- sweep width in t_1 (ppm)

sw2 - sweep width in t_2 (ppm)

ns – number of scans per FID

dl – interscan delay (sec)